ABSTRACT

Title of Dissertation:	MOLECULAR AND BIOPHYSICAL BASES OF INTRACELLULAR ELECTRIC FIELDS IN POLLEN TUBES
	Custódio de Oliveira Nunes Doctor of Philosophy, 2022
Dissertation directed by:	Professor José A. Feijó Cell Biology and Molecular Genetics

Pollen tubes are the male gametophyte of flowering plants. They are arguably one of the fastest growing cells in nature and inherently an excellent model for studying cellular processes like apical growth, polarity and chemotropism. Pollen tube development is associated with a unique choreography of ion fluxes and cytosolic ion gradients of Cl^-, Ca^{2+}, H^+ and K^+, creating a unique electrochemical environment, where alternating depolarizing ionic currents at their growing apex are spatially separated from hyperpolarizing currents in their shank. We hypothesize that these electrical differences generated by the opposite ionic patterns could sustain a standing membrane potential gradient at the growing apex. In agreement with evidence from other cellular electrotaxis phenomena, we further hypothesize that a standing electric field gradient could be mechanistic in terms of cell polarity and chemotropism of pollen tubes.

Here we show, for the first time, the existence of a standing membrane potential gradient in pollen tubes, confirmed in three different species, thus suggesting a conserved role in apical

growth. This conclusion was achieved using three complementary methods, two membrane potential dyes with opposite fluorescence kinetics, and a genetic probe for cytosolic potassium (K^+). The K^+ gradient is focused at the pollen tube tip, and is compatible with previous information on the individual ion features. Of relevance, K^+ shows a negative gradient from the tip, the first ever described in a living cell, suggestive of K^+ apical efflux that contributes to the depolarized state. Quantifications of the fluorescent dyes estimate an apical depolarization of approximately 30mV compared to the shank. Screening of ion-channel mutants inducing male-fertility phenotypes supports the hypothesis that this bioelectric oddity is mechanistic for pollen tube's critical functions, fast invasive growth and chemotropism. Furthermore, we determined that anionic lipids determine the emergence of the pollen tube and correlate with the apical depolarization area, suggesting that they may act as physical determinants of the growing apex. These results open important questions in our understanding of the bioelectrical processes determining cell growth, polarity, morphogenesis, and chemotropic reactions.

MOLECULAR AND BIOPHYSICAL BASES OF INTRACELLULAR ELECTRIC FIELDS IN POLLEN TUBES

by

Custódio de Oliveira Nunes

Dissertation submitted to the Faculty of the Graduate School of the
University of Maryland, College Park, in partial fulfillment
of the requirements for the degree of
Doctor of Philosophy
2022

Advisory Committee:
Professor José A. Feijó
Professor Caren Chang
Professor Ricardo Araneda
Professor Angus S. Murphy
Professor Sergei I. Sukharev

To my family,

For indulging my curiosity about the natural world.

"As individual emerges from individual along the line of species, so does species emerge from species along the line of life, and every animal and plant, in spite of its separateness and individuality, is only a part of the single, continuous, advancing flow of protoplasm that is invading and subduing the passive but stubborn stuff of the inorganic."

Julian Huxley, in *The Individual in the Animal Kingdom*

Acknowledgements

To my co-workers, for their friendship, generosity, transfer of skills and knowledge that made all this work possible : Michael Lizzio, Maria Teresa Portes, Daniel Santa Cruz Damineli, Alexander Simon, Erwan Michard, Michael Wudick, Juan Barbosa-Caro, Sandra Correia, Franscisco Neves, and José A. Feijó.

To the people involved in the collaborations, who made the best of the opportunity to work as a team: Marcela Hernández-Coronado, Ramin Rahni, Kenneth D. Birnbaum, and Michael Palmgren.

To João Santos, for the development of an image analysis pipeline that refined my quantifications.

To the people from the CBMG department and Biological Sciences doctoral program - staff, professors and students - who have made my time at UMD a memorable life experience. In particular to my fellow graduate students, for personal support and encouragement during my PhD.

To Richard Teague, for taking my mind off of the empirical sciences, even if just for a moment, and make me rediscover philosophy.

Table of Contents

List of Tables

List of Figures

List of Abbreviations

PT – Pollen tube

MPG – Membrane potential gradient

EF - Electric field

VSD – Voltage Sensitive Dyes

PS – Phosphatidylserine

PtdlInst(4,5)P_2 – Phosphatidyl-inositol-4,5-bisphosphate

Declaration of scientific collaborations

Portions of the dissertation have been published in the following manuscripts, where I share authorship:

Wudick MM, Portes MT, Michard E, Oliveira Nunes C, et al. **CORNICHON sorting and regulation of GLR channels underlie pollen tube Ca^{2+} homeostasis.** Science, 2018;(May):533-536. doi:10.1126/science.aar6464

Wudick MM, Michard E, Oliveira Nunes C, Feijó JA. **Comparing plant and animal glutamate receptors: Common traits but different fates?** Journal of Experimental Botany, 2018;(May):1-13. doi:10.1038/pr.2015.58

Hoffmann, RD, Portes MT, Oliveira Nunes, C, et al. **Plasma membrane H^+-ATPases regulate an oscillating cytosolic pH and sustain actin organization in pollen tubes.** Nature Communications, 2020 (May):14;11(1):2395. doi: 10.1038/s41467-020-16253-1

Hernandez Coronado, M, Oliveira Nunes, C, et al. **Repel or Repair: Plant Glutamate Receptor-Like Channels Mediate a Defense vs. Regeneration Tradeoff.** Developmental Cell, 2022 (Feb) 28;57(4):451-465.e6. doi: 10.1016/j.devcel.2022.01.013.

The data presented in the Results section was completed by myself under the supervision of my doctoral advisor, Professor José A. Feijó.

Chapter 1: Introduction

1.1 Bioelectricity, a signal as old as Life

The formulation of the concept of Life has been addressed by many disciplines in Science, but the definition most commonly used is an individual organism in a continuous self-producing activity (metabolism) and in continuous interaction with their respective environments, including other organisms (Maynard Smith, 1986). The 'individual' aspect of this definition is recapitulated in many different views as it requires the existence of a compartment, the separation of the individual from the environment by a communicating barrier, where exchanges with the environment may follow (De Loof, 2015, 2016). The cell surface, or plasma membrane, is a thin sheet about 4nm in thickness consisting of two lipid leaflets that keeps ions, proteins, and other molecules within the intracellular space because the non-polar hydrocarbon interior constitutes an energy barrier to most hydrophilic solutes inside the cell. To overcome this barrier, specialized membrane proteins like channels, pumps and carriers are embedded into the lipids to transport ions, metabolites and other molecules across the membrane (L. Wang, 2012). The selective permeability to certain ion species results in a difference in ion concentrations at the two sides of the PM leading to an imbalance of charge and electrical potential difference across the membrane, coined transmembrane potential. This bioelectricity is carried by simple inorganic ions such as H^+, K^+, Na^+ , Ca^{2+}, Cl^-, rather than by electron-based electricity because membranes are permeable to electrons and could not easily confine and concentrate electrons in the cytosol (Hille, 2001). All the living systems have this self-generated electrical

dimension and losing the ability to realize it eventually leads to cell death. It is not surprising that from an evolutionary perspective, the transmembrane potential can be hypothesized to be one of the first signals used by primitive cells to monitor membrane integrity. Especially when considering unicellular stages, in which organisms are challenged by environment fluctuations, the maintenance of the plasma membrane integrity is a matter of life and death. Any small rupture in the plasma membrane, even if repaired in time to allow survival, would always imply the loss of some intracellular materials and the dissipation of charges from the intracellular space to the exterior, attenuating the transmembrane potential across the membrane. Over time, these small depolarization events might have been the common origin and the first signals for membrane repair after injury (Lipchinsky, 2018).

Before discussing the electrical properties of biological membranes, it is important to remember the relations which describe electricity in the physical systems. Ohm's law states that the current through a conductor between two points is directly proportional to the voltage across the two points and inversely proportional to the resistance in the circuit $I = V/R$, where V is the potential difference (Volts), I is the current (Amperes) and R the resistance (Ohms). Ohm's law is valid in biological systems with a slight difference on how the current is carried, which is by ions and not by electrons. A simple model to represent the electrical properties of the biological membranes considers that the membrane behaves electrically as a resistor and capacitor in parallel (Hille, 2001) (fig.1).

The resistor (R) is the representation of ion channels which change permeability and thus conductance according to the opening and closing states. The capacitor

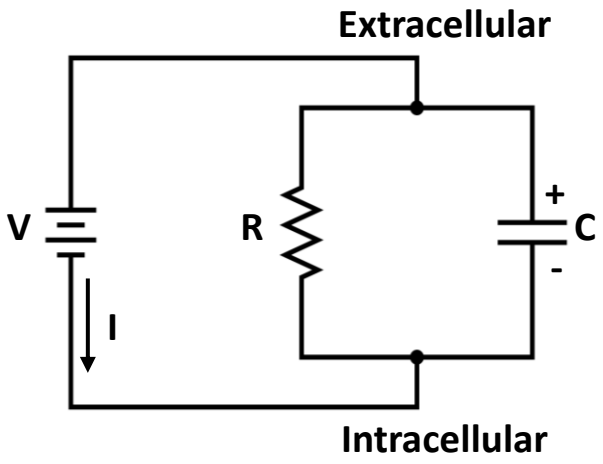

Fig. 1 | The phospholipid membrane behaves electrically as a resistance (R)-capacitance (C) network, shunted in parallel. V is the potential difference over the membrane or Membrane Potential. The current (I) is the movement of ions across the membrane

represents the membrane, because of its lipid bilayer structure which acts as an insulator. If a potential (V, in Volts) is applied across the membrane (C, in Farads), a quantity of charge (Q, in Coulombs) proportional to the difference, builds up on the plates of the capacitor. This is given by the formula Q = VC. When the voltage changes, the capacitor resists the change in voltage by drawing current from the changing source if the voltage is rising, or supplying current if the voltage is decreasing, with a capacitive current I = C(dV/dt), which states that the current flow onto a capacitor equals the product of the capacitance and the rate of change of the voltage . This expression just demonstrates that when ions cross membranes, the voltage difference is not instantaneous, and depends on the capacitance of the biological membranes. This lag between the ion currents and the voltage establishment happens in the millisecond time scale, nevertheless it is an important feature for biological membranes because it allows transient longitudinal gradients of membrane potential within the same cell when the membrane capacitance is low enough (few channels open)(Abbott & Kepler, 1952). Cells may take advantage of this when focusing ion fluxes and implement

thermodynamically and kinetically far-from-equilibrium states where growth and morphogenesis processes take place.

1.2 A Brief History of Bioelectricity

The earliest bioelectric phenomenon, of which mankind became aware, was the electrical discharge of certain types of fish, with the first reports of these events dating back to Aristotle in *Historia animalium* (cited in (Kellaway, 1946)). In the 18th century, bioelectrical phenomenon started to be formally studied by Luigi Galvani, conducting experiments with dead frog legs and discovered that muscle legs can be triggered by external induction although it was not required. Galvani thought that the nature of the contraction was caused by a sort of "animal electricity", different from the "frictional" electricity (Piccolino, 1997). Later, Alessandro Volta repeated these experiments, to conclude that the frog contractions were more evident when using a bimetallic conductor, and that the electricity involved in this phenomenon was of the same kind as the one produced by the electrostatic machines, the frog anatomy was just a very sensitive detector (Croswell, Cecchini, & Pelosi, 1992). It was not until the 19th century, that the mechanism behind Galvani's and Volta's observations was understood by the Biophysicist Julius Bernstein which is largely recognized by his 'membrane hypothesis' that correctly proposed that excitable cells are surrounded by a membrane selectively permeable to K^+ ions at rest, and during excitation permeable to other ion species that now we know to be mainly Na^+ in animals (Bernstein, 1912). Around the same time, in 1888, Walther Nernst, physical chemist and physicist devised the equation to determine the equilibrium reduction potential of a half-cell in an electrochemical cell. Named after him, the Nernst equation was adapted to biological

systems and used to study neurons (squid axon) and to predict resting membrane potential based on K^+ ion concentrations.

In 1901, Jagadish Chandra Bose, a physicist in training but a biologist by vocation, started experimenting with bioelectric potentials and movements in plants, believing that the essence between the physical, inorganic world and the world of living was to be found in the action of electromagnetic waves (Shepherd, 1999). Over the next thirty years, Bose performed hundreds of experiments on electrical signaling in plants, and gifted us with works like "Research into the Irritability of Plants"(Bose, 1913) and "The Nervous mechanisms of plants"(Bose, 1926). One of the main conclusions from these experiments using *Mimosa pudica* (telegraph plant), known by the drooping movement of the leaves after mechanical stimulation, was that electric stimulation alone triggers the same movement. Bose proposed that plant's electrical communication was done via the phloem and that electrical stimulation mimicked mechanical stimulation. In the 1920s and 1930s, E.J. Lund focused on ion currents and showed that anatomical polarity was predicted and controlled by the bioelectric polarity of ion fluxes in vivo (Lund, 1923). Between the 1930s and 1940s H.S. Burr, focused on measuring and correlating voltage gradients with future developmental patterns in a wide range of systems, from corn growth to human physiology (Burr, 1944; Burr & Northrop, 1935); his measurements showed that voltage gradients are quantitatively predictive of morphology, suggesting that the measured electric fields (EFs) carried patterning information. During this time, many scientists came up with their own terms for this 'immaterial force' that could be measured in all the organisms, namely Fields of life (L-fields) (Burr, 1973) or Entelechy by Hans Driesch (Churchill, 1969).

Whereas previous research was more descriptive, Marsh and Beams used a more functional approach showing that the anterior-posterior polarity in planarian regeneration could be controlled via external electrical stimulation of the worm segments (Marsh & Beams, 1947, 1949, 1952). The seminal work by Lionel Jaffe (L. F. Jaffe, 1981; Lionel F. Jaffe & Nuccitelli, 1977) and coworkers were of extreme importance after developing a non-invasive vibrating probe to measure extracellular ionic fluxes and showing that these precede pattern formation and accompany polarized growth and cell migration (Lionel F. Jaffe & Nuccitelli, 1974). At a single-cell level, ion currents were shown to traverse migrating amoebas creating an asymmetric front-rear pattern where currents enter the back and exit the front of the cell, according to the migration axis (Richard Nuccitelli, Poo, & Jaffe, 1977). These type of currents, similar in magnitude and spatial organization were also mapped in fungi, water molds, and pollen tubes undergoing polarized tip growth (Gow, 1984; Schreurs & Harold, 1988; Weisenseel, Nuccitelli, & Jaffe, 1975).

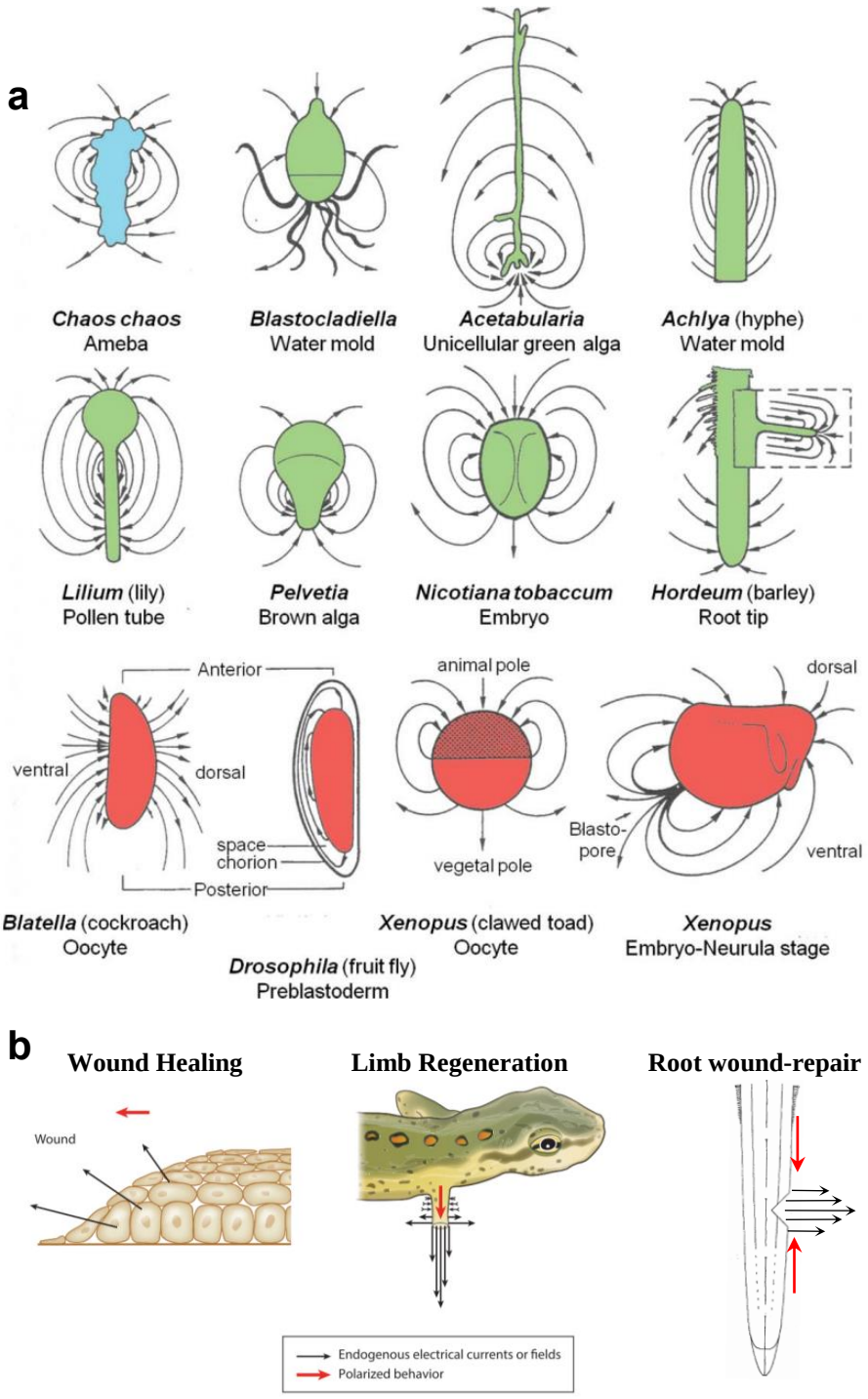

Fig. 2 | Electric currents in different systems. **(a)** Schematic diagrams of the electric currents around a variety of systems, as measured by the vibrating probe technique developed by Jaffe (1974) (adapted from De Loof (2016). **(b)** Electric current patterns around polarizing tissues (adapted from Chang & Minc (2014) and Mayer & Weisenseel (1997))

Other examples correlating these currents with polarity include measurements during the early cleavage of *Xenopus* eggs (Kline, Robinson, & Nuccitelli, 1983) as well as the currents associated with the light-triggered polarized outgrowth of the embryo in the brown algae Fucus and Pelvetia (fig.2) (Lionel F. Jaffe, 1966; Richard Nuccitelli & Jaffe, 1975, 1976) .

At a multicellular level, bioelectrical currents have been associated with large-scale tissue behavior. One of the most well-characterized example is probably wound healing in which outward currents are oriented away from the wound in animals (R. Nuccitelli, 2003; Reid, Nuccitelli, & Zhao, 2007) and in the roots of plants (fig.2 b) (Meyer & Weisenseel, 1997). It is thought that the currents associated with wounding arise from the rupture of trans-epithelial electrochemical organization that is established when tissues are intact (Zhao, Agius-Fernandez, Forrester, & McCaig, 1996). Other examples of bioelectrical control and asymmetric currents can be found in limb and tail regeneration (Altizer et al., 2001; Borgens, 1982; Jenkins, Duerstock, & Borgens, 1996), tissue migration and rearrangements during vertebrate development (Hotary & Robinson, 1992, 1994; Lionel F. Jaffe & Stern, 1979), oogenesis (Woodruff & Telfer, 1980) and histological differentiation in amphibian, avian, and invertebrate model systems (Borgens & Shi, 1995)

These pioneer studies have shown that spatially organized currents surround cells and tissues when morphogenesis and/or polarity take place, which have led to speculating that the resulting endogenous electrical fields could guide cells and tissues during development. The generated steady electrical patterns during these phenomena can only arise from the spatial segregation of ion channels which, in turn, create areas

of influx and efflux of different ion species creating a compounded electrical current at morphogenetic hotspots.

1.3 Effects of exogenous electric fields on cell polarity

Many biological processes like cell migration, polarity establishment and cell division, create extracellular electric fields which are the result of spatially localized ion currents in the cells. The observations of such currents led many researchers to investigate the effects of applying exogenous electric fields in order to highlight the importance of electrochemistry in cell polarity and understand this elusive force in the most fundamental cellular processes. Most of the cells used for these studies were cells that were known by their migratory behavior like amoebas (Korohoda, Mycielska, Janda, & Madeja, 2000), keratinocytes (Nishimura, Isseroff, & Nucciteili, 1996), lymphocytes(Lin et al., 2008), neural crest cells (Cooper & Keller, 1984; Pan & Borgens, 2010), neurites (Pan & Borgens, 2010; N. Patel & Poo, 1982; A. Rajnicek, Gow, & McCaig, 1992) and pollen tubes (R. Malhó, Feijó, & Pais, 1992; Rathore, Cork, & Robinson, 1991). In most of these experiments, the magnitude of EF that these cells were subjected to were similar in magnitude to the observed electric fields measured *in vivo* and the common ground of these studies was the migration toward the cathode with a few exceptions that will be detailed later on.

In amoebas subjected to EFs, migration trajectory is oriented parallel to the EFs, the migration speed is more constant and the number of lateral pseudopods decreased, suggesting a more deterministic path in their migration (Korohoda et al., 2000). Keratinocytes exposed to EF of the same magnitude as measured in wounds migrate

faster than in lower EF (Nishimura et al., 1996) suggesting that cells in closer contact with a wound will migrate faster than the cells in adjacent layers from the wound. The directional keratinocytes response to EF was even higher when the substrate included type I and IV collagen from the extracellular matrix (Sheridan, Isseroff, & Nuccitelli, 1996), suggesting that EFs alone are not enough to reproduce the composite effects of the interaction cell-enviroment in the responsiveness of the cells to EFs. Similar experiments using corneal epithelial cells also found that these cells would respond better to EF when supplementing the media with an EGF (epidermal growth factor). In the case of the lymphocytes, EFs not only induced migration towards the cathode but also activated kinase signaling pathways that are shared with chemotactic responses, suggesting that EFs alone might be able to activate some cellular pathways (Lin et al., 2008). Neurons subjected to EF had their neurites changing direction towards the cathode too but EFs also stimulated growth of new neurites which could suggest that EFs could trigger cell morphogenesis by inducing a different electrochemical state in the cell (N. Patel & Poo, 1982). The previous studies were done under exogenous EF, but one particular study addressed the influence of endogenous EFs in cell division when the EFs are created by wounds in rat cornea epithelia: cells surrounding the wound had the axis of division perpendicular to the wound-induced EFs and when the EFs were disturbed by pharmacology blocking ion channels, the mitotic spindle lost polarity and cell division happened at random angles (Song, Zhao, Forrester, & McCaig, 2002). Other studies were conducted not in migrating cells but cells that have polarized growth like rod-shaped bacteria, fission yeast or pollen tubes, to understand if growth direction could be steered by exogenous EFs. In three different species of

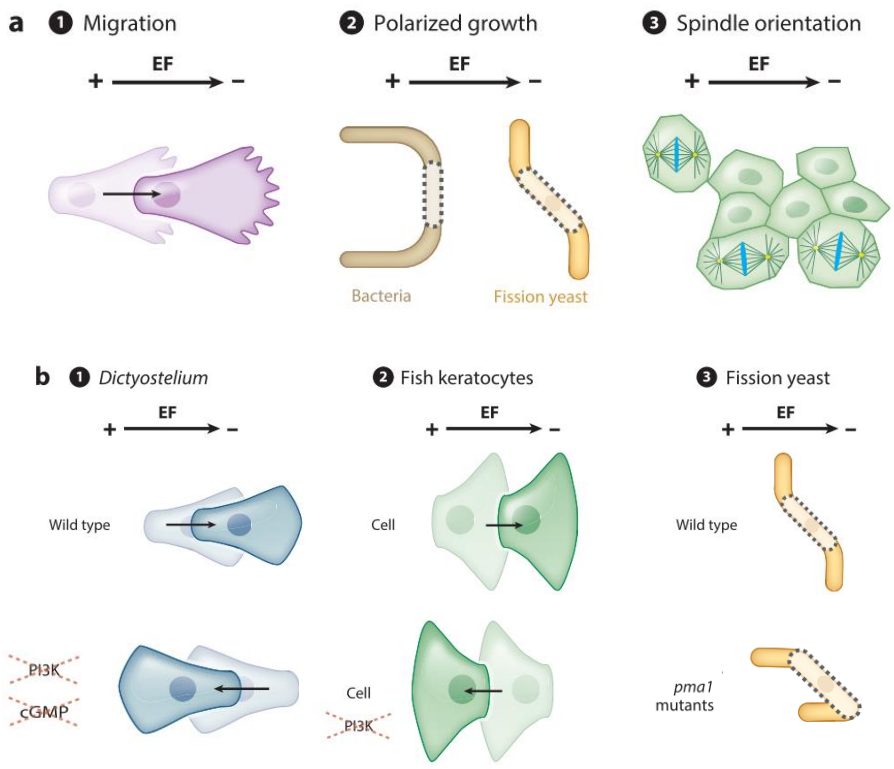

Fig. 3 | Effect of exogenous electric fields in cell polarity and growth. (a) Cells subjected to electric fields can orient **(1)** migration, **(2)** polarized growth, and **(3)** cell division. **(b)** Directionality changes in polarity under the effect of an electric field **(1)** Dictyostelium migrates toward the cathode, but when PI3K and cGMP signaling molecules are inhibited it migrates toward the anode. **(2)** Fish keratocytes migrate toward the cathode, but when PI3K is inhibited it migrates toward the anode. **(3)** Fission yeast apical growth is orthogonal do the EF but it becomes parallel in null mutant cells for the H^+-ATPase PMA1 (adapted from Chang & Minc (2014))

bacteria, EFs induced a curved growth towards the anode side and it was confirmed that this was not just passive bending but active growth because latex beads attached to the cell wall were tracked during growth and could show a faster growth rate in anode-facing ends of the cells than in the cathode-facing ends (A. M. Rajnicek, McCaig, & Gow, 1994). In fission yeast, the EFs reorient polarized growth in the direction orthogonal to the field (Minc & Chang, 2010) instead of the cathode or anode as in the previous examples, but null mutants for the H^+-ATPase PMA1 grow parallel

to the field. In plants, EFs orient growth toward the anode or cathode depending on the cell type (Schnepf, 1986), but probably one striking example is in Pollen tubes which, in specific conditions, grow to either sides of the EF (R. Malhó et al., 1992). In these experiments, the pollen tubes growing closer to the anode or the cathode grew parallel to the field but always towards the side that they grew closer to, whereas pollen tubes in the middle of the germination chamber grew randomly. Since this was only observed in agar solid medium, the authors reasoned that this disparity about a specific direction was the result of the distribution of ionic species in the plate due to the imposed electric fields in the media (R. Malhó et al., 1992). This uneven ion distribution could create ion gradients in the chambers which we know can steer PTs and affect their growth. Another explanation could be linked to the heterogeneous EF along the germination chamber, which could suggest that the field strength was more important to define the growth direction rather than the signal.

The effect of EF on cell's behavior was seen as epiphenomena because the mechanisms underlying cellular responses was elusive, and often was speculated rather than experimentally demonstrated. Since the 80's that researchers have thought that the actin filaments were responsible for EF-induced cell migration because the charged actin-based cytoskeleton assembly-disassembly dynamics dictates cell shape and therefore determines the direction of subsequent growth (A. M. Rajnicek et al., 1994). Many studies corroborate this hypothesis by showing the manipulation of assembly-disassembly velocity of actin filaments *ex vivo*, and reversing polymerization growth in function of direction and strength of the EF (Kim, Kao, Hasselbrink, & Meyhöfer, 2007; Riveline et al., 1998; Stracke, Böhm, Wollweber, Tuszynski, & Unger, 2002).

In vivo, migrating cells under EFs were shown to produce a strong fringe of actin filaments on the side migrating towards the cathode and that actin distribution in the cell is asymmetrical, being preferentially distributed on the lamellipodia forming at the migrating front (Li & Kolega, 2002; Luther, Peng, & Lin, 1983).

However, a more recent hypothesis posits that membrane potential plays an upstream role in electrotaxis because one of the most immediate effects on cell physiology upon exposure to EF is an asymmetric change in membrane potential that can be observed using voltage sensitive dyes (Flickinger, Berghöfer, Hohenberger, Eing, & Frey, 2010). In a cell electrically silent and with low voltage conductance, the side facing the anode hyperpolarizes whereas the side facing the cathode depolarizes. The hyperpolarized side facing the anode attracts Ca^{2+} by passive electrochemical diffusion which creates contractile forces through the interaction of Ca^{2+} with the cytoskeleton dynamics, thereby propelling the cell towards the cathode (Mycielska & Djamgoz, 2004). When using a Ca^{2+} depleted medium or Ca^{2+} channel blockers, intracellular calcium does not increase upon the EF action and cells lose electrotaxis (Onuma & Hui, 1988). In a study using Dyctiostelium, electrotaxis was significantly affected by manipulating the extracellular K^{+} concentration and pH in order to depolarize the cell, which suggests that if the electrochemical gradient and membrane potential of the cell are dissipated, the action of EF does not have the same effect in triggering migration (Gao et al., 2011). These studies place membrane potential asymmetries in the spotlight to explain electrotaxis, but how would that explain different directions in migration towards the anode or the cathode? In cells expressing voltage-gated channels, the membrane potential asymmetry would trigger currents that

could redefine the default migration pattern, thus a possible explanation is that the direction of cell movement will depend on the balance between contrasting contractile forces created by the different ion currents driven either by passive diffusion and/or voltage-gated ion channels (Mycielska & Djamgoz, 2004).

The different polarity orientations induced by exogenous EFs highlight the complexity of cellular responses and are likely to happen because of the existence of competing signaling platforms used to steer cells. Overall, these findings show that most cells are electrotactic and robustly reorient their polarity, directional cell movement or division plates to the applied EF, suggesting that electrotactic signals may be as essential as chemotactic or mechanotactic signals for cell guidance and polarity (Chang & Minc, 2014).

1.4 Membrane potential in cell polarity and guidance

The membrane potential of a cell arises from gradients of charges segregated across the insulating plasma membrane. Membrane potential is dynamically regulated by ion channels and pumps, whose function is exporting and importing ions through the membrane. Thus, the value of resting membrane potential is usually a function of the channels that a specific cell is expressing at the time. Levin and colleagues have promoted the idea that the bioelectrical state of a cell influences the progression through the cell cycle (Levin, 2012; Levin & Stevenson, 2012), being a key parameter in mediating proliferation or differentiation state. The concept came from an early experimental observation correlating resting membrane potential and the degree of mitotic activity in Chinese hamster ovary cells. When the external medium was modified to have these cells hyperpolarized (approx. -75mV), the DNA synthesis

measured by [^{3}H]thymidine incorporation was inhibited. Upon washing the hyperpolarizing medium, the cell cycle was recovered and DNA synthesis proceeded (Cone, 1971). Inversely, it was reported in the 70's that ouabain-induced depolarization in neurons was followed by DNA synthesis and subsequent mitosis, although lacking cytokinesis (Cone & Cone, 1976). The analysis of the nuclei in the binucleated cells revealed that DNA synthesis was complete.

In an attempt to illustrate this, Levin and colleagues compiled information of resting membrane potential of many cell types, which partly corroborates the idea that bioelectrical hyperpolarized states are correlated with differentiated cells, whereas depolarized states with actively proliferating cells (fig. 4). At the top of the axis we have hyperpolarized states in highly differentiated cell types like skeletal muscle and neurons (both excitable cells), and at the bottom many cell types in the prolific state, like embryo cells, cancer cells or undifferentiated embryonic stem cells. The liver cells reside in an intermediate resting membrane potential because they show a highly regenerative capacity at the same time that they are differentiated. Resting membrane potential is normally a function of the K^+ conductance which is controlled by the amount of K^+ channels expressed in the cells at a given point. When cells are subjected to a wide-spectrum K^+-channels blocker, proliferation is inhibited and this has been repeatedly confirmed in many tissues and cell types (reviewed in (Blackiston, McLaughlin, & Levin, 2009)). In fact, many different K^+-channels show cell-cycle-dependent expression or activity, thus changing the cells K^+ conductance in the different cell cycle checkpoints (reviewed in (Urrego, Tomczak, Zahed, Stühmer, &

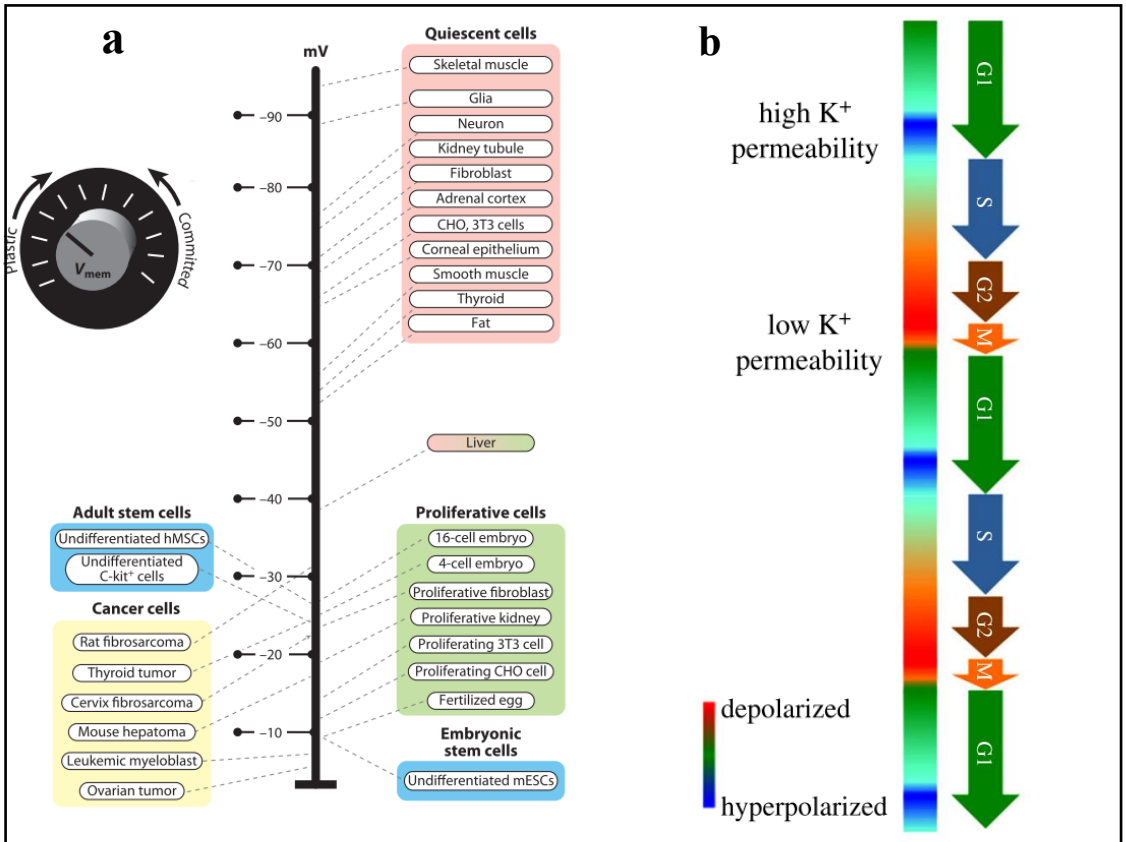

Fig. 4 | Membrane potential is a fundamental parameter regulating cell properties. (a) Cell types along the depolarized-hyperpolarized axis shows a correlation between membrane potential and cell fate. Highly plastic, undifferentiated, and proliferative cell types tend to be more depolarized and mature, quiescent and terminally differentiated cells types tend to be more hyperpolarized. (adapted from Levin, M. ,Stevenson, C. 2012). **(b)** Schematic representation of membrane potential throughout the cell cycle due to differential expression of K^+ channels, e.g. between G1 and S phases, there are more K^+ channels in the cell which in turn increases K^+ permeability, shifting membrane potential towards hyperpolarized values.

Pardo, 2014)), for example during mitosis, the cells are known to have low K^+ permeability and to be more depolarized (fig. 4 b).

A recent study in zebrafish skin cells presents a good example of how membrane potential changes are implicated in cell migration and cell identity (Inaba, Yamanaka, & Kondo, 2012). Zebrafish have pigmented skin stripes along their bodies,

alternating from blue and gold which correspond to different cell types; melanophores form the gold stripe, xantophores form the blue stripes. The underlying mechanisms of stripe patterning and the physical separation between these two cell types was not known, but several mutants from forward genetics screens were found that displayed defects in the stripes. One such mutant is called *jaguar* and its phenotype is having the two stripes overlapping due to the intermingled melanophores and xantophores. The jaguar mutant has a mutation on an inward-rectifying potassium channel Kir7.1, and it regulates resting membrane potential by letting K^+ into the cytoplasm of melanophores, but not xantophores. Melanophores membrane potential was analysed using the voltage sensitive dye DiBAC4 and shows that the jaguar mutant cells are more depolarized than the WT cells. Dynamic tracking of melanophores migration revealed that there is a transient depolarization upon contact with xantophores and a polarity switch, in which the melanophores migrate away from the xantophores. In the jaguar mutants, melanophores contact xantophores with no change in membrane potential resulting in no migration away from xantophores and an intermixing of pigment bands in the animal. Thus, membrane potential is sensitive to cell-to-cell communication and may regulate polarity and tissue patterning. More interesting is the question how the shift in membrane potential reprogrammed the cell to avoid the other cell type, as though the bioelectrical signal carried conditioning information.

Another study that shows a change in cell behavior correlated with a shift in membrane potential was done in *Xenopus* spinal neurons growth cone (Nishiyama, Von Schimmelmann, Togashi, Findley, & Hong, 2008). When growth cones are developing there are many different cues in the medium that trigger attraction or repulsion

behaviors, to avoid wrong neuronal connections. To test how neurons respond to these cues, neurons were tracked while given a source of attractants and repellents and membrane potential was indirectly measured by the voltage sensitive dye Di-2-ANEPEQ. When the growth cones were challenged by attractants, the growth cone hyperpolarized and the reverse happened with repellents, eliciting a depolarization. Both responses had approximately the same magnitude of 15 mV and were determinant of the direction of growth-cone turning. Although the guidance of these neurons relies on a specific membrane potential shift to steer towards or away from the chemical cues, the intracellular cascade and how growth is steered is not yet fully understood, but these responses rely on Cl^- and Na^+ currents. One feature that is worth noting is that the membrane potential response is only confined to the growth cone, the part of the cell that will respond to the external cues, rather than a whole-cell polarization shift. This unique example demonstrates that our knowledge of bioelectrical signal at a single cell level and especially subthreshold membrane potential differences along the plasma membrane are completely underrepresented in research, possibly because the tools to analyze such fine variations in voltage are not widely used yet.

1.5 Membrane electrostatics and cell polarity

Anionic lipid species are abundant components of biological membranes, are asymmetrically distributed within cells and can form longitudinal membrane domains (Spira et al., 2012; Van Meer, Voelker, & Feigenson, 2008). The asymmetry created by anionic lipids like Phosphatidylserine (PS), Phosphatidylinositol (PI), and Phosphatidic Acid may give rise to differently charged domains on the cytosolic inner

leaflet with strong affinity to cationic species such as Ca^{2+} ions or proteins (Olivotto, Arcangeli, Carla, & Wanke, 1996; Savtchenko, Poo, & Rusakov, 2017). The research on membrane electrostatic landscape has been developing fast in the last decade with the aid of the highly specific anionic lipid probes, to show that the combination of anionic lipids gives identity to the endomembrane system and plasma membrane (fig.5 a) (Platre et al., 2018).

As anionic lipids carry negative charges, the strength of this electrostatic fields depends on its relative concentration their respective nominal charges, varying from -1 for Phosphatidylserine (PS) to -5 for Phosphatidylinositol-4,5-bisphosphate ($PtdIns(4,5)P_2$). In plants, an electrostatic lipid gradient is formed from the PM to the tonoplast, which follows the endocytic route and specifies and electrostatic membrane territory from more negatively charged membranes at the Plasma membrane, to ER-derived compartments that are nearly neutral (Noack & Jaillais, 2020). The same electrostatic gradient was previously shown via artificial polybasic peptide fluorescence probes that have different nominal charges from +8 to +2/0. These polybasic electrostatic anchors localize in different cell compartments corresponding to their countercharges from anionic lipids, thus showing +8 probes only localized to the PM whereas +2/0 probes were localized only to endomembrane compartments (Simon et al., 2016).

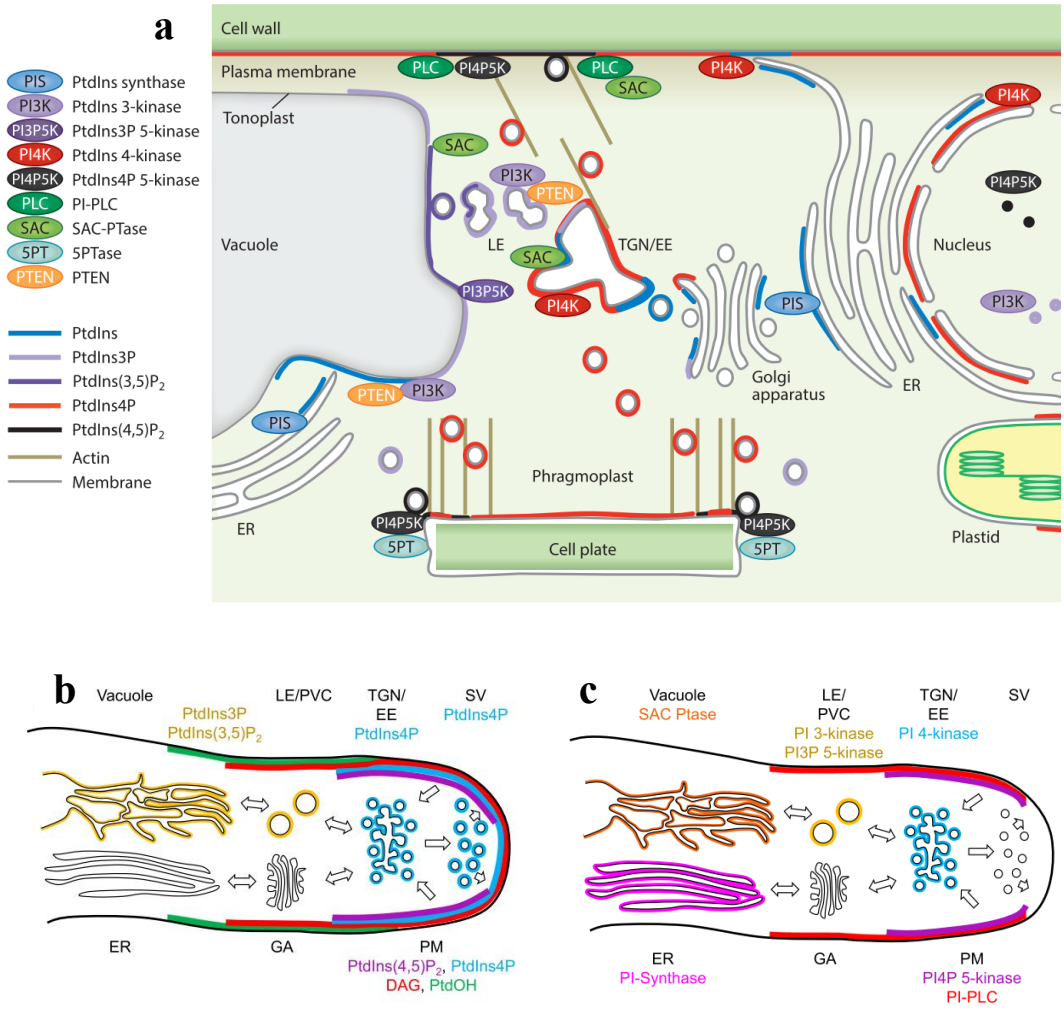

Fig. 5 | Lipids confer identity to membranes. (a) Electrostatic map of the subcellular localization of Phosphatidylinositol (PI) species and the respective enzymes that synthesize or modify them. Membrane trafficking to the cell surface or cell plate is correlated with 4-phosphorylated PIs, while trafficking to the LE (late-endosome) or vacuole involves 3-phosphorylated PIs. The progression of transitory vesicles toward fusion at a target membrane is correlated with the formation of PtdIns bisphosphates.
(b) Lipid and PI species in PTs and their polarized localization. PtdIns(4,5)P_2 are usually associated with the plasma membrane but in PTs, it is usually confined to the apical region. **(c)** Lipids biosynthetic enzymes and their distribution patterns in PTs .
Abbreviations: DAG diacylglycerol, ER endoplas- mic reticulum, GA; LE/PVC late endosome/pre-vacuolar compart- ment, PI synthase phosphatidylinositol synthase, PI3-kinase phosphatidylinositol 3-kinase, PI3P 5-kinase phosphatidylinositol 3-phosphate 5-kinase, PI4-kinase phosphatidylinositol 4-kinase, PI4P 5-kinase phosphatidylinositol 4-phosphate 5-kinase, PI5-phosphatase phosphatidylinositol 5-phosphatase, PI-PLC phosphoinositide-speci- fic phospholipase C, PM plasma membrane, PtdIns(3)P phos- phatidylinositol 3-phosphate, PtdIns(3,5)P2 phosphatidylinositol-3,5-bisphosphate, PtdIns(4)P phosphatidylinositol 4-phosphate, PtdIns(4,5)P2 phosphatidylinositol-4,5-bisphosphate, PtdOH phos- phatidic acid, SAC type SAC (suppressor of actin mutation) phosphatase, SV secretory vesicles, TGN/EE trans-Golgi network/ early endosome.

Not surprisingly, there is a high correlation of anionic lipid accumulation with processes related to polarity, e.g. in apical growing cells like pollen tubes (Ischebeck, Stenzel, & Heilmann, 2008; Sousa, Kost, & Malho, 2008; Yuelong Zhou et al., 2020), fission yeast (Haupt & Minc, 2017), or in migrating cells like Dictyostelium (Sato et al., 2009), and fish keratocytes (Sun et al., 2013).

When exposed to an EF, Dictyostelium cells move toward the cathode and the leading edge shows accumulation of PtdIns(4,5)P_2 and the enzyme responsible for PtdIns(4,5)P_2 signaling (PI3-kinase). Another pathway important to regulate cell migration and chemotaxis is the intracellular cyclic Guanosine Monophosphate (cGMP). When PI3-K or cGMP pathways were knocked down individually, cells displayed less directionality during migration. However, when PI3K and cGMP were supressed, cells migrated toward the anode of the EF instead of the cathode (Sato et al., 2009). Similarly, fish keratocytes do normally migrate towards the cathode, but when PI3K was knocked out, cells migrated toward the anode of the field (fig.3) (Sun et al., 2013).

In apical growing cells, PS and PtdIns(4,5)P_2 are pivotal for cell polarity establishment and are involved with vesicle trafficking, polar secretion and exocytosis. In fission yeast, PS accumulates at the sites of polarized growth during budding and mating. A mutant strain in the PS synthase (cho1Δ) exhibited major polarization defects with impaired enrichement of the Rho GTPase Cdc42p, a well-known polarity marker (Fairn, Hermansson, Somerharju, & Grinstein, 2011; Haupt & Minc, 2017). Cells depleted of PS show altered cell dimensions and growth impairment. Similarly in PTs, PS localizes to the growing tip and mutants for the Phosphatidylserine synthase are

dwarf sterile plants resultant of defects during sporophytic development (Yamaoka et al., 2011). Mutant PTs for ALA3, a class of flippases that uses PS as a substrate, show a decrease of PS accumulation at the apical region and defects in vesicle trafficking due to the important interaction between Rab GTPase RabA4d with PS during this process (Yuelong Zhou et al., 2020). Another described phenotype was ovule targeting because the mislocalization of PS consequently affects the localization of PRK3 and PRK6 proteins that are important for PT polarity and guidance (Yang et al., 2022). Arabidopsis RabA4d is typically localized at the inverted-cone zone of the PT and is responsible for targeted polar transport of vesicles. The lack of RabA4d activity leads to severe defects in the polarized growth phenotype of PTs, such as slow growth and increased width as well as swelling, partly phenocopying the ALA3 mutant PTs (Szumlanski & Nielsen, 2009). ROP GTPase 1 (Rho of Plant GTPase) is a well know membrane polarity marker in PTs and it is mainly involved in regulation of cytoskeleton dynamics and vesicle trafficking, moving in the apical region in a predictive way of the growth direction. ROP1 knock down or overexpression leads to non-polarized PT growth, in which instead of a tube, PTs grow spherically at the apical region (Gu, Vernoud, Fu, & Yang, 2003). In roots, ROP6 was found to bind to PS and organize in stable nano-domains, which is required for enhancing the ROP6 signaling (Platre et al., 2019). Although ROP1-PS nano-domain formation was not confirmed in PTs yet, the ROP C-terminus polybasic domain interacting with PS is conserved across different ROP family members (Smokvarska, Jaillais, & Martiniere, 2021).

The anionic lipid PtdIns(4,5)P_2 , with nominal charge -5 is usually synthesized at the PM and confers identity to this membrane by being the most negatively charged

anionic lipid in the cell. This lipid localizes at the PT tip where it is synthesized by specific PIPK (phosphatidylinositol kinase) isoforms that are maintained at the apical region throughout PT growth (fig.5 b,c) (Ischebeck et al., 2008; Sousa et al., 2008). PIPK mutants display slower tube elongation and reduced secretion of the cell wall materials, whereas overexpression of PIPK creates polarity defects, giving rise to PTs with split tip, or multiple branches and in some cases collapsed morphology of the apical dome (Ischebeck et al., 2008; Sousa et al., 2008).These phenotypes suggest that the amount of this lipid affects processes involved in vesicle delivery and fusion to the proper exocytosis sites in the apical region. To strengthen this hypothesis, PI(4,5)P2 is also known to participate in the PM targeting of SEC3 and EXO70, two subunits of the exocyst complex that is known to participate in the tethering and trafficking of post-Golgi vesicles to the plasma membrane (Bloch et al., 2016). In summary, anionic lipids are important for polar secretion, exocytosis and vesicle trafficking, and the electrostatic gradient, which comes from the different amounts of anionic lipids present in each organelle. This electrostatic gradient facilitates the movement of the required vesicles to be delivered to the polarity sites, the recruitment of specific proteins involved in these processes and protein-lipid nanodomains assembly that influence the distribution and function of the proteins in them. Moreover, morphogenetic processes like apical growth or cell migration have ion currents that accompany these cell behaviors, changing the electric properties of the cytosol and possibly the membrane potential. Especially in cells subjected to electric fields, membrane potential modulation is likely to happen if the fields are strong enough, and this leads to membrane destabilization and eventually to electrofusion of vesicles with the PM in a

process that should be mechanistically relevant when high rates of exocytosis take place (Ramos & Teissié, 2000).

1.6 Core Objective

The present thesis addresses the effects of the ion dynamics in the bioelectric state of pollen tubes. The objective of the data shown is to characterize and quantify the biophysical properties of the bioelectrical signal, focusing on its genetic and molecular foundation as well as the implications in the plasma membrane electrostatics. Using different imaging tools and mutants, I aim to illustrate the involvement of bioelectricity in apical growth and chemotropism. The overall goal is to advance the relationship of bioelectricity as an integrator and processor of cellular functions in pollen tubes as well as understanding its origin and conservation in other systems that require depolarizing signals as effectors for morphogenesis and cell patterning.

Chapter 2: Membrane Potential Gradient in Pollen Tubes

2.1 Introduction

Pollen tubes, angiosperm's male gametophyte, are one of the most important cell models when it comes to studying processes involved in apical growth and polarity. The fast cell growth and the precise targeting of ovules requires that growth and cell polarity are well coordinated through cellular mechanisms based on electrochemical phenomena formed by polarized ion fluxes of Ca^{2+}, H^{+} and Cl^{-} (Michard, Simon, Tavares, Wudick, & Feijo, 2016). While Ca^{2+}, H^{+} enter the cell at the apex and exit in the tube shank, anions, and most notably Cl^{-}, move in the opposite direction, entering the shank and leaving the cell at the tip. *In vitro*, the magnitude of these fluxes depends on the plant species, growth conditions and it varies in time in an oscillatory fashion (Damineli, Portes, & Feijó, 2017; Gutermuth et al., 2018; Michard, Dias, & Feijó, 2008). In the pollen tubes tested to date, the magnitude of the Ca^{2+} and H^{+} fluxes through the apical domain range between 1-50 $pmol.cm^{-2}.s^{-1}$ (Michard, Alves, & Feijó, 2009; Michard et al., 2008; Portes et al., 2015). For anions, the apical fluxes exceed those of Ca^{2+} and H^{+} up to three orders of magnitude, oscillating between 50-8000 $pmol.cm^{-2}.s^{-1}$ (Michard et al., 2009; Zonia, Cordeiro, Tupy, & Feijo, 2002). Thus, in the pollen tube tip, these fluxes are coordinated not only to reduce the ionic strength of the apical cytoplasm by means of these high anionic currents, but also to depolarize the plasma membrane due to the influx of positive charges (Ca^{2+}, H^{+}) and the efflux of negative charges (Anions). While the net ion currents at the tip are predicted to depolarize the membrane, the PT shank is under hyperpolarization forces, because H^{+}

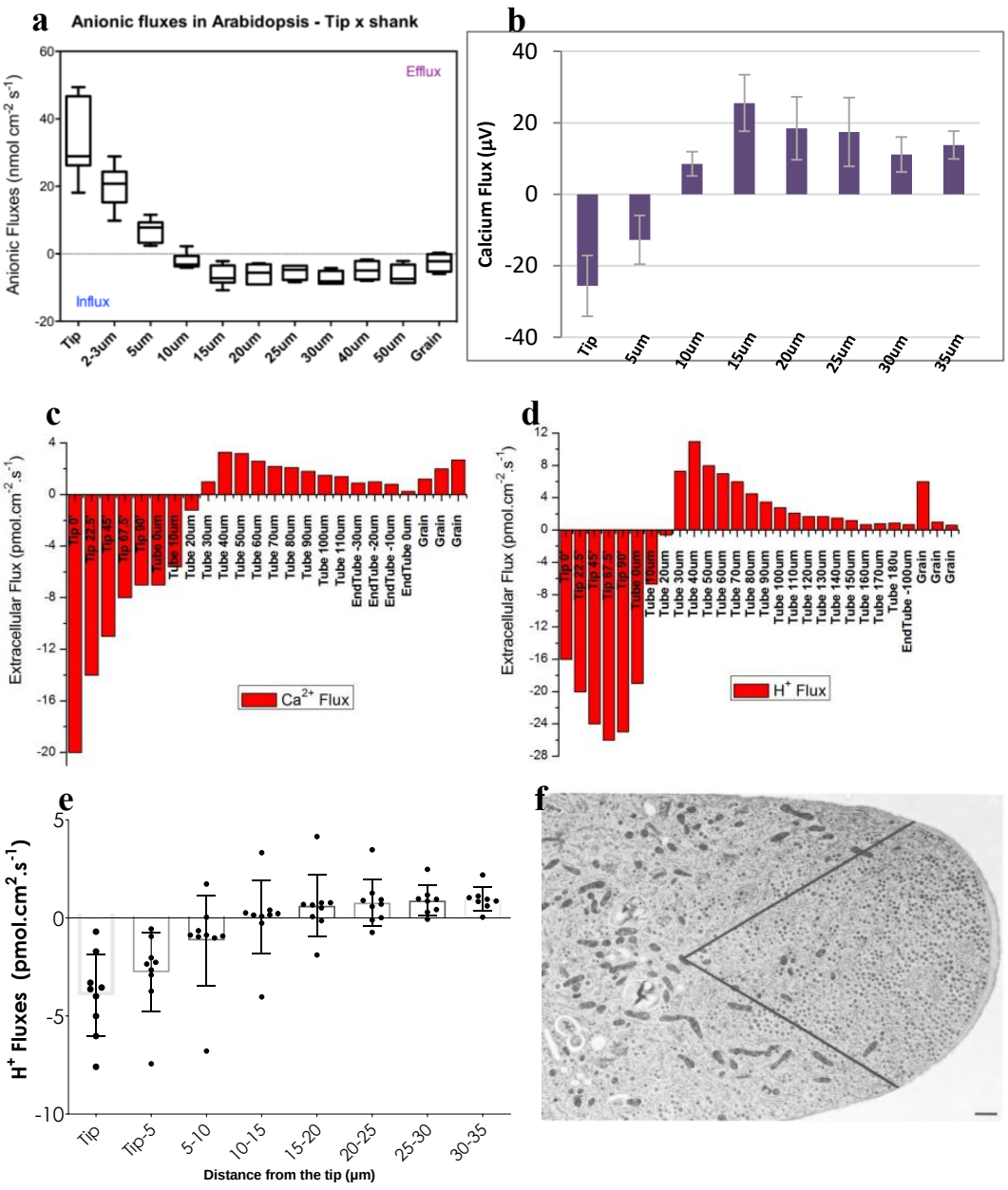

Fig.6 | Extracellular ion flux profiles in pollen tubes and the ion currents reversal points coincide with the clear zone. (a,b) Arabidopsis pollen tubes extracellular ion fluxes, anions (a) and Calcium (b) showing ion currents reversal points around 5-10µm away from the tip. **(c,d)** Tobacco pollen tubes extracellular ion fluxes, Calcium (c) and Protons (d) showing a reversal point farther away from the tip around 20-30µm from the tip. **(e)** Tomato pollen tubes extracellular H^+ fluxes showing ion currents reversal point at around 10-15µm away from the tip.(original result) **(f)** Electron micrograph of lily pollen tube showing an inverted cone of vesicles at the apex and the clear zone with smaller organelles (adapted from Lancelle & Hepler,1992), scale bar 1µm

and Ca^{2+} are leaving the cell and anions are going in, supporting the notion that this

region of the cell may be more negative (Lipchinsky, 2018; Michard et al., 2016).

The ion flux profiles along the PTs show that the higher fluxes at the tip decrease toward the shank and at a certain point, usually between 15-25µm from the tip, they reverse in the shank (fig.6 a,b,c,d,e). The ion reversal point is thought to be formed by the spatial segregation of ion channels/pumps along the membrane, potentially creating the anisotropic electrochemical potential as though the tip and the shank are contiguous compartments. The best example to date of this spatial segregation is the distribution of H^+-ATPases pumps (AHA), both in Tobacco and Arabidopsis PTs, that are evenly distributed in the shank and never progress to the tip area (Certal et al., 2008; Hoffmann et al., 2020). At a cytological level, the reversal point correlates with the clear zone, the high point of cyto-architectural polarization, in which the bigger organelles in the cell do not occupy the region of the tip. Although the cytoplasm in PTs is subjected to a reverse fountain streaming where cell components move toward the tip along the cortex, and stream backward through the lumen, there is a clear separation of organelles based on their size, and the clear zone consists mostly of small scecretory vesicles (fig.6 f) (Bove et al., 2008; Chebli, Kroeger, & Geitmann, 2013; Lancelle & Hepler, 1992; Alenka Lovy-Wheeler, Cárdenas, Kunkel, & Hepler, 2007). Spatial-Temporal Image Correlation Spectroscopy showed that in the apical region, these small vesicles exhibit irregular dynamics, quite different from the sustained vesicle movement in the shank which points to a vesicle transport mediated by diffusion and/or advection by the cytosol rather than motor proteins trafficking (Bove et al., 2008). Transmission electron micrographs show evidence that the level of vesicle compaction and fluidity at the tip

are higher than in the shank where the cytosol is subjected to streaming. Although there is no physical separation between the tip and the shank, there are levels of cellular organization that create significant differences in the cytosol organization and possibly medium resistivity (fig.6 f).

In this connection, it is hypothesized that the ion flux density and the cytosolic architecture can result in a longitudinal membrane potential gradient (MPG). This hypothesis has been proposed before and theoretical approaches have demonstrated that it is plausible (Lipchinsky, 2018; Michard et al., 2016). When taking into consideration the dominant anion fluxes at the pollen tube tip and assuming an average flux density of 1000 $pmol.cm^{-2}.s^{-1}$ (Zonia et al., 2002), the estimation of current density is about 100 $uA.cm^{-2}$, comparable with that of an action potential in muscle and neuronal cells (Gray, Mashburn, Sidorov, & Wikswo, 2013; Lipchinsky, 2018). Such current density traversing the pollen tube apex can result in a longitudinal gradient similar to that observed in nerve impulses, but in PTs would cause a standing membrane depolarization at the PT tip. An action potential depolarizes the membrane when Na^+ channels open letting Na^+ into the cell and while it propagates, the cell repolarizes using K^+ efflux to get to the resting state (Hille, 2001). While in action potentials, these successive events happen in time, in PTs the similar mechanism might happen in space, where the tip is subjected to depolarizing currents while the shank is subjected to hyperpolarizing/ repolarizing currents. The co-option of the same molecular machinery in terms of space or time have also been considered when comparing PTs with stomatal opening (Michard et al., 2016).

There have been multiple attempts at measuring membrane potential in the pollen tube shank by using intracellular microelectrode recordings, with measured values ranging from -55 to -130mV (*Zea mays* - Amien et al., 2010; *Agapanthus umbellatus* - Malhó, Read, Trewavas, & Pais, 1995; *Lilium longiflorum* - Messerli, Danuser, & Robinson, 1999; *Arabidopsis thaliana* - Mouline et al., 2002). Unfortunately, microelectrode recordings at the pollen tube apical region are not feasible because of the rapid expansion and friable nature of the nascent cell wall, provoking the tubes to burst due to the high turgor pressure (Michard et al., 2016). Nevertheless, preliminary evidence has been reported for membrane potential depolarization at the pollen tube tip by employing voltage sensitive dyes (M. A. Breygina, Matveeva, & Ermakov, 2009; M. A. Breygina, Smirnova, Matveeva, & Yermakov, 2009; M. Breygina, Smirnova, Matveeva, & Yermakov, 2010; Maksimov, Evmenyeva, Breygina, & Yermakov, 2018; Podolyan, Luneva, Klimenko, & Breygina, 2021). With the aid of $DiBAC_4(3)$ and Di-4-ANEPPS dyes, a steep longitudinal gradient of membrane potential was observed at a distance of 4 to 20µm with a potential difference of 20mV at the tip in tobacco PTs however, calibration and precision were not adequately addressed in this report. One of the main problems in this work is the use of the slow-response monovalent anionic dye $DiBAC_4(3)$ (Bis-(1,3-Dibutylbarbituric Acid)Trimethine Oxonol) that is a Nernstian fluorescence indicator (Emri, Balkay, Krasznai, Trón, & Márián, 1998). This dye concentrates in the cytoplasm in favor of the chemical gradient as any other anion meaning that, the more depolarized (more positive) the cell is, the more increasing in fluorescence in the cytoplasm. $DiBAC_4(3)$ was used on small tissues (Beane, Morokuma, Lemire, & Levin,

2013) or as a complimentary essay on electrophysiology studies in single cells (Bosch Calero, Selga, Brugada, Scornik, & Pérez, 2014; Yamada et al., 2001) but, if the goal is to study bioelectrical signal at a single-cell level, a diffusible cytosolic dye does not work because the cytosol balances out any electric potential differences. Moreover, the baseline for this calibration was done using fixed cells, which the authors claim to be equivalent to the completely depolarized cell, i.e. 0 mV (M. A. Breygina, Matveeva, et al., 2009). This might be conceptually correct but no research was done to assess whether the process of fixation does not cross react with the dye, creating errors in the baseline. In subsequent work, the authors used Di-4-ANEPPS, a lipophilic fast-dye, to assess membrane potential which has the advantage of being ratiometric. However, the absolute values of membrane potential calculated for Di-4-ANEPPS were calibrated using DiBAC simultaneously to extrapolate the absolute values, thus adding the error of fixing the cells to this calibration as well (M. A. Breygina, Smirnova, et al., 2009). Although somewhat quantitative, the data from these studies should be read as a qualitative work by relative comparison of fluorescence. The apical depolarization in tip-growing cells has been demonstrated convincingly with microelectrode impalement in hyphae of the fungus Neurosopora crassa (Potapova, Aslanidi, Belozerskaya, & Levina, 1988). Neurospora hyphae are divided into ‘compartments’ by incomplete septa, and the cytoplasm streams continuously toward the growing tips. In these studies, they have shown that the tip compartment is usually 10-30 mV more depolarized than the contiguous compartment. Although cytologically similar to PTs, the electric potential differences are measured between compartments at a longer distance of

approximately 100µm, likely attributed to the slower growth rates and consequently the ion current magnitude at the hypha tip.

Independent lines of evidence suggest that the circulating ion fluxes at the PT tip give rise to a longitudinal electric gradient but this was never properly demonstrated. Here, I explore this hypothesis using voltage sensitive fluorescent dyes (VSDs) and quantify the membrane potential gradient formed at the tip of the PT. One of the most important ions that is predictive of membrane potential is K^+, but intracellular concentrations and K^+ gradients are not characterized in pollen tubes. Using a genetically-encoded K^+ sensor, I investigate the K^+ cytosolic gradient and concentrations to be able to estimate the membrane potential in PTs.

2.2 Results

2.2.1 Testing and selecting voltage sensitive probes in pollen tubes

The cytosol of all living cells has a negative electrical potential in relation to the extracellular space. Because the cytosol is conductive due to ions and it is electrically isolated by the plasma membrane, the interior of a cell is typically equipotential and the negative electrical potential drops across the membrane. Such potentials are classically measured using an intracellular microelectrode impaled into the cytosol and compared against an extracellular bath electrode. Unfortunately, in PTs, this technique is highly invasive and does not allow to measure the pollen tube tip, because PTs end up bursting. For this reason, I worked with different fluorescent probes to investigate the membrane potential along the pollen tube: VSFP Butterfly 2.1,

BeRST, Thioflavin T, Annine-6plus and FluoVolt. Thioflavin T is a cationic dye, which gets incorporated by the cell in the cytosol following the electrochemical gradient, which showed impressive results in bacteria (Prindle et al., 2015). Although this was not our first choice because of its localization in the cytosol, we thought that it would be complimentary to the membrane dyes, but Thioflavin T was found to be photocytotoxic despite not being cytotoxic as the dose response curves show (fig.7 a,b,c). After some minutes of fluorescence imaging, Thioflavin T signal increases in the cytoplasm, pollen tubes stop growing and eventually burst, thus we discarded this dye. BeRST is a voltage sensitive dye that increases fluorescence with depolarization, but did not labeled the PT tip and stained non-specifically the cell wall rendering it useless for plant cells (fig.7 e,f,g) (Huang, Walker, & Miller, 2015). VSFP butterfly 2.1 is a genetically-encoded FRET probe, based on the voltage-sensitive domain of a phosphatase from *Ciona intestinalis* (Dimitrov et al., 2007). From the 12 transgenic Arabidopsis lines expressing VSFP2.1, we never found one with a good signal at the pollen tube plasma membrane, thus we decided to stop working with this sensor (fig.7 h,i).

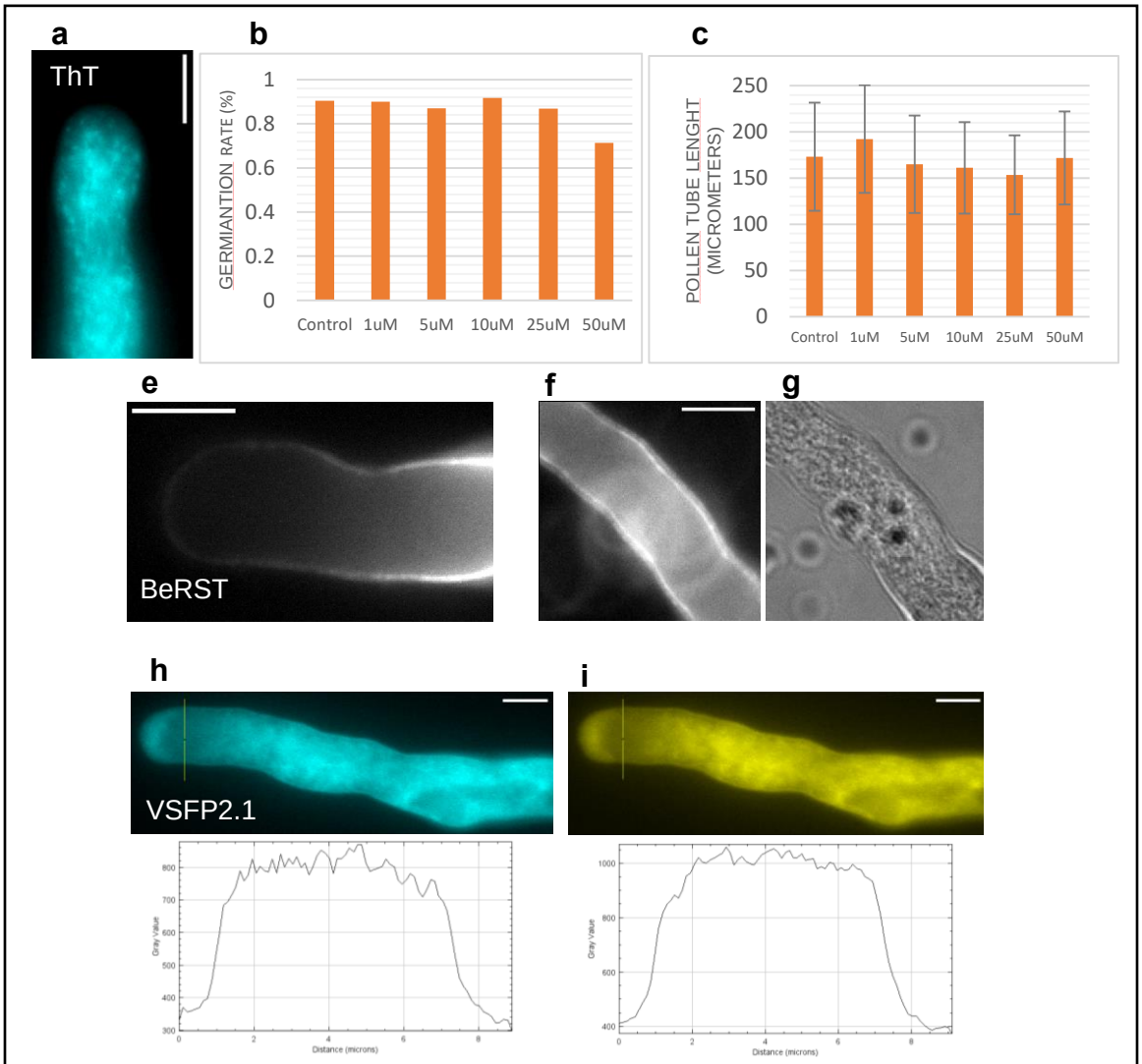

Fig.7 | Testing different voltage reporters in pollen tubes. (a) Thioflavin T cationic dye in pollen tubes gets compartmentalized in endomembrane compartments and mitochondria. ThT is not cytotoxic in normal conditions **(b,c),** not affecting germination rate **(b)** nor PT growth even at high concentrations, but the fluorescence imaging makes the dye photocytotoxic. **(e,f,g) BeRST** voltage sensitive dye that works by increasing fluorescence with depolarization. The PT tip does not get labelled properly and shows unspecific binding to the cell wall during plasmolysis **(f)** fluorescent imaging and **(g)** DIC image to show the plasmolysis. **(h,i)** VSFP2.1 genetically encoded sensor in the two difference channels CFP (h) and YFP (i) and the profiles of the respective cross section at the tip that do not show a high peak in fluorescence at the plasma membrane. This led us to conclude that VSFP2.1 does not get trafficked to the plasma membrane at high enough amounts for our research.

A voltage sensitive probe must be physically located inside the membrane in order to sense the electrical potential locally, or at least, within the Debye length of the membrane i.e., the length constant of the electrostatic field generated by charges close to the membrane surface that attenuates into the surrounding electrolyte (Kuhn & Roome, 2019). A molecular probe that randomly diffuses within the conducting cytosol (like ThioFlavin T) is not exposed to any significant potential changes, as any potential difference quickly shift charges until the cytosol is equipotential again. The voltage-sensitive dyes (VSD) used in this work, FluoVolt and Annine-6plus, were designed to be incorporated into the cell membrane by mimicking the phospholipid properties. At one end of the dye molecule there are hydrophobic membrane anchors and at the opposite end there is a charged hydrophylic group that aligns with the phospholipids negatively charged head group. In between is a hydrophobic chromophore consisting of aniline and anellated benzene rings that imbibe into the hydrophobic core of the membrane (Fig.8). FluoVolt and Annine-6plus work through Photo-induced Electron

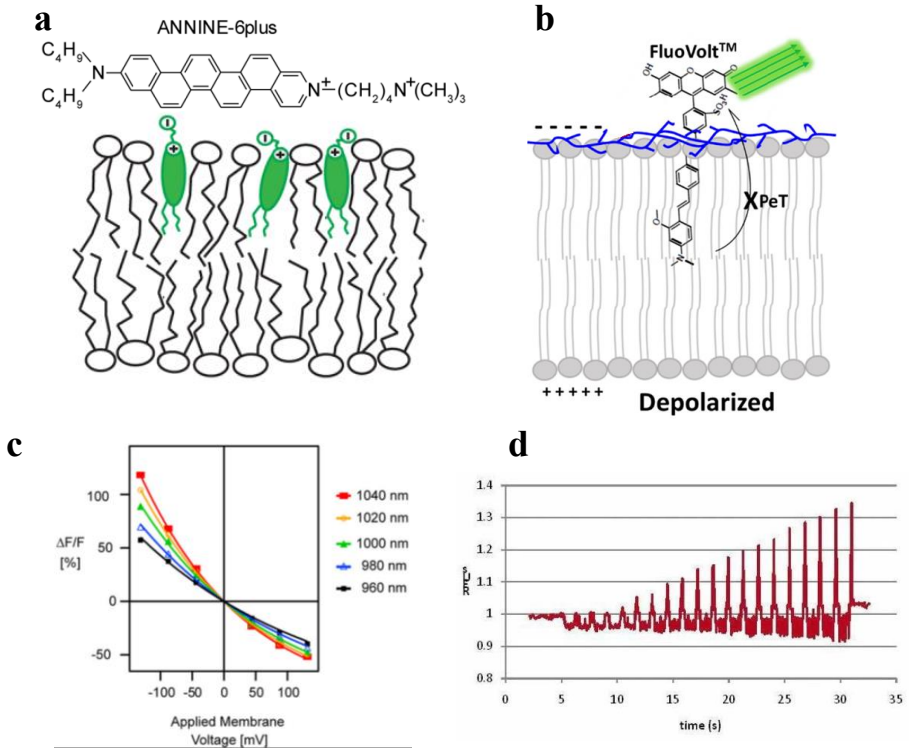

Fig.8 | Voltage sensitive dyes structure and membrane positioning. (a) Annine-6plus structure showing on the left side the membrane anchors that insert into the core of the membrane and the aniline and benzene groups that stabilize and make the structure rigid in hydrophobic environments (adapted from Kuhn & Rome 2019). **(b)** FluoVolt insertion into the membrane (disregard blue lines), showing a smaller membrane anchor and less benzene groups that being non-polar have more affinity to the hydrophobic core of the membrane. This dye requires a weak detergent in the staining protocol (adapted from Nag, et al 2020) **(c)** Annine-6plus traces at different imposed voltages in HEK cells imaged at 5 different wavelengths in two-photon microscopy. **(d)** Fluovolt traces show fluorogenic responses as cells are depolarized in single steps from -80 mV to 0 mV at 2 second intervals.

Transfer (PeT), a process whereby a fluorescent probe is enhanced or quenched by an electron-rich donor through a membrane spanning molecular wire. A change of membrane electric field alters the rate of electron transfer and, in turn, the intensity of the emitted fluorescence (Miller et al., 2012). We chose FluoVolt and Annine-6plus because they label the PT plasma membrane with a nice signal-to-noise ratio, little cytoplasmic signal, and were compatible with pollen tube's physiology as it is shown next.

2.2.2 Building a pipeline for plasma membrane fluorescence analysis

Analysis of membrane fluorescence is not an easy process because the few tools to contour an object including its the perimeter. These algorithms are usually made to select out some Region Of Interest (ROI) in an image rather than to measure the contour itself. To solve this problem, we came up with a protocol for membrane fluorescence analysis that would make it easier to trace the peaks of fluorescence in the membrane and that way make sure that we are measuring the plasma membrane. We developed a Macro in imageJ (Fiji) that creates transects along a selected rectangle drawn onto the picture, perpendicular to the pollen tube growth axis (fig. 9 a,b,c,d,e). The distance between transects can be defined at any length above one pixel, which means one can virtually screen the entirety of the plasma membrane. The distance chosen between transects in our analysis was 200µm. Each pixel of the transect is saved with one x,y coordinate and the respective fluorescent value.

The next part is the analysis in Jupyter using the protocol Membrane Identification at https://github.com/SantosJGND. This protocol runs two searches in parallel from the beginning and from the end of each transect and finds the first peaks in fluorescence (two sides of the pollen tube)(fig. 9f). Then, it takes the fluorescence value of the maxima, one value below (-1 pixel) and another above (+1 pixel) the peak itself and averages them to a final value of fluorescence. In our imaging protocols using the super-resolution mode of Zeiss LSM980, three pixels correspond to approximately 117nm of the membrane, corresponding to better than a tenth of the theoretical

resolution, and well above the Nyquist criteria in terms of resolution and device pixel resolution oversampling.

Membrane fluorescence are averaged from the 3 maxima pixel in each side of the membrane, then centered and plotted with a color code that indicates the fluorescence intensity (yellow to blue navy, high fluorescence to low fluorescence) (fig.9 g). This algorithm gives back a file that has the fluorescence in function of the

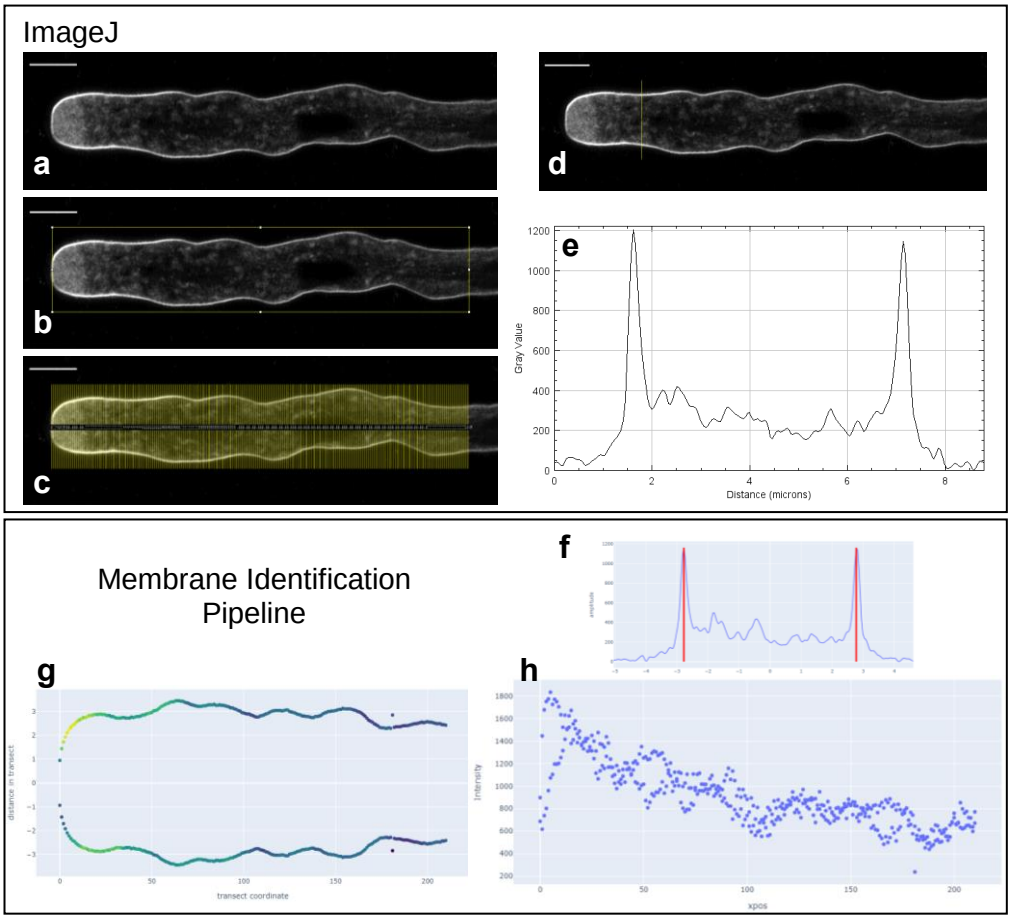

Fig. 9 | Methods for detecting plasma membrane fluorescence. (a) Image for analysis, (b) rectangle to select ROI to where transects (c) are drawn at a distance of 0.2µm, (d) each transect can be quickly visualized at a glance in imageJ (e). Using the Membrane identification algorithm in Jupyter notebook, all the transects from multiple PTs can be analyised at a time and there are 3 different steps: (f) finding the peaks in each transect, marked by red line, (g) ploting the peaks and the corresponding fluorescence intensity (average between the 3 maxima pixels) represented by a color-code (the brighter the more fluorescence intensity) and finally (h) all the points plotted of fluorescence in function of distance from the tip. Here represented only the two sides of the PT

distance from the tip in µm that can be exported to any other software. Each pollen tube has two traces associated with it, one from each side of the membrane (fig.9 h).

This pipeline made this measurements much more efficient, it allowed to increase transect sampling rate and analysis in batch. It is also a great tool for a quick visualization of the data set in the different kinds of plot at the transect or whole cell level.

2.2.3 Assessing FluoVolt and Annine-6plus dyes reliability and labeling efficacy in pollen tubes

The voltage sensitive dyes (VSDs) utilized in this work have opposite fluorescence kinetics: FluoVolt reports depolarization by increasing fluorescence when membrane potential increases (fig.8 a, c), whereas Annine-6plus reports hyperpolarization by increasing fluorescence when membrane potential decreases making them complimentary (fig.8 b,d)

FluoVolt is reported to have a fast response and 25% fluorescence change quantified by ΔF/F per 100 mV. The few studies using FluoVolt published to date focus mainly on induced Pluripotent Stem Cells-derived cardiomyocyte monolayers (Bedut et al., 2016; McPheeters, Wang, Werdich, Jenkins, & Laurita, 2017) and neuronal cell cultures (Pakhomov, Semenov, Casciola, & Xiao, 2017). These studies have reported a ΔF/F of 12-20% per 100mV in cardiomyocyte monolayers and 7% per 100mV in neuronal cell cultures. The downside of FluoVolt staining is the necessity for a weak detergent to help membrane incorporation, as older versions of VSDs, namely RH-421, di-4-ANEPBS, Annine-5, and Annine-6 that required either pluronic acid or sodium cholate. The addition of detergents in the staining protocols affects the viability of cells

and most of the times membrane integrity and fluidity (Kuhn & Fromherz, 2003). In the other hand, Annine-6plus is water soluble and does not require any other specific solvents to load the dye into the membranes and shows a fractional fluorescence intensity change of 30% ΔF/F per 100mV (Fromherz, Hübener, Kuhn, & Hinner, 2008). For this reason, Annine-6plus is used throughout the whole pollen tubes incubation period while FluoVolt is added only 30min before imaging, to reduce PTs exposure to detergents (methods section for more details).

To test different staining protocols and whether these dyes can label the plasma membrane effectively, I used pollen tubes from Arabidopsis (fig. 10 a,d), Tomato (fig.10 b,e) and Tobacco (fig.10 c,f). The germination media for the 3 species differs in its constituents and osmolality and the PTs are different in size and growth rates, which allows to test the labeling of the dyes in media with different ionic strengths and its incorporation in cells with different growth rates. To make the sampling more homogenous, all the pictures were acquired when PTs were growing more than $1\mu m.min^{-1}$ because when PTs stop, the tip-focused gradients and their ion dynamics choreographies decrease in magnitude and consequently the electrochemical gradients are expected to be dissipated.

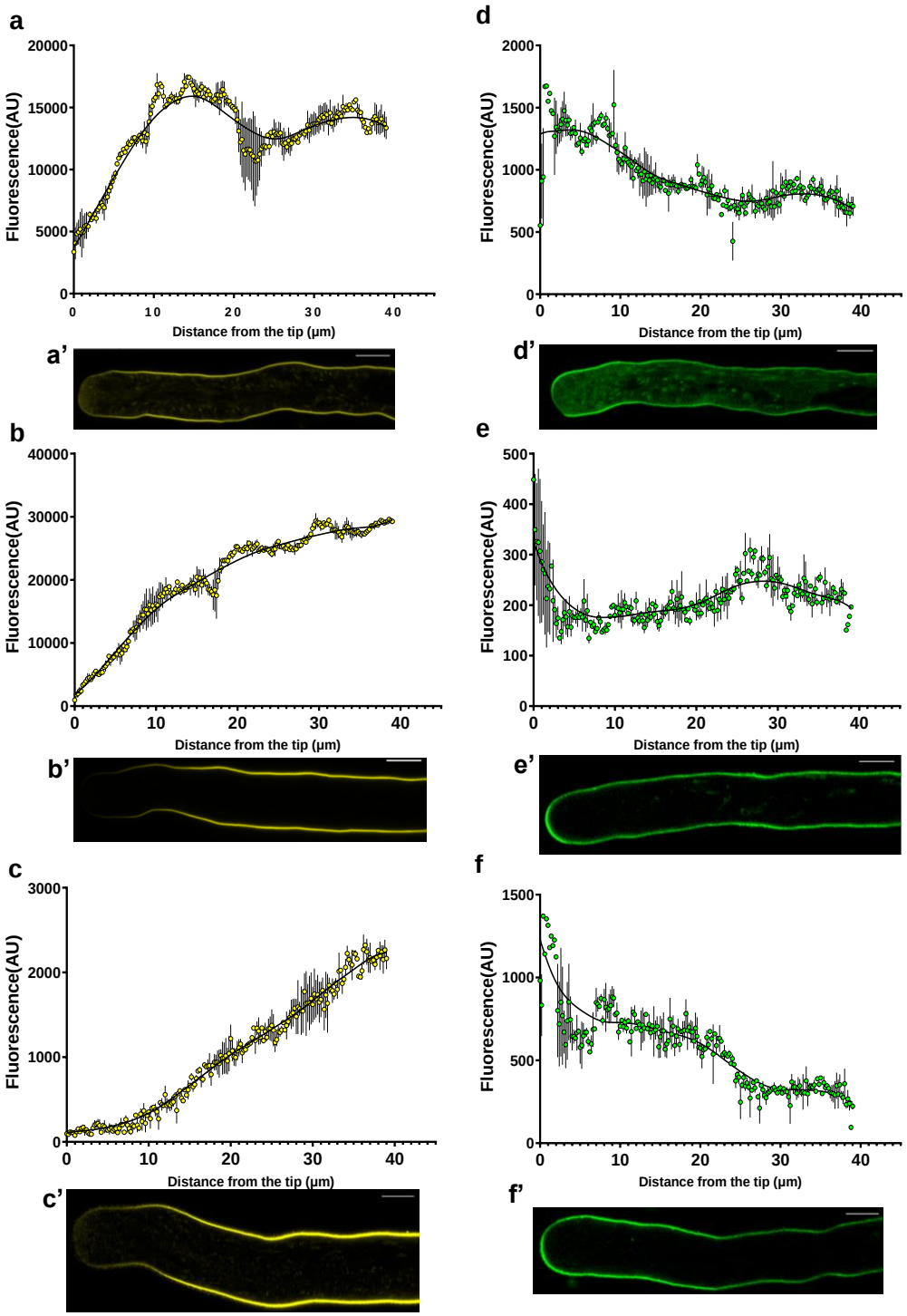

Fig. 10 | Pollen tubes from three species labeled with VSDs show a membrane potential gradient (MPG). Representative images of Arabidopsis **(a',d')**, Tomato **(b',e')**, and Tobacco **(c',f')** labeled with Annine-6plus **(a',b',c', yellow)** and FluoVolt **(d',e',f', green)**. Fluorescence intensity plots **(a,b,c,d,e,f)** from the representative pictures. Each side of the membrane is analyzed, and ploted together, each dot represents the average of the two values in each side of the membrane at the same position. All the species show a MPG that spans from the tip. The shortest gradient is from Arabidopsis and the longer is Tobacco. Sampling rate of 0.2um. Scale bar = 5um

All three species show a similar membrane pattern accordingly with each VSD kinetics: Annine-6plus labeled PTs have low fluorescence intensity in the tip and increases to the shank (fig.10 a,b,c) whereas FluoVolt shows high fluorescence intensity at the tip and decreases along the shank (fig. 10 d,e,f). A membrane potential gradient (MPG) spans the tip region from more depolarized potentials to the more hyperpolarized potentials at the shank. It is worth noting that the size of the gradient varies for all the species but it also varies within species as I elaborate further below. Between the 3 species, the most striking MPG is from the tobacco, because it is much longer than the other species, up to 30-40µm away from the apex but the observed inversion points of the H^+ and Ca^{2+} fluxes match this distance (fig.1 c,d).

VSDs are typically tested in neurons or cells without wall which raises questions on the labelling effectiveness of these dyes in plant cells. To test whether these dyes have nonspecific affinities to the cell wall, Annine-6plus and FluoVolt labelled pollen tubes were subjected to plasmolysis with sucrose, to allow for a physical separation of the plasma membrane from the cell wall. Upon plasmolysis, PT's tip retracts from the cell leaving a hollow part of the tube behind (fig.11 b,c,d). Another approach was to look at callose plugs (fig.11 a), the floodgates of pollen tubes that confine the cytosol to the foremost growing region. In callose plugs, the plasma membrane is separated leaving a space without membrane, where we can distinguish membrane and cell wall clearly. Plasma membrane shows a good labeling with these dyes and despite some dotted structures in the cell wall when increasing contrast (fig. 11 a,b, white arrows), these do not over impose with the plasma membrane fluorescence. When compared with other studies using the lipophilic FM dyes in cells

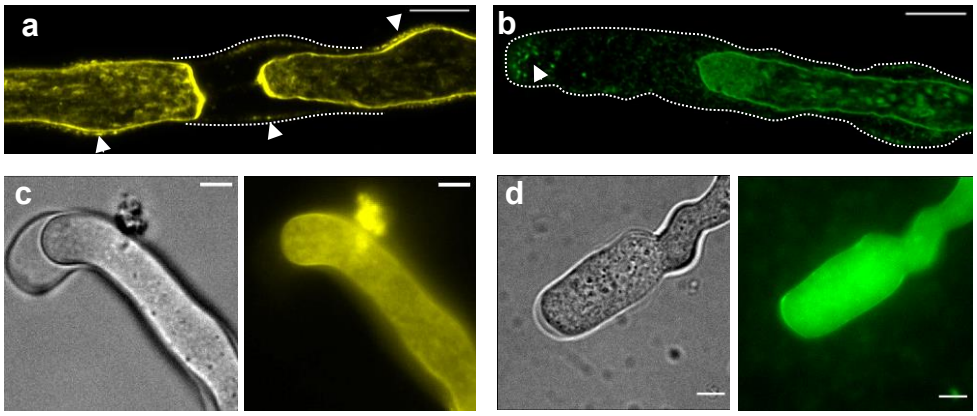

Fig. 11 | VSDs do not show unspecific stainig of cell wall. Arabidopsis (a,b) and tobacco (c,d) PTs under plasmolysis, labeled with Annine-6plus (a,c) and FluoVolt (b,d). (a) Callose plug showing a good staining of PM and some residual fluorescence of in the cell wall (white arrows). The signal intensity from the cell wall is much lower than the membrane and does not overimpose PM fluorescence. (b) PT tip collapsed inside the tube (dotted line) and some low fluorescence dots can be seen in the cell wall tip. (c) PT tip collapsed (d) PT slightly collapsed not showing any fluorescence signal in the wall. Dotted structures associated with hechtian. Scale bar = 5um

under plasmolysis, these dotted structures throughout the wall are similar to residual plasma membrane from Hechtian Strands that break apart when the plasmolysis negative pressure is too strong (Yoneda, Ohtani, Katagiri, Hosokawa, & Demura, 2020). Given that the signal from these structures in the cell wall are much lower in intensity than the plasma membrane labelling and do not over impose the PM signal, these structures do not influence the PM image analysis.

2.2.4 Membrane potential gradient variation is implicated in pollen tubes growth rate

PTs growth rate is oscillatory, changing from fast to slow regimes that are usually accompanied by changes in the ion dynamics and, consequently, in the intracellular ion concentrations and gradients (Damineli et al., 2017). As a consequence

of the ion oscillations, the electrochemical potential of the cell changes too, which can impact the MPG in the PT tip.

In FluoVolt labeled PTs, it is clear that there were two different populations based on the fluorescent signal profiles thus, I divided them in two categories based on the size of the MPG and the shape that features low fluorescence at the tip:

.Long MPG, shallow slope, in which the first 5um from the tip show low fluorescence but then it increases and the MPG extend up to 25-30um (fig.12 e)

.Short MPG, steep slope, in which the first 10um from the tip have high fluorescence that quickly decreases to low fluorescence (fig.12 f)

These two populations were also seen in tobacco and tomato pollen tube samples.

The two different populations not only show a difference in the MPG at the tip, but the overall fluorescence of the shank varies too, reaching low levels in the short MPG population (fig. 12 d). That would imply that shorter MPG are correlated with more hyperpolarized PTs and vice-versa.

Annine-labelled PTs show some variation on the steepness of the gradient too (fig.12 a), but it is difficult to divide them in two categories because there is no clear cut feature like the unlabeled tip in the samples with FluoVolt. Moreover, the fluorescence intensity of the shank does not seem to change considerably between the two states so I chose two representative PTs featuring a long (fig.12 c) and short (fig.12 b) MPG.

The existence of such variance in MPG sizes seems to imply that PTs can change from one to another depending on their ion dynamics, thus we investigated whether MPG size is correlated with growth rate. In a time-lapse series using FluoVolt

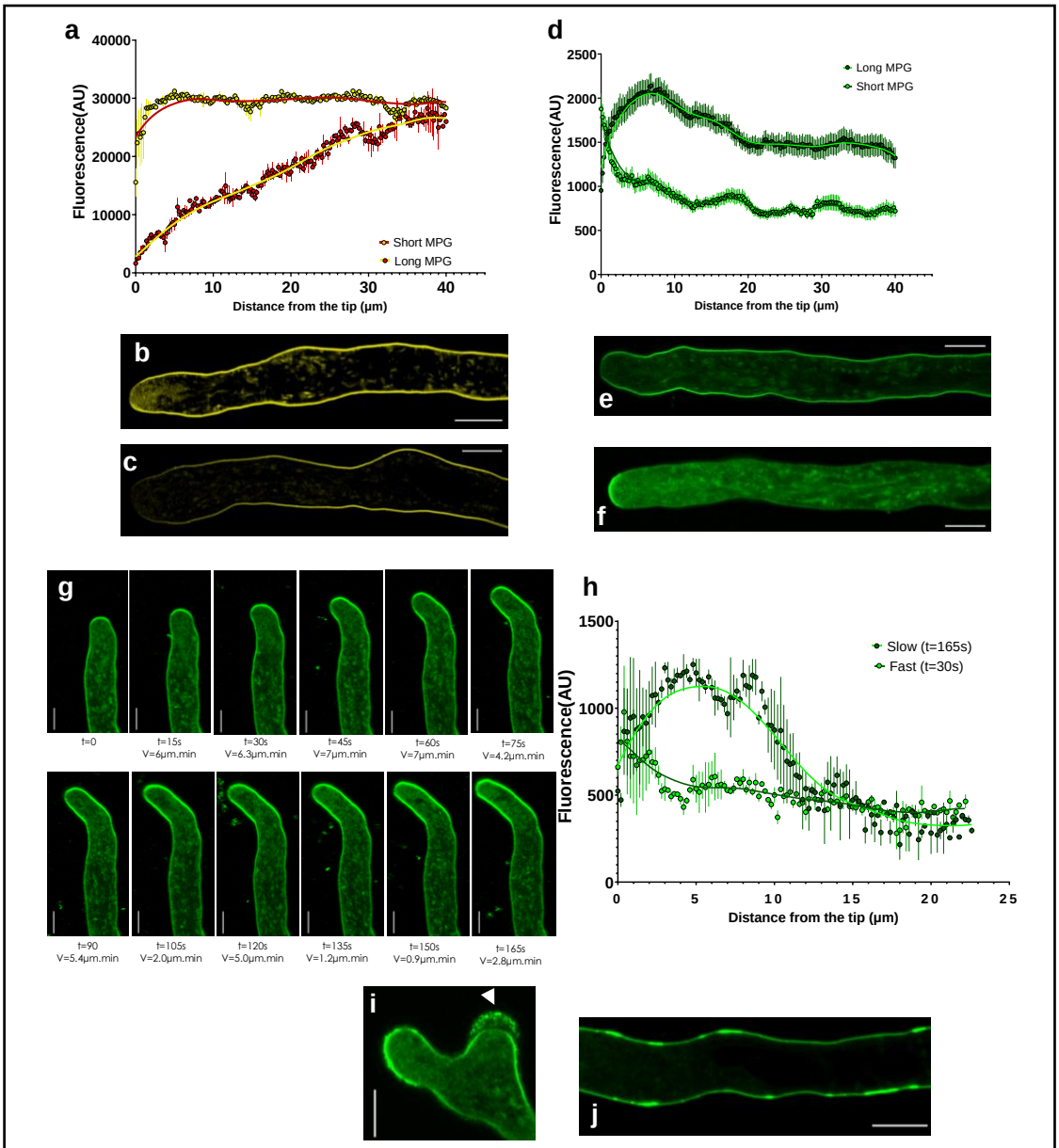

Fig.12 | Membrane potential gradient variation in Arabidopsis. (a) two representative traces of short (b) and long (c) MPG in annine-6plus labeled pollen tubes. (d) population analysis of short (n=14) and long (n=16) MPG and representative PTs (e) long, (f) short. (g) Time-lapse series showing transition from short to long MPG and associated instant growth rates. (h) FluoVolt fluorescence profiles of two points in (g), representative of the two types of MPG. (i) FluoVolt branched PT showing the stopped branched due to cell wall deposition (white arrow) and other growing tip. Arrested branch is unlabeled at the apex of the tip whereas the growing tip is well labeled with the dye. (j) evidence for solvatochromism when given a high osmotic shock with KCl (250mM). Scale bars = 5um

(fig.12 g), the MPG is seen changing from the short to the long form and the growth rate analysis reveals that the short form is related to a faster growth whereas the long

form to a slower growth rate. In a more detailed analysis of the time-lapse sequence showing the fastest (t=30s) and the slowest (t=165s) growth rates, we can see how the fluorescence profiles (fig.12 h) are similar to the population analysis (fig.12 d). One possible reason that can contribute to the unlabeled feature at the tip of slower PTs is the fact that even when PTs slowdown, the rates of endo- and exocytosis may not change in a relevant way. This means that slow growth would imply more endocytosis to compensate the lack of membrane that is not contributing to growth, and in the process, the dye would be parted from the tip through vesicles. Another evidence for this phenomenon comes from the observation of a PT that branched in two tips (fig.12 i), where one of them not growing developed a thick cell wall deposit and low membrane fluorescence (similar to the long MPG example), while the other active growing tip shows high fluorescence at the tip as in the short MPG. Other examples of low fluorescence at the tip include mutants with slow growth rates and will be described in the next chapter. Moreover, the characteristics of FluoVolt could also explain these variations because while Annine-6plus is water soluble, FluoVolt is solubilized in DMSO and relies on a weak detergent to get into the membrane, which by itself is evidence that diffusion alone is not enough for membrane incorporation. The protocols for FluoVolt also require longer incubation periods, between 15-30min, whereas Annine-6plus only requires 5 min which is a good approximation for the incorporation rate of the dyes.

Another possible explanation for differences in labeling at the tip is solvatochromism i.e., the phenomenon of changes in the excitation and emission spectra caused by the local solvent shell of the dye. The local solvent pertains to the

solutes concentration in the extracellular or intracellular environment and/or the lipid composition, which impacts the plasma membrane-water interface and consequently the position of the dye relative to the membrane that relies on hydrophilic and hydrophobic interactions (Fromherz, 1995; Kuhn & Fromherz, 2003; Lambacher & Fromherz, 2001). A change in the positioning of the dye relative to the membrane, being closer to the hydrophobic core or more at the PM surface, influences the quantum yield. In fact there is evidence that high extracellular KCl concentrations (250mM) have a detrimental effect on homogenous fluovolt labelling (Fig.12 j). The dye changes its distribution to *puncta* along the membrane that are an artifact of a high ionic strength in the medium. Another piece of evidence that FluoVolt might be more affected to external compounds is the fact that the staining protocol for tomato PTs requires two times more dye than Arabidopsis and Tobacco, and I suspect that the difficulty in membrane binding comes from the PEG (24%) used in the media, which by being slightly negatively charged can change the dye conformation in the membrane. Although solvatochromism could explain the problems in labelling with FluoVolt the same does not hold true for annine-6plus because extended studies have shown evidence that this dye is not affected significantly by this phenomenon due to its rigid structure when imbibed in the membrane (Fromherz et al., 2008; Kuhn & Roome, 2019).

Overall, the results obtained with FluoVolt indicate that the first 5um at the tip might have labeling problems and should be taken prudently. If the low fluorescence in the FluoVolt unlabeled tip PTs was truly reporting membrane potential, we should see PTs showing the same pattern with Annine-6plus but with higher fluorescence, and

no such gradient shape was ever recorded. So far, our data is not sufficient to assert that growth rate and MPG size correlate perfectly due to the difficulty in capturing the exact moment when the growth rate changes during time-lapses.

The existence of different MPG sizes is indicative that the MPG might be as dynamic as the ion oscillations and growth rates observed in PTs. The correlation of PTs growth rate with MPG size is an important feature to understand the mechanism by which the MPG affects apical growth, or vice-versa.

2.2.5 Annine-6plus responsiveness to depolarization

VSDs response to changes in the membrane potential differs depending on cell type and tissues (Kuhn & Roome, 2019; Salerno, Garten, Smith, Stølen, & Kelly, 2020) due to the characteristics of membranes and the surrounding solvents. To test whether Annine-6plus responded to depolarization in pollen tubes, I ran a ionophore-driven depolarization protocol (Feijó, Sainhas, Hackett, Kunkel, & Hepler, 1999a) that employs a mix of ionophores composed by valinomycin (K^+), nigericin (H^+/K^+ antiporter) and extracellular [K^+] up to 150mM to dissipate the electrochemical

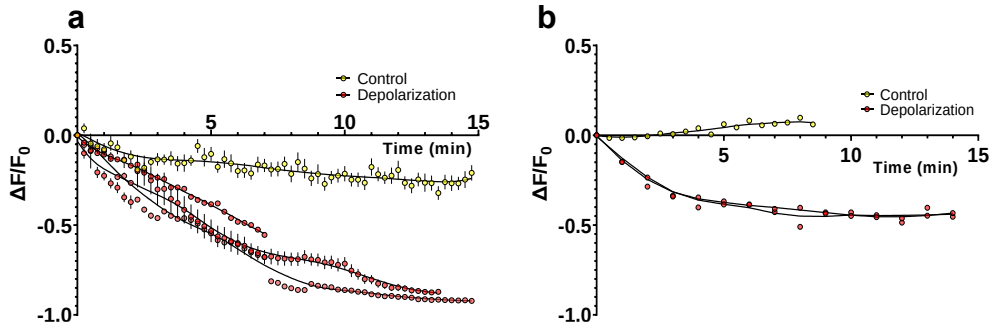

Fig.13 | Annine-6plus response to depolarization protocols. Analysis of Fluorescence change in segments of PTs shank after the Depolarization cocktail is added in the medium: Valinomycin (30uM) Nigericin(25uM) Niflumic acid (10uM), and 150mM KCl. (a) Sampling rate every 15s (b) sampling rate very 30s (control) or 60s (treatment). Each trace corresponds to one cell

gradient of K^+. As an addition to the published protocol, I decided to use the Cl^- channel blocker, Niflumic acid, because it is well known that Anionic currents have the highest magnitude in PTs and it is likely that these could partly counteract the effects of the ionophores.

When the ionophore mix is added to the medium, fluorescence starts to decrease and eventually plateus at a very low fluorescence (depolarization) (fig 13 a,b). This was the prediction since the ionophore mix dissipates the electrochemical gradient of K^+, H^+ and the Cl^- fluxes get decreased. The two graphs show different sampling rates (15s or 30s/60s) during time-lapses because it was observed some photobleaching in the col-0 sample (fig.13 a). The analysis using $\Delta F/F0$ shows some variation of how much depolarization occurs between the PTs, which can happen depending on the initial state of membrane potential.

Although the ionophores action is usually reproducible, in some rare cases pollen tubes can compensate for this changes, and still show the reverse fountain streaming that can be seen in growing PTs and counteract the depolarization tendency. Depolarization protocols cause a multitude of undesirable responses in PTs, from bursting, to detachment from the coverslip or complete collapse of the tube when it plasmolyses, which make these experiments time-consuming and extremely challenging. The bursting of PTs in the vicinity of the field of view create movement in the media and often the PTs get carried away, as was the case in one of the samples that I stop recording at approx. 7min (Fig.13 a).

2.2.6 Investigating Cytosolic K+ gradient and intracellular concentrations

Potassium (K^+), the most abundant intracellular cation, is an essential macronutrient for plant growth and development. Potassium is involved in many physiological processes, such as osmo- regulation, enzyme activation, electrical neutralization, and membrane potential maintenance (Y. Wang & Wu, 2017). Despite its abundance in every cell type and importance in so many physiological processes, K^+ has been difficult to study by live-cell imaging due to the unavailability of specific probes until recently. As soon as the newly Genetically-Encoded Potassium Ion Indicator (GEPII) (Bischof et al., 2017) became available, we transformed it into Arabidopsis driven by a pollen specific promoter LAT52 to study K^+ ion dynamics in PTs and to investigate whether intracellular [K^+] could partly explain the existence of a MPG.

Growing PTs expressing GEPII were imaged while growing (fig.14 a) and then analyzed using one transect drawn across the center of the PT in the ratiometric image (methods). The tip-focused K^+ gradient spanning from the tip is inverted (fig.14 b), showing lower K^+ concentration at the tip and increasing to the shank. The inverted K^+ gradient seen with GEPII implies an outward K^+ current and the PT tip, previously confirmed for tobacco and lily PTs with extracellular flux measurements (Dias, P. unpublished). The K^+ gradient is quite consistent between PTs (fig.14 b), and spans the first 40µm from the tip, revealing the longest cation gradient described in Arabidopsis PTs.

In order to quantify the K^+ concentration, GEPII was calibrated in PTs, using known concentrations of KCl in the extracellular media and permeating the membrane

to K^+ using the K^+-specific ionophore valinomycin. To assess the concentration of valinomycin necessary to equilibrate the extracellular and intracelllar [K^+], I ran time-lapse essays following the PTs fluorescence upon using different Valinomycin concentrations (fig.14 c). Between 50-10µM of valinomycin, the Fluorescence ratio decreases quickly reaching approximately the same values of ΔF/F0, while the control with DMSO (valinomycin + solvent) decreases only slightly due to photobleaching. At 5um valinomycin, PTs do not equilibrate with the medium and PTs can still grow for some time, having no significant differences in fluorescence ratio. This is important because 5uM valinomycin can increase K^+ conductance without affecting the intracellular K^+ concentrations, which is a useful tool that is used later on. When using 50µm valinomycin, many tubes lost integrity, either collapsing or plasmolysing slightly, so I decided to use 30µM to run this calibration essays.

The extracellular [KCl] used in the calibration protocol were the following: 0.5, 2.5, 5, 25, 50, 100, 150, 250, 400 mM. An equation for one-site total binding was deployed to fit the data showing a R^2=0.95:

$$y = \frac{Bmax \cdot x}{(Kd + x)} + Ns \cdot x + Bckg$$

Where:

Bmax is the maximum specific binding in the same units as Y.

Kd is the equilibrium dissociation constant, in the same units as X. It is the K^+ concentration needed to achieve a half-maximum binding at equilibrium.

NS is the slope of nonspecific binding in Y units divided by X units. **Background** (Bckg) is the amount of nonspecific binding with no added K^+.

$$y = \frac{0.7434x}{(3.313 + x)} + 0.001x + 0.4656$$

From this equation (fig.14 d) and the values of the gradient (fig.14 b) we can calculate that the amount of K+ in the tip is ≈250mM and increases to a concentration of ≈425mM. If we assume that K^+ alone would define the values for membrane potential, we could use the Nernst equation to estimate the variation that spans the MPG.

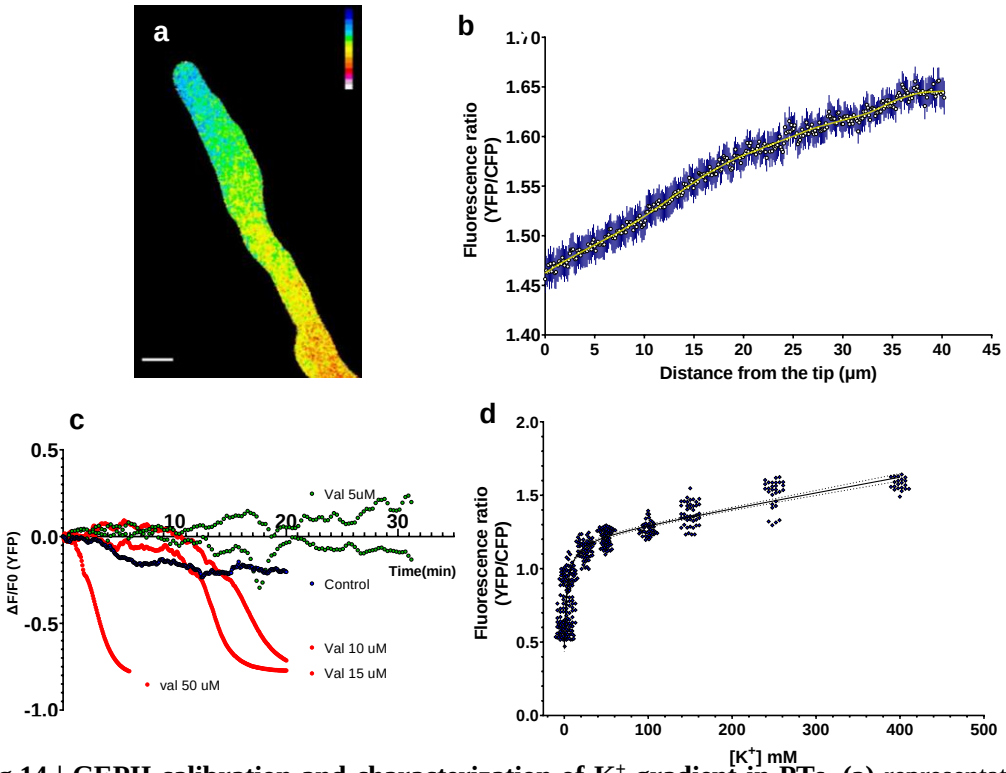

Fig.14 | GEPII calibration and characterization of K^+ gradient in PTs. (a) representative ratiometric image of the inverse K+ gradient in Arabidopsis pollen tube. Scale bar=5um, calibration bar: blue- low [K^+] white – high [K^+]. (b) Average K+ gradient in PTs (n=25). (c) Testing valinomycin concentrations that permeabilize PTs to K+. In red valinomycin concentration that dissipate K^+ electrochemical gradient, shown by the decrease of the Fluorescence ratio do low levels. In blue control shows some photobleaching. In Green, valinomycin concentration that increases K^+ conductance but does not dissipate K+ electrochemical gradient. (d) Calibration curve from the points 0.5, 2.5, 5, 25, 50, 100, 150, 250, 400 mM, with a nonlinear fit equation for one-site total binding of GEPII.

$$V_{Eq.} = \frac{RT}{zF}\ ln\left(\frac{[K^+]out}{[K^+]in}\right)$$

Where:

$V_{Eq.}$ is the equilibrium potential (Nernst potential) for K^+

R is the universal gas constant and is equal to 8.314 $J.K^{-1}.mol^{-1}$ (Joules per Kelvin per mole).

T is the temperature in Kelvin ($K = 23C^o + 273.15$)

z is the valence of the ionic species. ($K^+=1$)

F is the Faraday's constant and is equal to 96485 $C.mol^{-1}$ (Coulombs per mole).

$[K^+]_{out}$ is the concentration of K^+ in the media, 0.5mM

$[K^+]_{in}$ is the concentration of K^+ in the cytosol, 250mM at the tip, 425mM at the shank

The estimated values of membrane potential given the K^+ gradient in PTs are V_{tip}= -158.6 mV and $V_{shank(40um)}$= -172.1 mV, a difference of 13,5 mV. These values are a rough estimation, assuming that the membrane potential in pollen tubes follows the equilibrium potential for K^+, but we do know that in PTs, anionic currents can be up to 3 orders of magnitude higher than the cation currents. If these anion outward currents from the tip are taken into consideration, the tip would be even more depolarized for lack of negative charges, which would imply an underestimation on our account from the actual values.

The use of GEPII allowed us to see for the first time an inverted K^+ gradient spanning the first 40µm from the tip. Unfortunately, cytosolic $[K^+]$ are so high that the probe is working at the limit of its dynamic range, and as consequence, did not allow for a more comprehensive study about the ion dynamics and oscillation of this gradient. In the case of Ca^{2+} and H^+, the gradients oscillate and there are bursts of ions coming into the cytosol, while with GEPII, we cannot see significant changes in ion

concentration during PTs growth. This could mean one of two things, either the [K^+] at the tip do not change within the dynamic range of the probe, or the gradient is continuously created through a process without bursts of big effluxes of K^+. The latter possibility, although completely different from the other cations studied so far, is not farfetched due to the long gradient formed up to 40µm away from the tip, which would be more easily explained by a steady-state like K^+ efflux rather than an oscillatory efflux with bursts and periods of dynamic equilibrium.

2.2.7 Calibration of voltage-sensitive dyes and quantification of Membrane potential gradient

One of the challenges of quantifying membrane potential in PTs when using VSDs was the problem of not having a reference point to convert fluorescence into voltage. The previous studies using VSDs in PTs used relative comparison of WT with different treatments (M. A. Breygina, Matveeva, et al., 2009; M. A. Breygina, Matveyeva, Andreyuk, & Yermakov, 2012; M. A. Breygina, Smirnova, et al., 2009; Maksimov et al., 2018) and calculated estimates of membrane potential based on the fractional fluorescence intensity change of the VSDs that was previously published. However, it is known that the VSDs respond differently depending on the tissues and extracellular media (Bedut et al., 2016; McPheeters et al., 2017; Pakhomov et al., 2017). Another approach used double-barrel voltage-clamp to deliver hyper- and depolarizing pulses while having a read out of the fluorescence, but these classical methods of electrophysiology are invasive, creating artifacts on the longitudinal

distribution of the dye through the PM, and disrupt the normal development and growth of PTs (Gutermuth et al., 2018)

The most preferred calibration method for ion probes usually uses ionophores to make the cells permeable for a specific ion, then changes the extracellular concentrations for that specific ion so that the interior of the cell balances out with the extracellular concentrations, similar to what it was described for GEPII. However, resting membrane potential is the result of the compounded contribution of each ion in a cell, which can be described by the simplest and most widely used Goldman–Hodgkin–Katz equation (Hille, 2001):

$$V_{Eq.} = \frac{RT}{F}\ ln\left(\frac{P_K[K^+]o + P_{Na}[K^+]o + P_{Cl}[Cl^-]i}{P_K[K^+]i + P_{Na}[K^+]i + P_{Cl}[Cl^-]o}\right)$$

Where:

$V_{Eq.}$ is the equilibrium potential (Nernst potential) for K+.

R is the universal gas constant and is equal to 8.314 J.K-1.mol-1 (Joules per Kelvin per mole).

T is the temperature in Kelvin (K = 23C^o + 273.15).

F is the Faraday's constant and is equal to 96485 C.mol-1 (Coulombs per mole).

P is the ionic permeability

$[Ion]_{out}$ is the concentration of monovalent Ions in the extracellular media

$[Ion]_{in}$ is the concentration of monovalent Ions in the cytosol

This equation is usually simplified to the Nernst equation, because the permeability/ conductance for K^+ is so much higher than for the other ions, that the

values of a simplified equation are usually a very close approximation of the resting membrane potential. This approach for the VSDs calibration can be used because the K^+ concentration inside PTs is already known and the germination medium too. Moreover, the tests ran before using different valinomycin concentrations show how to make PTs permeable to K^+, while being kept alive (fig.14 c, green traces). Here, I used 5µM valinomycin because PTs are viable for at least 30 minutes without changing intracellular K^+ concentration (fig. 14c) and have high permeability for K^+, which is a condition that should be met to use the Nernst equation. The extracellular K^+ concentrations used for the calibration were 0.1, 1, 10, and 100mM , corresponding to -206.61998, -155.37, -96.81, -38 mV, respectively.

Annine-6plus calibration shows a negative correlation between membrane potential and fluorescence (fig15 a), while FluoVolt shows a positive correlation (fig.15 a,b) as it is expected from the respective VSDs properties. Annine-6plus samples is clearly more variable than FluoVolt, especially in intermediate points of membrane potential nevertheless, these results show that the VSDs respond in the range of membrane potential that was tested, and the linear regressions have a good fit (Annine-6plus R^2=0.72, FluoVolt R^2=0.86, fig.15 a,b). Using the linear regression equations, we can convert fluorescence values into millivolts and compare the results of each VSD side by side. When comparing both VSDs membrane potential profiles in WT PTs, there is a discrepancy between the two, especially at the MPG level (fig.15 c). Annine-6plus has a very steep gradient and the first values of the tip are -50 mV whereas FluoVolt shows values around -160 mV. However, it should be noted that the Fluovolt profiles shown here consist in a pool of both Short and Long MPG populations

(fig.12d), which skews the results to a lower membrane potential at the tip due to the unlabeled tip problem. Even though, annine-6plus does not seem to have this problem with labeling, endo- and exocytosis might still decrease the dye concentration from the tip. Thus, it was decided that the first 5µm from the tip should be excluded when comparing samples because this is the area that shows a decreased fluorescence in the FluoVolt long MPG population (fig.12 d). I define the tip zone between 5-10um and the shank between 25-40um. The average membrane potential at the tip in Annine-6plus labeled PTs is at -104.8 mV and the shank at -145.7 mV, while in FluoVolt samples, the tip is at -164.0 mV and the shank at -190.4 mV. The VSDs seem to be roughly 50mV apart from each other but despite these differences, the MPG (shank-tip) in the two species is roughly the same, in Annine-6plus is -40.9mV and with FluoVolt is -26.4mV.

I believe that the difference between VSDs comes from the calibration protocols where we assume that the valinomycin effect is greatly enough that K^+ has the highest permeability and the Nernst equation can be used as a fare estimate, though it is likely that the permeability of anions is still quite high and the calculations of equilibrium potential using the Nernst equation depart from the real values. Pollen tubes are still alive during the calibration protocols and it is possible that anions are trying to compensate the higher permeability induced by valinomycin, thus our calculations using the Nernst equation would be under- or overestimated. This experimental error is the same for both calibrations and because the VSDs have opposite dynamics, the VSDs averaged values may be the best approximation of membrane potential in PTs.

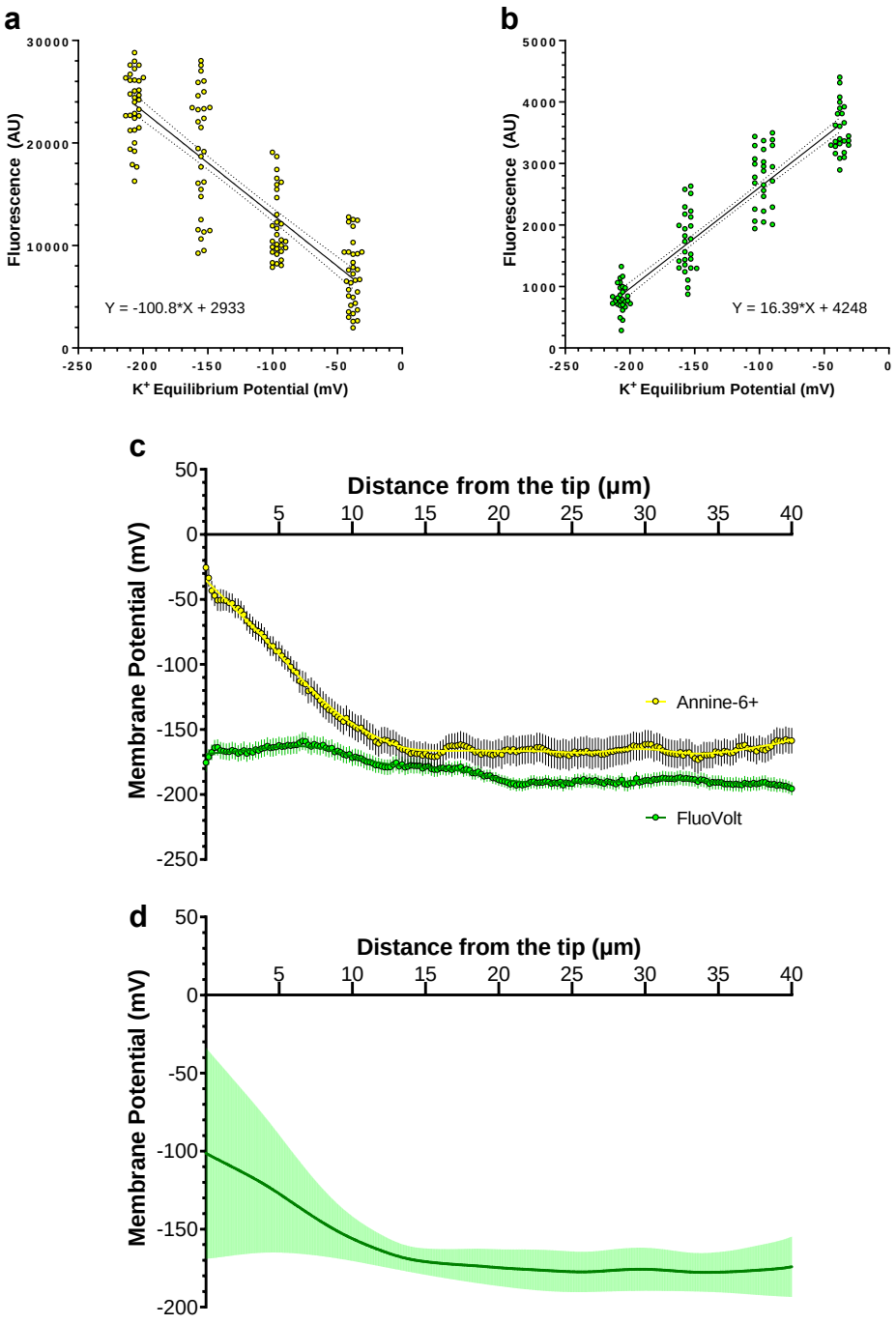

Fig.15 | VSDs calibration and calculation of membrane potential in pollen tubes. Annine-6plus **(a)** and FluoVolt (b) were calibrated using 0.1, 1, 10 and 100 mM KCl with 5uM valinomcyin and measuring fluorescence intensity. K+ Concentrations were converted to equilibrium potential for potassium using the Nernst equation and the known values of intracellular [k+]. (c) Population analysis of WT PTs labeled with Annine-6plus (n=36) and FluoVolt (n=28), in which fluorescence was converted to membrane potential using the linear regressions in (a) and (b). FluoVolt data is a pool of both long and short MPG types

2.3 Discussion

Bioelectrical phenomenon at a single-cell level has been a subject heavily dominated by neuroscience because it was thought that only propagating electrical signals could bring cells to a far-from equilibrium state so that different electrical potentials could be created in the same cell transiently, at time-intervals of milliseconds and then coming back to the equipotential state. All the other cells that depart from the type of morphology that allows electric propagation or excitation were thought to have a homogeneous electric potential in relation to the extracellular environment. Even though asymmetric ion currents have been studied for a long time in PTs, the consequence of these fluxes in setting asymmetries in membrane potential have not been well studied, mostly due to the technical limitations of the classical electrophysiology approaches.

Using voltage sensitive reporters is a way of circumventing these limitations because they are non-invasive. While testing different reporters, most of them were discarded because they were cytotoxic, or were not delivered to the plasma membrane, or because of non-specific binding to the cell wall. Annine-6plus and FluoVolt labeled well the plasma membrane, presenting a good signal-to-noise ratio and little cytoplasmic internalization. Annine-6plus showed a fractional fluorescent intensity change of 55% per 100mV while FluoVolt showed 24.4% per 10 mV, values that are comparable to previous publications (Kuhn & Roome, 2019; Salerno et al., 2020). Both VSDs are compatible with live cell imaging but FluoVolt requires a weak detergent in order to label the plasma membrane homogeneously, which makes it cytotoxic for longer periods of incubation and imaging. One of the limitations of using VSDs in PTs

is the high rates of endo- and exocytosis at the tip (Ketelaar, Galway, Mulder, & Emons, 2008), which affect the VSDs incorporation into the membrane. Other works using di-4-ANEPPS reported similar problems with VSD labeling within the first 5µm from the tip (M. A. Breygina, Smirnova, et al., 2009; M. Breygina et al., 2010; Maksimov et al., 2018) but this problem cannot be addressed without perturbing the normal electrophysiology of the PT and consequently the MPG dynamic. The use of VSDs showed that a MPG focused at the tip may be a characteristic feature of pollen tubes given that the three species tested showed a similar pattern of depolarization at the tip.

The average between VSDs shows that the potential at the tip (5-10µm) is -143 ± 1.7mV and in the shank (25-40µm) is approximately -180mV ± 0.5mV with a difference between the tip and the shank of about 34mV. This difference may be even larger if we were certain the values between the apex and the first 5µm, which the dye report as having -100mV. The values obtained by the VSDs in the shank are more hyperpolarized than any other microelectrode measurements done previously that recorded the most depolarized shank to be at -130mV (Mouline et al., 2002). The difference between using VSDs and microelectrode recordings could be mainly because the impalement causes cytoplasm leakage and depolarizes the cell.

Another evidence that supports the existence of a MPG is the results of GEPII, showing a tip-spanning K^+ gradient with less K^+ at the tip than in the shank. The observed gradient suggests that K^+ does not follow the same path as the other cations like H^+ and Ca^{2+}, which usually have inward currents at the tip and exit the shank. Instead, K^+ accumulates in the PT shank to be extruded at the tip, which contributes to the depolarization. The K^+ fluxes at the tip are estimated to depolarize the tip by

13.5mV in relation to the shank. The K^+ concentrations only account partly to the MPG because the value of the averaged MPG calculated from the VSDs is 34mV in relation to the shank. The difference between the two values is expected to come from the anions (Zonia et al., 2002), which are the highest magnitude currents measured at the tip, and a smaller contribution from H^+ and Ca^{2+} (Hoffmann et al., 2020; Michard et al., 2009).

The existence of a standing MPG affects many other cellular processes because it presupposes the creation of an electric field at the PT tip. Any sustained electric field like the one generated by the MPG has an immediate effect in many cellular components which consequently triggers electrotaxy responses (Flickinger et al., 2010; Mycielska & Djamgoz, 2004). Pollen tube growth requires exocytosis from the small apical vesicles that accumulate in the apical cytoplasm. There is evidence showing that these vesicles when isolated and exposed to an EF move toward the anode side (Heslop-Harrison & Heslop-Harrison, 1982). The reason of this movement to the anode side comes from the lipid content of the membranes of these vesicles that is negatively charged. Apical vesicles contain high amounts of enzymes of the phosphoinositide metabolism that are implicated in PtdIns4P biosynthesis, with a nominal charge of -3 (Gerth et al., 2017; Heilmann & Ischebeck, 2016; Ischebeck et al., 2010). Negative charges are likely to be drawn to the tip because it has a higher voltage than the shank, thus considered the anode side if we consider the PT a battery. The MPG-generated EF can bring these smaller vesicles to the PT tip, where the Ca^{2+} inward currents occur and can trigger the exocytosis. This mechanism has a lot of similarities with the pre-synaptic neuron, in which it receives the depolarizing action potential that triggers

depolarization-activated Ca^{2+} channels that in turn help in the exocytosis of neurotransmitter vesicles into the synaptic cleft (Pedersen, 2011). The transduction of the Ca^{2+} signaling is thought to occur via two proteins Synaptogamin-1 and complexin, which interact with the SNARE proteins on vesicles (Ramakrishnan, Bera, Coleman, Rothman, & Krishnakumar, 2020). Synaptogamin orthologs are highly expressed in PTs and RNA interference studies suggest that they have a role in pollen tube germination and growth (H. Wang et al., 2015). No depolarization-activated Ca^{2+} channels were ever described in PTs, but in root hairs, another tip growing cell, there is evidence showing that such channels exist, and elicit Ca^{2+} inward currents at imposed voltages in the range of the root hair physiological conditions (Véry & Davies, 2000). The existence of a MPG-generated EF at the PT tip may be important for sustaining growth by electrostatically carrying the small vesicles to the apex and maybe even drawing them from the cytosolic reverse fountain streaming to the apical cytoplasm. This effect may be critical because there is evidence that the vesicle transport in the apical region of the tube is not mediated by motor proteins but can be driven by a combination of other physical forces like diffusion, electrophoresis and osmophoresis (Bove et al., 2008; Chebli et al., 2013; Hepler & Winship, 2015; Lipchinsky, 2018).

The MPG-generated EF not only acts on the cytoplasmic components but it has a direct effect on the charged membrane components that, if free to move laterally on the plane of the membrane, should undergo redistribution in response to an EF applied along the membrane (Y. C. Zhou, 2012). The phenomenon of lateral electro-diffusion at the plasma membrane level has long been postulated by Jaffe as a possible mechanism underlying the effects of biogenic electric fields in developing organisms

(Lionel F. Jaffe, 1977; Lionel F. Jaffe & Nuccitelli, 1977). Subsequent studies revealed that when subjected to EF, Acetylcholine (Ach) Receptors accumulate in clusters at the cathodal side in the muscle membrane (Orida & Poo, 1978), and positively charged artificial fluorescent lipids (DiI) migrate toward the cathode side(McLaughlin & Poo, 1981; Poo, 1981). Lateral electro-diffusion may explain partly the segregation of ion channels at the plasma membrane that give rise to the flux profiles with different directions in the tip and in the shank. This way, the different ion channels with either positive or negative nominal charges could be maintained in certain parts of the membrane without invading each other's domains due to the effect of attractive or repelling forces from the EFs. Moreover, the reversal point of the ion fluxes could be a readout of the area where the MPG-generated EF is at the weakest point which would make this area more depleted from the channels that are subjected to electrodiffusion.

The MPG difference in voltage between the tip and the shank is also another possible ion channel regulatory mechanism, in which channels at the tip are subjected to a different voltage than in the shank. Even if some channels are not under the effect of electro-diffusion due to their nominal charge, the membrane potential difference can be sufficient to have them active at the tip and not in the shank and vice-versa, but this will be further explored in the next chapter. The effect of electro-diffusion in anionic lipids along the MPG is also an important factor for the control of ion channels because the lipidic microenvironments can confer stability to particular allosteric states of ion channels (Tillman & Cascio, 2003). Some ion channels have an obligate requirement for one species of phosphoinositide, whereas others may accept a broader range of phosphoinositides or anionic lipids (Hille, Dickson, Kruse, Vivas, & Suh, 2015). In

some extreme cases, *e.g.* the potassium channel Kv7.1, specific lipid species are required to couple the voltage sensing domain to the pore opening, meaning that in the absence of a specific lipid species the pore cannot open (Zaydman et al., 2013). Unfortunately, similar work has been far behind in the plant field and there are no evidence for ion channel modulation by lipid interactions.

There are a multitude of ways in which the MPG and MPG-generated EF can affect directly cellular processes that would explain the maintenance of pollen tube growth and polarity. Hopefully, the MPG concept can give rise to new and testable hypothesis that will further our understanding of morphogenesis processes that rely on bioelectrical phenomena at a single-cell level.

Chapter 3: Genetic foundations to establish a membrane potential gradient in Pollen Tubes

3.1 Introduction

In the previous chapter, I described how pollen tubes have a membrane potential gradient formed at the tip as a consequence of a defined ion dynamics that establish different electrochemical states between the tip and the shank. The most plausible explanation to such pattern would be the asymmetrical distribution of channels throughout the pollen tube such that the ion currents and their electric equivalents at the tip have the opposite direction than in the shank, creating a dynamic equilibrium sustained by two counteracting forces: depolarizing at the tip, hyperpolarizing at the shank (Domingos et al., 2019; Michard et al., 2016). In this collaborative work, we show evidence of the key molecular players that are involved in creating the K^+ and H^+ gradients that give rise to the membrane potential gradient and how the lack of these specific molecular players disrupts the bioelectrical state that seems fundamental for normal pollen tube growth and guidance.

3.1.1 Plasma membrane H^+-ATPases sustain pollen tube growth through pH homeostasis

Pollen tubes possess conspicuous ion gradients at the tip of the cell (H^+, Ca^{2+}, Cl^-, K^+) that are thought to be involved in creating polarity by modulating cellular processes and structures implicated in apical growth (Lipchinsky, 2018; Michard et al., 2016). The apical cytosolic pH ion gradient ranges from 10-30um from the tip and can vary up to one pH unit along this distance, i.e. one order of magnitude in the

concentration gradient. Molecular cell biology and pharmacology approaches support the idea that AHAs sustain the cytosolic pH gradient and that the plasma membrane localization of AHAs define the length of the gradient (Feijó, Sainhas, Hackett, Kunkel, & Hepler, 1999b; Michard et al., 2016). The observed H^+ gradients are maintained through the activity of the plasma membrane H^+-ATPases (AHAs for Autoinhibited H^+-ATPase), the main family of H^+ extrusion in plants (Lang, Pertl-Obermeyer, Safiarian, & Obermeyer, 2014; Palmgren, 2001; Sze, 1985). The plasma membrane Proton-ATPases (AHA) are electrogenic pumps that export H^+ to the apoplast at the expense of ATP. The use of energy stored in the ATP molecule is necessary to export H^+ against its electrochemical potential to regulate not only pH homeostasis inside the cell but also membrane potential. As H^+ are imported to the cytosol at the tip passively, positive charges leave the cell in the shank hyperpolarizing the membrane to more negative values and regulating the extension of the pH gradient to the foremost 30 µm of the PT. The process of hyperpolarizing the membrane is paramount to cell's function because it is a form of storing energy at the plasma membrane level for solute transport (Palmgren, 2001).

In tobacco pollen tubes, NtAHA1 localizes the plasma membrane only in the shank, and it is completely excluded from the tip (Certal et al., 2008), which correlates well spatially with the data of extracellular H^+ fluxes and the pH cytosolic gradient. Thus it is thought that the H^+ flow through the pollen tube creates a H^+ short-circuit, in which the tip influxes compensate the net effluxes along the pollen tube shank (Michard et al., 2009). In the present work, we showed that three AHAs are highly expressed in Arabidopsis PTs as revealed by histochemical staining of GUS activity of the

transgenic lines pAHA6::GUS, pAHA8::GUS and pAHA9::GUS (fig16a). The transgenic lines of AHA-GFP fusions showed that these pumps indeed localize to the plasma membrane being excluded from the tip, closely resembling the previous work with tobacco (Certal et al., 2008). AHA6 localized along the entirety of the shank, while AHA 8 was absent in regions further away from the tip, and AHA9 was present only at the most posterior regions of the shank close to the pollen grain (fig16a). The mutant lines of these three pumps were analyzed and crossed with each other to generate double and triple mutants in order to understand the possible synergistic effect of AHAs activity in pollen tube growth and development. *In vivo*, double mutants showed a different degree of pollen tube arrest in the pistil and reduced fertility but the most striking combination is aha6/8, the AHAs at closest proximity from the tip, suggesting that their activity at the apical region is most relevant in sustaining apical growth (fig.16 b). The triple mutant aha6/8/9 is even more severe, not only in seed production but also in pistil growth arrest (fig16 b,c). The fact that the mutation in AHA9 in the double mutant aha6/9 affects the initial growth stages in the pistil (*in vivo)* and that in the triple mutant aha6/8/9 the germination rate is down to 10% indicates that AHA9 might be more important in the initial stages of pollen tube development (fig.16 b).

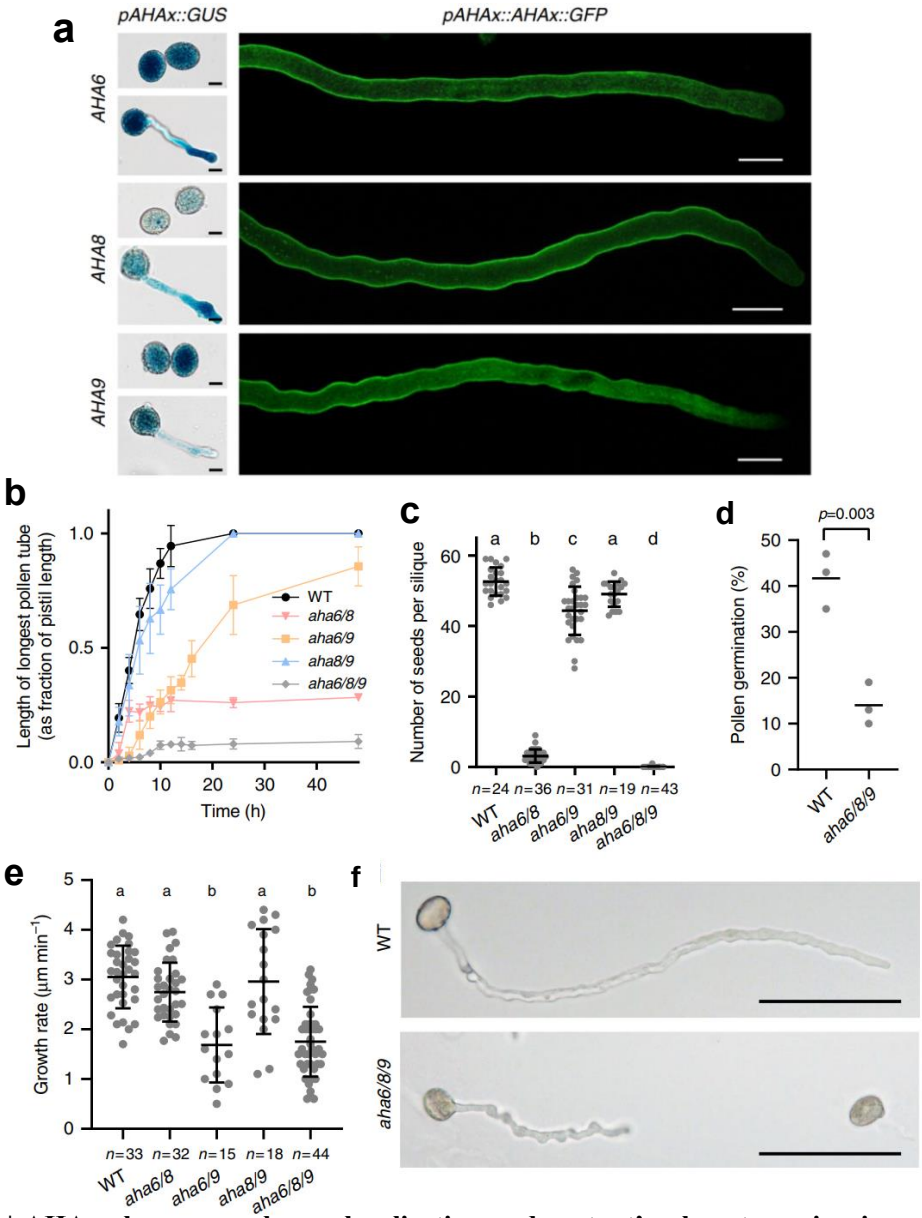

Fig.16 | AHAs plasma membrane localization and mutant's phenotypes in vivo and in vitro. (a) Left, Histochemical staining for GUS activity in pollen grains and grown pollen tubes stably expressing AHA promoter::GUS fusions and observed using a light microscope. Right, Pollen tubes stably expressing GFP-tagged AHA proteins under control of their endogenous promoters and observed using a confocal microscope, scale bar = 10µm. **(b)** In vivo pollen tube growth rate (as a fraction of pollen tube length over pistil length)($n \geq 3$ for all genotypes and time points; error bars show SD). **(c)** Number of seeds per silique (one-way ANOVA and Bonferroni's Multiple Comparison Test; $p < 0.01$; error bars show mean with SD). **(d)** In vitro germination rate for WT and aha6/8/9 triple mutant pollen. Means from three individual experiments with ≥ 100 scored pollen grains for each genotype and replicate are shown (two-sided t-test; $p < 0.003$). **(e)** Average pollen tube growth rate assayed in vitro (one-way ANOVA; Bonferroni's test; $p < 0.01$; error bars show mean with SD). **(f)** Light microscopy images of WT and aha6/8/9 pollen tubes grown in vivo. The triple mutant is characterized by short and wavy pollen tubes. Scale bar = 100 µm.

To understand how these mutations affect cell physiology, extracellular H^+ fluxes were measure along the pollen tube length as a read-out of AHA's activity. All the mutant combinations lacking AHA6 show reduced H^+ influx at the tip and virtually no net H^+ effluxes at the shank when compared to WT, correlating the localization of AHA6 at the shank near the tip with the H^+ fluxes measured (Fig.17 b, c). This effect is consequential to the cytosolic pH gradient where the mutants lacking AHA6 have lower pH and, more relevant, a less pronounced gradient, resulting in a less alkaline cytosol than the WT and aha8/9 (fig17 e).

Given that pollen tubes growth relies in many different ionic currents, we hypothesized that changing the dynamics of H^+ would have an impact in the other ion dynamics. Anion effluxes were measured at the tip as they are the largest fluxes in pollen tubes, 3 orders of magnitude higher than H^+. Since anions are counterions to the H^+, that makes anion fluxes more likely to be affected by the H^+ imbalance. Indeed, a striking reduction of anion effluxes at the tip is observed in mutants lacking AHA6 when compared with WT and aha8/9 thus suggesting that the H^+ and anion dynamics are interdependent (fig17 d).

The role of cytoskeleton was also investigated not only as a cause for the aberrant phenotype of the triple mutant but as a downstream target of the imbalance of cytosolic pH, since pH is known to regulate of the ADF/cofilin family of actin remodeling proteins (Hepler, 2016; Yonezawa, Nishida, & Sakai, 1985). Actin is

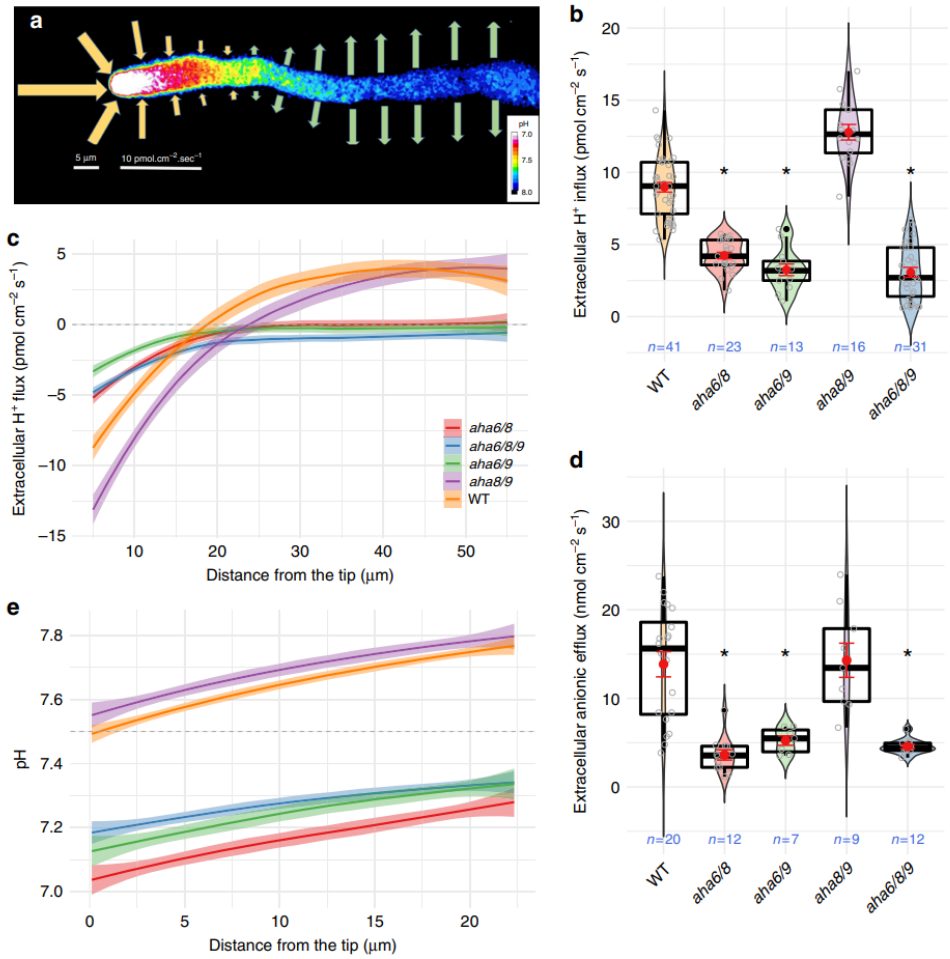

Fig.17 | Reduced pollen tube growth in aha6 double and triple mutants is associated with reduced extracellular ion fluxes and intracellular pH gradients. (a) Representative WT pollen tube summarizing H+ fluxes measured at the surface (arrows) and cytosolic pH gradient (false color). Arrow size is scaled with the flux intensity shown on the bottom bar, while direction denotes influx or efflux. **(b)** Extracellular H+ fluxes at the pollen tube tip. Violin plots show the probability density with color-filled curves obtained from individual observations (open gray circles), with boxplots (thick black lines and outliers as black dots) overlaid with the mean and standard error (red circle and lines). **(c)** Extracellular H+ fluxes throughout the pollen tube sampled every 5 µm, averaged and interpolated with a local polynomial fit (loess) with n > 10 for all genotypes. Negative values indicate influx and positive values efflux. **(d)** Extracellular anion efflux at the tip. **(e)** Cytosolic pH throughout the tube averaged with loess for each genotype (n > 16), obtained by fluorescence imaging of a calibrated pH probe (pHluorin). Media pH indicated by dashed line.

distributed in PTs in bundles along the shank of the tube, ending in a fringe like structure in the sub-apical region (3-6um in Arabidopsis), and a mesh of very short microfilaments in the apical dome (Cheung et al., 2008). In the aha6/8/9 pollen tubes, the sub-apical region is depleted of the actin fringe and the apical-dome was completely

devoid of actin, whereas the other mutants did not show a significant departure from the WT.

Altogether, these results show that H+-ATPases control dynamic H^+ fluxes in growing pollen tubes and are required for normal pollen tube elongation. The effect of these pumps in creating an electrochemical pH gradient along the tube is necessary for establishing different actin polymerization states and directs actin bundling towards the apical region. Moreover, H^+-ATPases generate the proton motive force that drives the anion effluxes and the H^+ influxes at the tip.

3.1.2 K^+ transport in pollen tubes

In the previous chapter, I have shown through a genetically-encoded K^+ probe that Pollen tubes have a negative K^+ gradient at the tip. This cytosolic K^+ gradient can only be formed if there are K^+ outward currents at the PT tip and K^+ inward currents at the shank, following the same flux pattern for anions. However, the studies investigating K^+ fluxes in PTs so far were not reproducible and were likely to be artifacts of the techniques and the ionophores used(Messerli et al., 1999). Thus, most of the work on K^+ currents in pollen tubes stems from the classical electrophysiology approach through single-channel recordings or whole-cell patch-clamp/voltage-clamp by using pollen grains or protoplasts because pollen tubes do not withstand these invasive techniques.

Studies using single-channel patch clamp in lily pollen grain protoplasts found that there are two main K^+ channel populations opening with depolarizing membrane potentials (Obermeuer & Kolb, 1993). Using a double-barrel pipette to follow voltage

and apply current in pollen grain protoplasts showed that there is K^+ outward currents at more depolarizing values above -100mV whereas K^+ inward currents were activated at values between -200 and -100mV (Obermeyer & Blatt, 1995). More recently, inward K^+ currents were also measured in Arabidopsis protoplasts but only the hyperpolarization-activated currents were reported when clamping the cell to voltages below -80mV. These currents were interpreted as specific for K^+ because when the K^+ channel blocker Ba^{2+} was used, it inhibited 80% of the currents. Moreover, these currents are pH-dependent and peaked at external pH of 5, almost two units away from the in vitro germination media for Arabidopsis (Fan, Wang, Wang, & Wu, 2001). K^+ channels pH-dependence seems to be a common feature in plants as hyperpolarization is usually associated with the extracellular acidification of the medium/apoplast conducted by H^+-ATPases (Thiel, MacRobbie, & Blatt, 1992).

An important advance was the identification of a pollen specific K^+ channel from the Shaker family, named SPIK for Shaker Pollen Inward K^+ channel (Mouline et al., 2002). Studies using patch-clamp to study this channel's activation in COS cells showed that SPIK's half-maximal potential was at -205mV and it was pH sensitive shifting the half-maximal potential to -160mV when changing pH to 5, a unit away from the control. Patch-clamp in pollen grain protoplasts of the *spik-1* mutant showed a strong reduction in the current magnitude and the inward rectifying feature of the channel was no longer observed confirming that SPIK is an important player in homeostatic inward K^+ currents during pollen tube development. To understand whether SPIK is involved in K^+ uptake during PT growth, the authors measured membrane potential in early developing pollen tubes showing that PTs are

hyperpolarized around -120 to -134mV, which is within the activation range measured for the SPIK channel .Pollen tubes from spik-1 plants show a lower germination rate and growth rate *in vitro*, and *in vivo* are less competitive than WT producing 1.6 times fewer seeds (Mouline et al., 2002). Although SPIK -driven K^+ inward currents are the most prevalent in pollen grains, the fertility phenotype of *spik-1* mutant pollen tubes is not that severe indicating that K^+ transport could be mediated by other transporters that were not identified in these patch-clamp experiments.

One other player responsible for K^+ inward currents is the Tandem-Pore K^+ channels (AtTPK4), exclusively expressed in pollen and it is the only member of this family targeted to the plasma membrane (Becker et al., 2004; Marcel, Müller, Hedrich, & Geiger, 2010). Double-barreled impalement techniques showed that tpk4-1 pollen tubes had reduce voltage-independent K^+ currents in comparison with WT. A distinct feature of this channel was its sensitivity to cytosolic pH rather than extracellular pH concentrations. A change from 7.5 to 6.3 cytosolic pH suppressed TPK4-mediated currents when expressed in oocytes. Moreover, TPK4 currents were mostly blocked by elevated extracellular Ca^{2+} in a voltage dependent manner at voltages more negative than -100 mV. The activity of the channels SPIK1 and TPK4, responsible for inward K^+ currents in the shank of the pollen tube complement each other. TPK4 is weakly voltage dependent and is active at membrane potentials above -100mV, a range at which SPIK1 is closed, thus it is considered an open-rectifier, i.e. voltage-independent instantaneous gating and saturating K^+ currents at increasing positive membrane voltages (Becker et al., 2004). Furthermore, TPK4 is sensitive to extracellular Ca^{2+} and intracellular pH whereas SPIK1 is sensitive to external pH but insensitive to

extracellular Ca^{2+}. The complementarity voltage, pH and Ca^{2+} dependent properties of TPK4 and SPIK1 may account for most of the K+ physiological responses and inward currents that keep K^+ at such elevated concentrations in PTs because these channels function at a wide range of bioelectrical states.

The inward K^+ currents responsible to maintain cytosolic K^+ can be attributed at least partly to SPIK1 and TPK4 but little is known about the K+ outward currents. One possible candidate as K^+ outward transporter is CHX family of transporters, predicted as Cation/Proton exchangers. This prediction comes from the similarity between the hydrophobic domains of CHX with the Cation/Proton Antiporter-2 proteins (CPA2)(Sze et al., 2004). CHX21 and CHX23 are highly expressed in pollen but only CHX23 seems to be pollen specific. Single mutants do not have a phenotype but the double mutant chx21/23 plants rarely produce seeds, having at best 1 seed/silique and this phenotype was attributed to a defective pollen tube's chemotropic response because PTs do not steer toward the ovules. Heterologous expression of CHX23 in an E. coli strain lacking three important K^+ transporters allowed growth of this strain, suggesting that CHX23 mediates K^+ uptake. In this experiments, bacterial growth was enhanced by CHX23 expression at a more basic pH of 7 rather than the more acidic (pH 5.8), indicating that CHX has a pH dependent activation (Lu et al., 2011). Double mutants *chx21/23* have slightly decreased H^+ influxes at the tip and effluxes in the shank (fig 18 a,b) which points to a potential role of CHX21/23 in regulating the homeostasis of H^+, K^+ or both. CHX23 in an E. coli strain lacking three important K^+ transporters allowed growth of this strain, suggesting that CHX23 mediates K^+ uptake. In this experiments, bacterial growth was enhanced by CHX23

expression at a more basic pH of 7 rather than the more acidic (pH 5.8), indicating that CHX has a pH dependent activation (Lu et al., 2011). Double mutants *chx21/23* have slightly decreased H^+ influxes at the tip and effluxes in the shank (fig3a,b) which points to a potential role of CHX21/23 in regulating the homeostasis of H^+, K^+ or both.

Here we investigate the impact of loss of function of AHA and CHX channels on the overall bioelectrical state of the pollen tube. Until now, assessing membrane potential in pollen tubes was not possible without invasive impalement techniques that

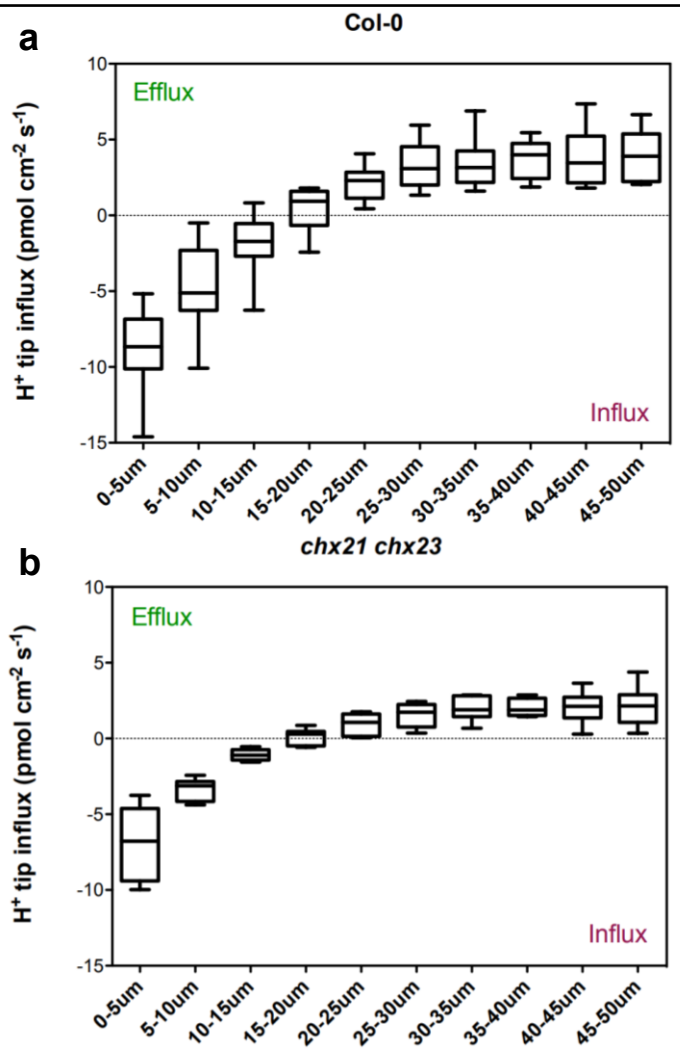

Fig.18 Extracellular H+ flux profiles in chx21/23 mutants. (a) WT (Col-0) **(b)** chx21/23. Negative values indicate H+ influx and positive values efflux. Chx21/23 mutant pollen tubes show a slightly reduced H+ flux overall

dissipate longitudinal membrane potential patterns. Longitudinal membrane potential patterns could provide mechanistic insights on apical growth and cell polarity. By comparing different VSDs in response to these genotypes we can assess the reliability and accuracy of these dyes.

3.2 Results

Pollen tube growth relies on ion dynamics and homeostasis to perform their functions. The mutations in specific ion transporters like AHAs and CHXs disrupt the normal physiology of the pollen tubes to a point that fertility is highly reduced to being almost sterile. These sets of mutants are interesting case studies because the mutations in AHAs affect apical growth whereas mutations in CHX disrupt the chemotropic response. One similar phenotype with two different mechanistic origins could provide insight on how these two processes work. The comparison between these genotypes using different VSDs also provides a way to validate these dyes' relative accuracy.

3.2.1 CHX subcellular localization

In previous work (Lu et al., 2011), the authors were only able to clone CHX23-GFP, claiming that their attempts to clone CHX21 failed due to persistent errors on the DNA sequence. Nevertheless, CHX23-GFP was expressed in pollen tubes and shown to co-localize with an ER marker.

We cloned CHX21-GFP and CHX23-RFP driven by LAT52 promoter and expressed them in the chx21/23 background to rescue the phenotype. PTs from the transgenic plants were imaged under airy-disk confocal microscopy in the super-resolution mode. Our findings show that CHX23-RFP localizes to the plasma

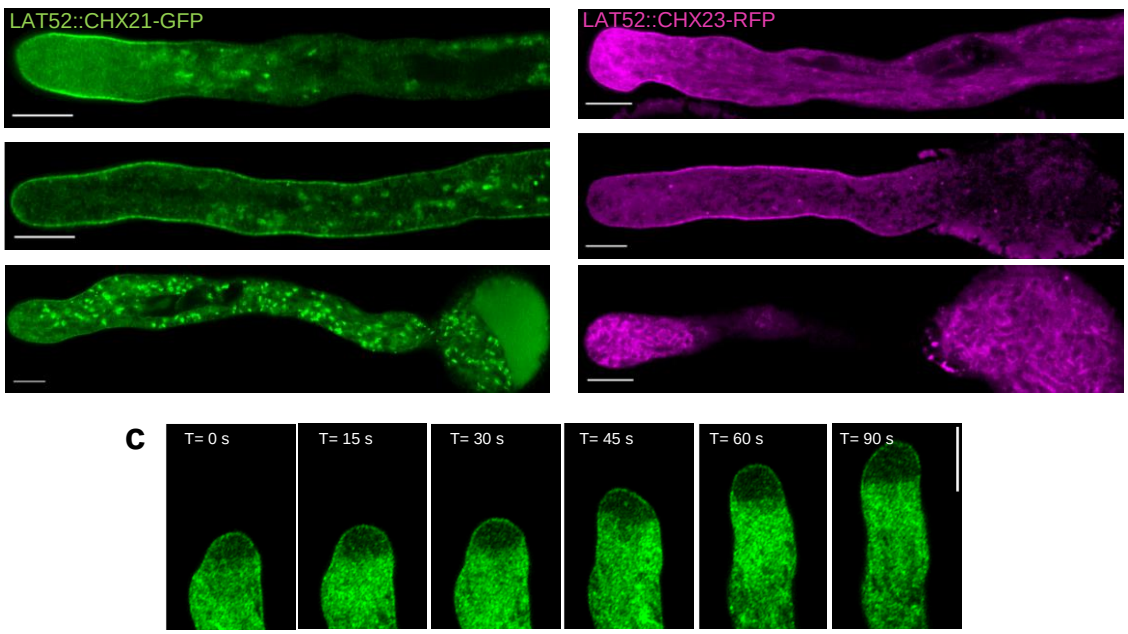

Fig.19 | CHX 21 and 23 subcellular localization in the *chx21/23* background. **(a)**Lat52::CHX21-GFP pollen tube shows localization at the tip especially in the subapical area where there is more fluorescence **(top)**, in some cases the localization is extended to the shank but showing lower fluorescence than in the tip **(middle)**. CHX21-GFP also localizes to endomembrane comparments of a smaller size, thought to be Golgi **(bottom)**. **(b)** LAT52::CHX23-RFP pollen tube showing localization at the tip of the PT **(top)**. In the first instances of growth, CHX23-RFP localizes to the subapical region too **(middle)**. When z-scanning pollen tubes, the cortical region of the tube also shows some patterns that resemble ER as it was described in Lu, et al, 2011 **(bottom)**. **(c)** Frames of a time-lapse sequence showing CHX21-GFP localizing to the membrane apex in the newly formed membrane. CHX23-RFP follows the same pattern.

membrane at the PTs tip in the first 20µm, but during the first stages of pollen tube germination it seems to localize to the shank too (fig.19 b). When z-scanning the tubes in the cortex, we could also detect some fluorescence signal similar to the ER as it was described before (fig19.b bottom). CHX21-GFP localizes to the plasma membrane on the pollen tube tip, showing high fluorescence intensity in that region, but some of the pollen tubes also show labeling back along the shank but at a lower fluorescence intensity, suggesting that the distribution of CHX21 is mostly at the tip (fig19a).

Moreover, there is an endomembrane localization to a structure that was not yet identified by co-localization studies, but by analogy it could be Golgi (fig19. A bottom). When imaged in time-lapse sequences, both CHX21 and CHX23 appear at the apex of the pollen tube with each new increment of membrane during growth.

These transgenic plants were created using the chx21/23 double mutant and the complementation of either of the CHX rescued the fertility phenotype thus increasing the seed yield to normal levels, indicating that the GFP/RFP fusions were successful and did not disrupt protein function. Overexpression of proteins, and especially ion channels that are not too abundant, could create artifacts in cellular localization, but since the fertility phenotype was rescued (unpublished data), we consider that our observations agree with the endogenous localization of CHXs in pollen tubes.

3.2.2 Male-fertility phenotypes linked to membrane potential homeostasis

Given the severe male-fertility phenotypes in these ion transporter mutants, we wanted to investigate the bioelectrical state of pollen tubes to understand how the lack of these ion transporters influence membrane potential. VSDs labeled mutants were analyzed and the fluorescence intensity converted to membrane potential using the calibration curves obtained in chapter 2.

At a first glance, the genotypes have the same relative distribution from more hyperpolarized states to more depolarized membrane potentials following the order chx21/23, WT, aha6/8 and aha6/8/9, regardless of the VSD used (fig20. a,b). It is important to note that the variation in mV from one genotype to another is conserved between the VSDs, e.g. the difference between chx21/23 and WT is roughly the same

using FluoVolt or Annine, and the bigger difference between WT and aha6/8 is conserved too. This relative distribution is reassuring that the VSDs are reporting a similar trend within the genotypes but, the absolute values for membrane potential do not match when comparing the two VSDs. The discrepancy in the absolute values of membrane potential between the VSDs is in the order of 50mV and could be attributed to the error in the calibrations when we assume that the cell is completely clamped to K^+. If it is not the case that can skew the calibration curves through the influence of Cl^- in membrane potential. Chloride currents in the tip are 3 orders of magnitude higher that H^+ and $Ca2^+$ and it is difficult to predict whether Cl^- transporters are not functionally trying to rectify membrane potential homeostasis during the calibration protocols.

The mutants *aha6/8* and *aha6/8/9* are more depolarized in relation to WT because AHAs are highly electrogenic, using up ATP to extrude H^+ against the concentration gradient (fig.20 a,b). Thus, the cell is losing positive charges at the expense of ATP, becoming more negative, or hyperpolarized. By mutating these AHAs localized to the shank, pollen tubes become more depolarized. This also explains that the triple mutant has a more severe phenotype than the double mutant. Another consequence of not having these pumps active, is that the H^+ concentration in the cytoplasm is much higher, and thus it decreases the H^+ driving force to go inwards at the tip as a compensatory way.

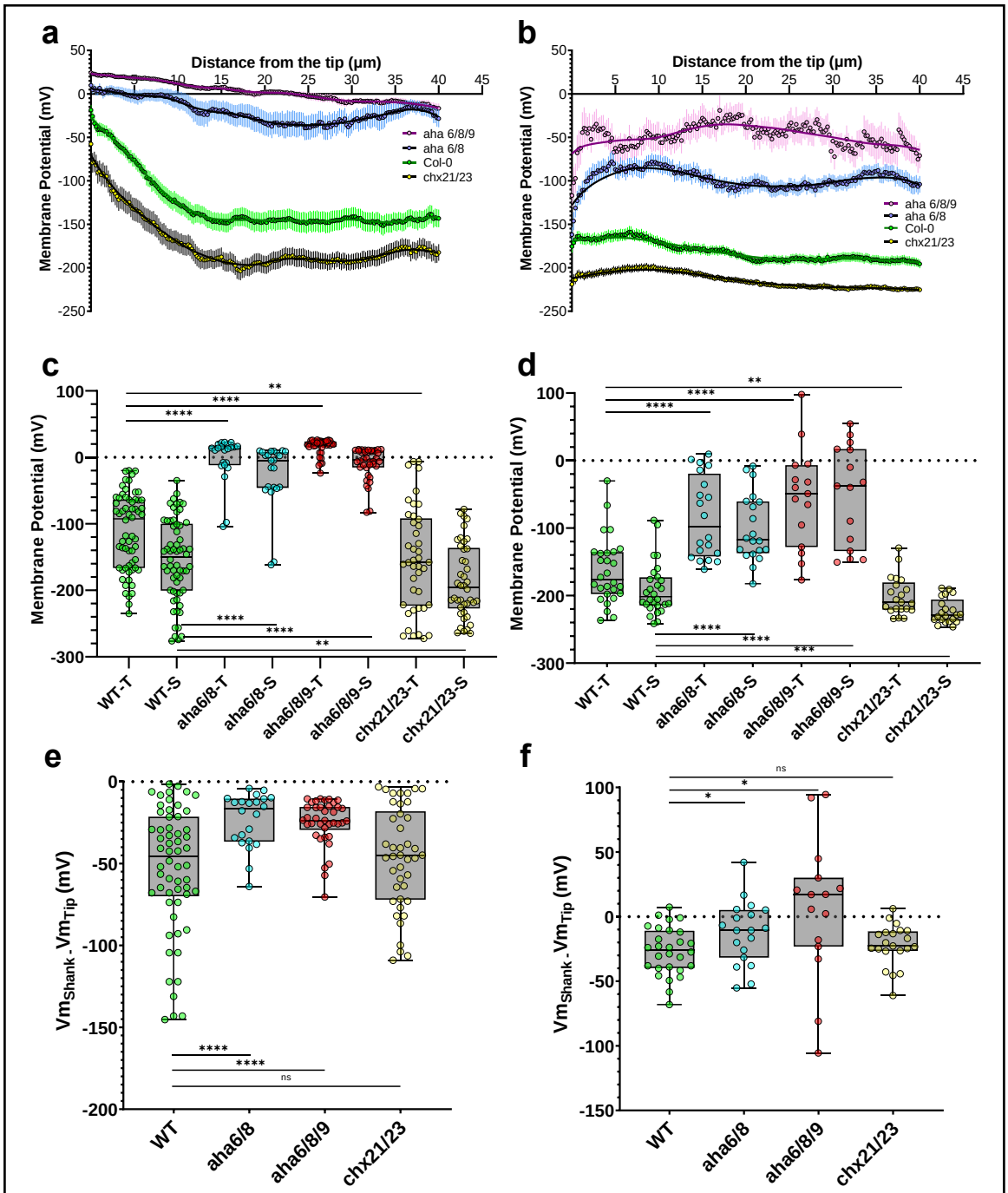

Fig.20 | VSDs in different genotypes reveal differences in pollen tube's bioelectrical state. (a,b) Pollen tubes membrane potential profiles with Annine-6plus **(a)** and FluoVolt **(b)** of WT, chx21/23, aha6/8, and aha6/8/9 calculated from fluorescence intensity using the calibration curves from the previous chapter. The lines over the dots represent a Lowess regression on each sample **(c – Annine-6plus, d - FluoVolt)** Comparison between the tip and shank regions between genotypes using Welch's T-tests showing that all the genotypes are significantly different from WT in both tip (T) and shank (S) regions. **(e – Annine-6plus, f – FluoVolt)** Metric to define the MPG steepness in the different genotypes using paired samples and subtracting the tip from the shank values. Welch's T-test was employed to compare the samples, showing that aha6/8 and aha6/8/9 are statistically different but not chx21/23.

In the case of the CHX mutants, pollen tubes become more hyperpolarized in relation to the WT but CHX function is still not completely elucidated which makes it difficult to draw conclusion on what is the mechanism that drives the hyperpolarization in the cell. Assuming that the hyperpolarization is a direct effect of CHXs loss of function, that would imply that these channels are electrogenic and that the antiport mechanism is asymmetrical as hypothesized before (Sze & Chanroj, 2018). Based on comparative bioinformatics, the author's hypothesized that the stoichiometry of CHXs is $2H^+$ in/ K^+ out, which would slowly depolarize the tip of the pollen tube and would contribute to maintaining the K^+, H^+, and membrane potential gradients that we observe.

To statistically analyse the membrane potential profile curves (fig20 a,b), we subdivided pollen tubes in two different regions, the tip between 5-10µm and the shank between 25-40µm and averaged all the points in these regions. We did not consider the tip between the apex-5µm because FluoVolt showed problems in labeling especially when tubes are growing slower (previous chapter), and here we can see the same effect when looking at the slow growing mutants *aha6/8* and *aha6/8/9*, which have a pronounced decreased in fluorescence in the apex. The comparison between tip and shank regions between genotypes show that there is a statistically significant difference from the WT in both VSDs labeled PTs (fig.20 c,d).

Taken together, these results indicate that membrane potential homeostasis is important for the normal function of PTs, namely in terms of chemotropism. Bioelectrical imbalance to more depolarized or more hyperpolarized values than WT have implications in growth and chemotropism, either because membrane potential has

a direct effect in membrane proteins or because ion imbalance causes structural or organizational problems at a cellular level.

3.2.3 Membrane potential gradient is correlated with growth rates

We showed that the overall bioelectrical state of the mutants is different from the WT PTs, but we wanted to investigate whether these changes in overall membrane potential presuppose a difference in the steepness of the MPG. We explore whether the MPG steepness is correlated with growth in the different genotypes because we believe that the MPG is key to establish cell polarity in PTs.

To investigate the difference in the membrane potential gradient between the tip and the shank, we subtracted the values from the shank and the tip regions from the same pollen tube, to be able to quantify the voltage difference or in other words, the steepness of the MPG. The two VSDs reported the same general trend between the genotypes in which the MPG in aha6/8 and *aha6/8/9* mutants is different from the WT but not from CHX (fig.20 e,f). Since *aha6/8* and aha*6/8/9* mutants have slower growth rates, these results suggest that the steepness of the MPG could affect apical growth in these cells. The mutants *chx21/23* do not have differences in growth rate and the MPG is comparable in magnitude to the one of WT PTs. In FluoVolt samples, there are some positive values, in which the tip is more hyperpolarized than the shank. These outliers are in most cases instances where the shank between 25-40um would have a decrease in fluorescence along the tube, and because the sampling area is bigger than the tip, the integrated value would be lower than the tip resulting in a positive MPG. It is hard to understand these positive values, but they are only present in the FluoVolt samples.

3.2.4 Combining the VSDs data for a more reliable estimate

Throughout this work, we realized that the VSDs have discrepancies and report membrane potential differently in absolute values, but there is also a sensitivity issue between VSDs when reporting within the same cell because Annine-6plus always reports a higher difference between the tip and the shank. We think that the discrepancy in absolute values can derive from the calibration protocols not being perfect, creating a slightly over- or underestimation of the real membrane potential. One striking example of that can be seen in the data pertaining to Annine-6plus (fig.20 a) because the AHA mutants reach positive values, and this should not be possible in a cell that lacks the most important pumps to energize the membrane. If the membrane is not hyperpolarized like in the AHA mutants, it is very unlikely that the cell has enough energy to create currents that bring membrane potential do positive values. These over- and underestimations could indicate that either the calibration protocols are not clamping K^+ completely, or that even when the K^+ is clamped there are other ion currents that could bias the membrane potential and our fluorescence signal. In either way, the effect of the protocol should be the same in the samples, and because the VSDs fluorescence dynamics work in opposite directions, I summarized the data by averaging the Lowess regressions in fig. 21 and table I.

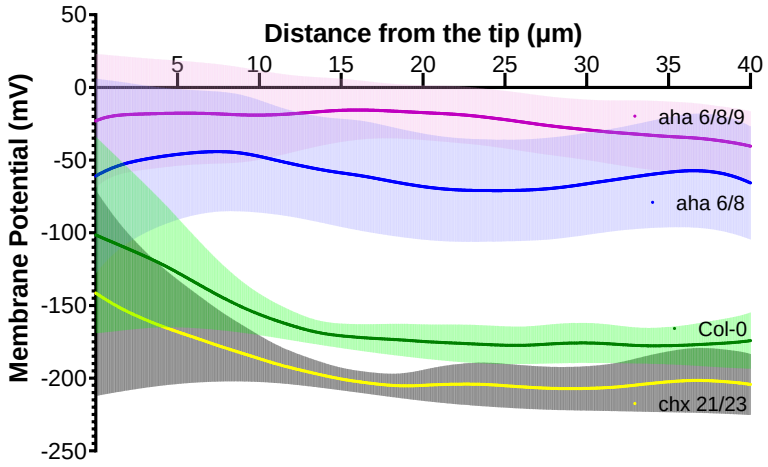

Fig.21 | VSDs average is a closer estimate of the real membrane potential. Lowess regressions in fig. 5a, b were averaged to create this plot (n=2). WT and chx21/23 have a very similar profile, almost parallel, showing roughly the same MPG and a stable hyperpolarization in the shank. AHA mutants are more depolarized and show a high variance along the entire profile, indicating a bioelectrical state far from homeostatic.

When we average the VSDs membrane potential profiles (fig. 21), it is noticeable that in WT and chx21/23 there's a bigger variance in the apex region (<5µm) than in either the tip (5-10µm) or the shank, which was expected since this is where the labeling of VSDs can be more easily influenced by cellular processes such as endo- and exocytosis. The AHA mutants are usually so out of the physiological homeostasis that they represent the highest variance between samples, and here, when combined the two VSDs, this variance is even more pronounced, but the relative position is still preserved, and *aha6/8/9* is still the most depolarized genotype from the two.

Table I summarizes the results from VSDs and the estimations drawn from the K^+ concentrations to allow a quick comparison between the techniques. GEPII estimates of membrane potential in the shank are very close to the VSDs average but the values from the tip depart from the prediction, especially when we calculate the

MPG difference. GEPII estimates show that K^+ concentrations might only account for -13.5 mV of the MPG, which is less than half of what is predicted by averaging the VSDs. This suggests that the depolarization at the tip has the contribution from other anions like Cl-, and since we know that these currents are higher in magnitude this would be a plausible explanation. From all the MPGs (ΔΨ shank-tip), the AHAs mutants have the lowest, almost comparable to the MPG estimates in GEPII. Given that these mutants have a slower growth rate, this suggests that the steepness of the MPG could be predictive of apical growth rate. Inversely, *chx21/23* has a very strong phenotype *in vivo*, but no growth rate impairment and the MPG is comparable to the one in WT, implying that the hyperpolarization in the shank is critical to chemotropism.

Table I - Membrane potential comparison between VSDs, genotypes and MP estimates. This table summarizes the results from fig.20 to allow a quick comparison between the different dyes. The GEPII estimation is based on the K+ concentrations observed in WT pollen tubes and then its estimated using the Nernst equation. VSDs average was calculated using the values in fig.21 (in mV)

Genotypes	Probe	Tip (5-10µm)	Shank (25-40µm)	ΔΨ(shank-tip)
Wild Type	GEPII	-158.6 ± 10	-172.1 ± 16	-13.5
	Annine-6+	-111.2 ± 7.4	-154.2 ± 7.9	-43.0
	FluoVolt	-163.9 ± 9.2	-190.5 ± 7.3	-26.6
	VSDs Avg.	-142.6 ± 1.7	-179.6 ± 0.5	-34
aha 6/8	Annine-6+	-2.5 ± 7.5	-26.0 ± 10.5	-23.5
	FluoVolt	-84.0 ± 13.5	-99.8 ± 11.25	-15.8
	VSDs Avg.	-45.1 ± 2.6	-63.6 ± 1.4	-18.5
aha 6/8/9	Annine-6+	16.0 ± 2.0	-9.0 ± 3.9	-25
	FluoVolt	-50.0 ± 19.2	-55.8 ± 19.1	-5.8
	VSDs Avg.	-18.3 ± 2.1	-31.2 ± 0.8	-12.9
chx 21/23	Annine-6+	-153.0 ±12.1	-186.4 ± 8.6	-33.4
	FluoVolt	-200.8 ± 6.2	-222.9 ± 4.0	-22.1
	VSDs Avg.	-177.5 ± 1.7	-204.7 ± 0.7	-27.2

3.2.5 Competition essays with the mutant lines

The bioelectrical state of AHA mutants and CHX mutants are opposite. In one hand AHA mutants are more depolarized than the WT, and this depolarization increases with the number of AHAs mutated. In the other hand, the *chx21/23* double mutant is more hyperpolarized than WT. Following this reasoning, if chx21/23 mutants had a mutation in one of the AHAs, the hyperpolarized state should be recovered to levels closer to the WT, or at least partly. One problem with this approach is generating lines with these mutants that already have severe fertility phenotypes, making it difficult to have a good seed yield to recover homozygous plants for a specific combinations of 3 mutations. In order to circumvent this we thought in using pollen competition experiments that only require haplotypes (table II), rather than homozygous plants for a specific genotype.

The double mutants *chx21/23* and *aha6/8* were crossed with each other to create a plant heterozygous for all the loci, which was later used as a pollen donor, because it would create all the mutant combinations. This pollen was crossed to a WT plant and the progeny was screened for the mutations. This approach is a good shortcut but we do not know if some combinations are incompatible with pollen viability, which means that any allele combination not present in the progeny could be creating defects at the pollen grain level rather than PT level. If our hypothesis was correct, chx21/23/aha6 or chx21/23/aha8 combinations should be passed onto the progeny because chx21/23 do not have any problems in growth and a single mutation in one of the AHAs would just depolarize slightly the PT.

Our results show that there was no instance in which triple and quadruple mutant PTs were able to fertilize seeds, which directly contradicts our hypothesis but we cannot exclude that sporogenesis and pollen grain formation was not defective when three or four mutations were combined. One surprising result pertains to the transmissibility of *chx21* mutation that is two times more likely to be passed on to the next generation than WT. That means that *chx21* mutation works as a gain-of-function because they are more transmissible than WT, while *chx23* works as a loss-of-function that decreases pollen transmissibility. CHX21 mutations is so beneficial for transmissibility that even when together with AHA8 mutation it still outperforms WT, although the same is not true for *chx21/aha6* haplotype. CHX21 localizes to the plasma membrane tip, very close to AHA6 that is expressed immediately below the apical region. CHX21 and AHA6 localize and function at the same region of the pollen

Table II – Competition essays with pollen from a heterozygous plant for all the mutations in CHX21 and 23, AHA6 and 8. The segregation of 4 different loci are going to create 16 different pollen haplotypes. The gene annotation identifies the pollen haplotype focusing on the transmission of the mutant alleles. Observed frequency is calculated from the number of seeds carrying a specific mutation. Expected frequency if there was no effect of the genotypes in the transmissibility of the mutant alleles. Adjusted expected frequency is based on data of how transmissible the combination of chx21/23 or aha6/8 are. The rest of the frequencies was adjusted from that. Significantly different from the segregation ratio of the expected frequency adjusted (χ^2, $P < 0.0001$)

Pollen haplotypes	Gene annotation	Progeny #Seeds	Observed Frequency	Expected frequency (no effect)	Expected Frequency (adjusted)
ABCD	WT	32	0.16	0.06	0.10
aBCD	chx21	62	0.31	0.06	0.10
AbCD	chx23	5	0.03	0.06	0.10
ABcD	aha6	25	0.13	0.06	0.10
ABCd	aha8	13	0.07	0.06	0.10
aBCd	chx21/aha8	41	0.21	0.06	0.10
aBcD	chx21/aha6	8	0.04	0.06	0.10
AbcD	chx23/aha6	5	0.03	0.06	0.10
AbCd	chx23/aha8	5	0.03	0.06	0.10
ABcd	aha6/8	1	0.01	0.06	0.02
abCD	chx21/23	1	0.01	0.06	0.00
abCd	chx21/23/aha8	0	0.00	0.06	0.00
aBcd	chx21/aha6/8	0	0.00	0.06	0.02
Abcd	chx23/aha6/8	0	0.00	0.06	0.02
abcD	chx21/23/aha6	0	0.00	0.06	0.00
abcd	21/23/6/8	0	0.00	0.06	0.00
		198.00	1.00	1.00	1.00

whereas AHA8 localizes much farther back in the PT which may explain the lower transmissibility of chx21/aha6 haplotypes.

The CHX21 and CHX23 genes seem to have a synthetic interaction which is a consequence of the robust buffering schemes at the molecular level that confer phenotypic stability. The genetic robustness is the result of parallel redundant pathways that conceal the effects of mutations without interfering with important cellular process, so that the process does not rely on any one individual component.

3.3 Discussion

The fertility phenotypes associated with the ion transporter mutants *aha6/8*, *aha6/8/9* and *chx21/23* are correlated with differences in PTs bioelectrical state. These differences are seen when comparing either the apical regions or the shank regions, but the differences are also reflected within the same cells because the MPG steepness differs between the genotypes. PT growth is especially affected by MPG differences as demonstrated in the genotypes *aha6/8* and *aha6/8/9*. The lack of AHAs in the PT shank deregulates pH homeostasis decreasing the intracellular pH gradient by approximately 0.5 which consequently affects many other cellular processes relevant for PT development and polarity maintenance. Indeed, studies in lily PTs have shown that either alkalinization or acidification treatments reorganize the actin cytoskeleton, especially at the apical region, likely because the apical region is the first being affected by external pH changes (A. Lovy-Wheeler, 2006). In other apical growth systems like yeast, Pma1 is the ortholog of AHAs and does localize to the plasma membrane on the sides of the cell, largely excluded from the growing zones, like AHAs do. In fission

yeast, *Pma1* null cells are not even viable, but hypomorphic allele cells, although alive, show polarity and apical growth defects and the cells lose their elongated shape to become more spherical due to the disorganized and faint actin cables. Moreover, Pma1 hypomorphic cells were affected differently when exposed to an EF. Instead of orienting the apical growth perpendicular to the EF, growth was parallel to the EF which suggests a role of pH or H^+ currents in mediating electric effects on polarity (Minc & Chang, 2010). In fibroblasts, mutations in the Na^+/H^+ pump NHE1 cause cell migration defects and loss of directionality and focal adhesion remodeling was impaired (Choi, Webb, Chimenti, Jacobson, & Barber, 2013; Denker & Barber, 2002). In the single-cell *Dictyostelium discoideum*, Na^+/H^+ pump DdNHE1 is localized to the leading edge of the polarity region during cell migration. DdNHE1 null mutants still have directional sensing to cyclic-AMP, but cannot attain polarized morphology during growth, extending pseudopodia around the cell which makes them much slower (H. Patel & Barber, 2005). Additionally, pharmacological inhibition of NHE1 has been reported to inhibit migration in leukocytes, neutrophils, endothelial cells and, epithelial cells (Denker & Barber, 2002). These examples are evidence that transporters that regulate pH at the plasma membrane are critical for cell migration and cell polarity establishment.

Another effect from the AHA mutations is the effect in electrochemical gradient and the changes in the cytosolic polyelectrolyte solution that affects other ion dynamics like the anions. This is an important note, because the depolarization in the AHAs mutants is the result of a complete reshaping of the ion dynamics due to the compound effect of the pH changes in the cytosol and H^+ currents that in turn affect the anion

dynamics too. The less steep MPG in the AHA mutants also accounts for a smaller EF at the pollen tube tip that can affect the processes dependent on electrotaxy like vesicle fusion, thus it may explain the slower growth rate in these mutants.

In the case of the CHX21/23 mutant, PTs are more hyperpolarized, approximately 25mV, in relation to the WT. The MPG in this mutant is also comparable with WT and does not present any difference in the growth rates. This is another instance in which the MPG seems to be correlated with growth rates in PTs. This mutant fails to target the ovules which suggests that either the chemotropic pathways are being disturbed by the change in either the bioelectrical state or the cytosolic K^+ concentrations. We would have liked to express GEPII in the *chx21/23* background to investigate whether the cytosolic K^+ concentrations are affected, but we have not been successful so far due to the fertility phenotype and low seed yield of these mutants. A study in rice PTs have shown that RUPO from the *Catharanthus roseus* Receptor-Like Kinase (CrRLK1L) family interacts with members of the K^+ transporter family HAK. RUPO PT mutants have an early burst phenotype and pollen grains have 35% more K^+ content than WT. RUPO gets auto-phosphorylated and interacts physically with HAK channels to regulate their function and in turn regulate K^+ homeostasis (L. Liu et al., 2016). HAK belongs to the family classified as proton-coupled KT/HAK/KUP-type K^+ transporters which are associated with fine tuning of K^+ uptake, like the voltage-independent K^+ channels of the TPK family or the voltage-gated K^+ channels of the SHAKER-type (Gomez-Porras et al., 2012). Members of the CrRLK1L family were identified in many processes involving PT-ovule interaction, control of cell-elongation and cell expansion like FERONIA, ANXUR1/2, THESEUS 1, HERCULES1/2 and

BUPS1 (RUPO ortholog) (Kessler, Lindner, Jones, & Grossniklaus, 2015). Not surprisingly, the reproductive phenotypes associated with CrRLK1L mutants are precocious PT burst in the case of ANXUR and BUPS that are expressed in pollen tubes, while FERONIA, expressed in the ovule and not in pollen, yields phenotypes where PTs do not burst in the contact with the ovule (Kessler et al., 2015; X. Zhou et al., 2021). The work with BUPS shows that CrRLK1L receptors interact and contribute to the phosphorylation state of H^+-coupled K^+ transporters, a key step in the regulation of these channels and in turn in controlling K^+ homeostasis (Y. Wang & Wu, 2013). CrRLK1L are a subfamily that belongs to the family of Receptor-like kinases (LRK) that includes another subfamily of Leucine-rich repeat receptor kinases (LRR-RK)(Galindo-Trigo, Gray, & Smith, 2016). PRK6 is an LRR-RK and is the only receptor identified for LUREs, the chemoattractant secreted by ovules (M. Liu et al., 2021; Zhang et al., 2017). Although PRK6 mediated pathway is not solely required for PTs attractions, it does play a role during the chemotropic response especially in conspecific PTs attraction(M. Liu et al., 2021). The indication that CrRKL1L receptors can interact with K^+ channels and that this interaction may be important for K^+ homeostasis could point to possible interaction of LRR-RK proteins with other K^+ transporters like CHX. We can only hypothesize that *chx21/23* PTs may be lacking the interaction with receptors that directly transduce the chemotropic sensing. CrRKL1L receptors are activated by Rapid Alkalinization Factors (RALFs) opening also an obvious interface between pH regulation and the activation of these recetpors

CHX21 and 23 are H^+/K^+ exchangers but antiporters usually work in both ways. Given the influxes of H^+ and the K^+ gradient shown by GEPII, it follows

that CHX21 and 23, localized at the PT tip are uptaking H^+ in exchange by K^+ from the cytosol. In order to understand CHX function at the PT tip, the electrochemical gradient of H^+ and K^+ were calculated in table III. The electrochemical gradient for each ion was calculated to understand which ion is following its electrochemical potential, because antiporters usually use the energy of the ion that is crossing the membrane in favor of its electrochemical potential to take the other ion against it.

$$\Delta G = RT\ ln\left(\frac{[A^+]in}{[A^+]out}\right) + F.z.\Delta Vm$$

The first parameter is the Nernst equation and represent the concentration/chemical gradient and the second parameter pertains to the electrical gradient where:

z is the valence of the ionic species. (K^+=1)

F is the Faraday's constant and is equal to 96485 $C.mol^{-1}$ (Coulombs per mole).

ΔVm is the voltage difference across the membrane.

The ΔG for H^+ are all negative values, which means that H^+ may enter the cell passively. The ΔG for K^+ goes from positive to negative with increasing hyperpolarization, meaning that between 0 and -50mV it is required energy to make K^+ go into the cell which is the same to say that K^+ can passively cross the membrane from the cytosol to the outside because it is the reverse direction. In the WT scenario, where

the apex is at approximately -100mV, H^+ enters the cell passively while K^+, being very close to equilibrium, will require the H^+ excess energy to move out of the cell.

At -150mV, which is closer to the apical values between 5-10um, both H+ and K+ can passively be transported into the PT because both have negative ΔG but the H^+ electrochemical gradient is three times higher than that for K^+. Hence, H+ should go into the cell and the exceeding energy will carry K+ out of the cell. In spite of not knowing the stoichiometry of CHX channels, it has been previously hypothesized that $2H^+ \leftrightarrow K^+$ as a response to alkaline stress, in which the cell would have this mechanism to maintain the cytosolic pH close to neutral (Sze & Chanroj, 2018). This mechanism suits the PT model perfectly, because the ion currents created match the ones observed, and the uneven movement of positive charges into the cell (with a net gain of +1) would depolarize the cell. Given *aha6/8/9* PTs bioelectrical state, at approximately -18mV, ΔG for H+ is near equilibrium while K+ can passively be transported out of the cell. In aha6/8/9 PTs the reverse happens in WT, because the energy from the passive K+ transport is used to bring H+ inside the cell.

Table III - Calculations of the electrochemical gradient for H+ and K+ given the intracellular and extracellular concentrations at different membrane potentials (kJ/mol)

	pH (H+)		**K+**	
Concentrations (tip)	7.5 out/7.5 in		5mM out /250mM in	
mV	ΔG(H+)	H+ driving force	ΔG(K+)	K+ driving force
0	0.0	equilibrium	9632.7	strong outward
-50	-4824.3	inward	4808.4	outward
-100	-9648.5	strong inward	-15.8	near equilibrium
-150	-14472.8	strong inward	-4840.1	inward
-200	-19297.1	strong inward	-9664.4	strong inward

This calculations exemplify how the apical MPG can change ion transport dynamics along the PT by impacting the electrochemical gradient and the driving force of each ion, but in this antiporter example, either H+ or K+ can use their energy to transport the other when voltage changes. However, if we consider a passive channel for a specific ion, these differences in voltage along the PT may translate into a more drastic response of the direction of the currents. The same for voltage-dependent channels that can be active at a region of the MPG and not in the shank, or vice-versa.

Chapter 4: Effects of membrane potential on lipid lateral segregation and micro-domain formation

4.1 Introduction

Biological membranes have three kinds of potentials: 1) the transmembrane potential that is the readout of the electric potential between the cytoplasm and the bulk of extracellular medium, 2) the surface potentials that result from the accumulation of charges at the membranes interface, and 3) the dipole potential, the potential arising from the dipolar components of the phospholipids and interface with water that spans the hydrophobic core of the bilayer (fig.22) (L. Wang, 2012). Here, I want to focus on the surface potential that is generated by the charged head groups of phospholipids and the adsorbed ions at the interface. Anionic lipids are ionizable and dissociate, resulting in electrostatic attraction between the charged head groups and the counterions in solution (Cohen & Venkatachalam, 2014). The electrostatic effect of the surface potential with the inner Helmholtz layer of cations – resultant of the electrostatic attraction of ion into a screening effect around the membrane - forms an electrical double layer or also known as sub-membrane voltage (Savtchenko et al., 2017). It is important to note that the sub-membrane voltage is generated by local charge accumulation and it is essentially what controls the voltage-dependent activity of membrane proteins. A common example is ion channels, in which their molecular sensors are driven by electric fields at the nanoscopic scale, in close proximity of the membrane surface, rather than the transmembrane potential readout obtained with electrodes, away from the membrane (Bezanilla & Perozo, 2003; Catterall, 2010).

Another effect that comes from the surface potentials attracting counterions to its vicinity is enhancing or depleting the availability of ions close to the ion channels, consequently affecting the rates at which the ions enter the pore. The same effect happens for charged ligands or drugs that can be attracted by surface potentials to then bind the target receptors in the membrane (Cohen & Venkatachalam, 2014; Savtchenko et al., 2017).

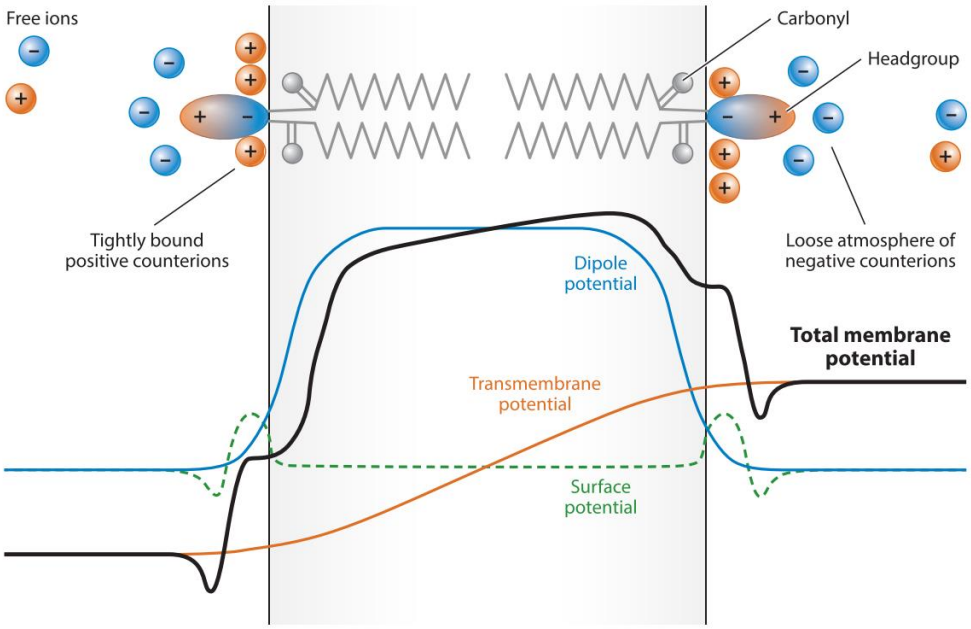

Fig. 22 | Representation of three potentials contributing to the electrical potential profile in a membrane. Charged anionic lipids create the surface potential and the dipole of the lipid headgroups create the dipole potential. This membrane is symmetrical in both leaflets, thus the surface and dipole potential are shown as straight lines. If either of these quantities is asymmetric across the lipid bilayer, then an electric field may permeate the membrane (similar to the black line). This intrinsic electric field is undetectable by conventional patch clamp and does not affect equilibrium ionic distributions in the bulk. However, it does act on the conformations of transmembrane proteins and regulates membrane permeability. (image adapted from (Cohen & Venkatachalam, 2014))

The surface potential difference is generated due to the inherent asymmetric lipid distribution between the inner and outer leaflet. Zwitterionic lipids like phosphatidylcholine (PC) are usually found in the outer leaflet, while aminophospholipids, such as phosphatidylethanolamine (PE) and Phosphatidylserine (PS) are predominantly located in the inner leaflet (Gurtovenko & Vattulainen, 2008; Wiese et al., 1996). The imbalance of anionic lipids in the inner leaflet and neutral lipids in the outer leaflet produce transmembrane electric fields, even in the complete absence of ion imbalance, indicating that the asymmetrical distribution of differently charged lipids is enough to produce nonzero transmembrane potentials (Gurtovenko & Vattulainen, 2007, 2008; Wiese et al., 1996). In fact, membrane asymmetry is so well regulated that the appearance of anionic lipids in the outer leaflet like PS, are indicative of cell death (Schlegel & Williamson, 2001).

The effects of surface potentials are usually studied in artificial membranes systems (liposomes or monolayers) and with mathematical modeling. In biological membranes, lipid composition is not stationary as in artificial membranes, and the composition of the different phospholipids changes over time and space. Thus, the effects of surface potentials can be even more pronounced in cases where there is the formation of lipid micro-domains or “rafts”. The concept of lipid rafts originated from animal studies on the polarization of sphingolipids in epithelia membranes and on glycosylphosphatidylinositol-anchored (GPI-anchored) proteins that were found to partition in low-density sphingolipid or cholesterol enriched phases (Brown & Rose, 1992). Lipid rafts, or microdomains, are isolated as non-ionic detergent resistant

membrane (DRM) fractions from animal, yeast and plant membranes, and are enriched in sterols and sphingolipids (Martin, Glover, & Davies, 2005). While animals and yeast seem to have only one class of sterol and sphingolipid, plants are much more diverse showing that DRMs contain several sterol molecules (24-methylcholesterol, sitosterol, and stigmasterol) and two distinct classes of sphingolipids (inositolphosphorylceramides and glucosylceramides) (Markham, Li, Cahoon, & Jaworski, 2006; Mongrand et al., 2004). Through non-random lateral separation of these particular lipids, the plasma membrane organizes in specialized micro domains that recruit proteins to specific areas and define regions of membrane function (Carland, Fujioka, Takatsuto, Yoshida, & Nelson, 2002). Lipid microdomains may recruit proteins with hydrophobic modifications, e.g. GPI anchors, transmembrane proteins like ion channels, and signaling protein families that include kinases, heterotrimeric and monomeric G proteins (Foster, De Hoog, & Mann, 2003), which, when brought together, may enhance and/or trigger signaling cascades (Field, Holowka, & Baird, 1997). Unfortunately, there has not been any advances on live-compatible sterol or sphingolipid probes, but research in fixed PTs using the sterol binding dye filipin showed accumulation of sterols in the apical region of the cell, suggesting microdomain formation (Moscatelli et al., 2015).

Anionic phospholipids may also organize in functional micro-domains/clusters that are often related to cellular processes related to polarity, for example in the cell plate establishment upon division, the casparian strip establishment, root hair and pollen tube growth, and even during biotic interactions with mycorrhizal symbionts or pathogens (reviewed in (Noack & Jaillais, 2020; Platre & Jaillais, 2017)). Recent work on Arabidopis roots have shown that phosphatidylserine (PS) clusters with ROP6 (Rho GTPases of Plants) and is required for ROP6 signaling during development. In fact, lateral distribution of membrane components has been the focus of research as a process of membrane functionality and regulation. Evidence suggests that the lateral redistribution of lipids into micro-domains is significantly regulated by membrane potential which affects the membrane structure in multiple ways: shift in phase-transition temperature (P. Herman, Malinsky, Plasek, & Vecer, 2004), destabilization of cholesterol-phospholipid complexes (Radhakrishnan & McConnell, 2000) and, theoretically, domain separation of lipids with different acyl chain lengths (Schäffer & Thiele, 2004). In yeast cells, it was shown that a sustained membrane potential depolarization always decreases the gel-like microdomains regardless of the depolarization protocol that the cells are subjected to (Petr Herman et al., 2015). In another study, in mammal cells, depolarization induces micro-domain formation of PS and PtdInst(4,5)P_2, and because K-Ras is targeted to the plasma membrane by electrostatic interaction with PS, depolarization amplifies K-Ras–dependent mitogen-activated protein kinase (MAPK) signaling (Yong Zhou et al., 2015). Thus, it is likely that the effect of membrane potential in lipid distribution and organization may control

the gain in signaling pathways by bringing lipid-proteins complexes together to enhance the downstream cascades.

In this chapter, I investigate the effects of membrane potential on phospholipid micro-domain formation and the possibility of lipid segregation along the MPG-induced electric field.

4.2 Results

4.2.1 Phosphatidylserine (PS) and Phosphatidylinositol-4,5-bisphosphate (PtdInst(4,5)P_2) accumulation pattern in pollen grains and pollen tubes

To investigate the localization of lipid domains, we created Arabidopsis transgenic lines expressing the $C2^{Lact}$-GFP that specifically binds to PS, and PH^{PLC}-GFP that specifically binds PtdInst(4,5)P_2, driven by the pollen specific promoter LAT52. We chose these two anionic lipids due to their roles in cell polarity and morphogenesis. In pollen grains, PS is localized to the sperm cells plasma membrane and it accumulates in the pole of the pollen grain, where the development of the pollen tube is going to take place (fig.23 a). As shown when the PT emerges, there are many small vesicles highly enriched in PS in the inverted cone of vesicles in the apical region, as PS is an important lipid that participates in vesicle fusion. Consequently, the apical region of the plasma membrane is also enriched in this lipid likely due to the PS-enriched vesicles fusion at the apex of the PT (fig.23 b left). Right after pollen grains are hydrated, there are highly fluorescent speckles in the PG highly enriched in PS, which may be multivesicular bodies enriched in PS (fig.23 b, right). PtdInst(4,5)P_2

localizes in the plasma membrane apical domain of the pollen tube and readily accumulates when the PT starts developing the protrusion in the pollen grain (fig.23 c), and in later stages maintains the apical domain at the apex (fig.23 d). This was expected as these two anionic lipids are always correlated with cell polarity.

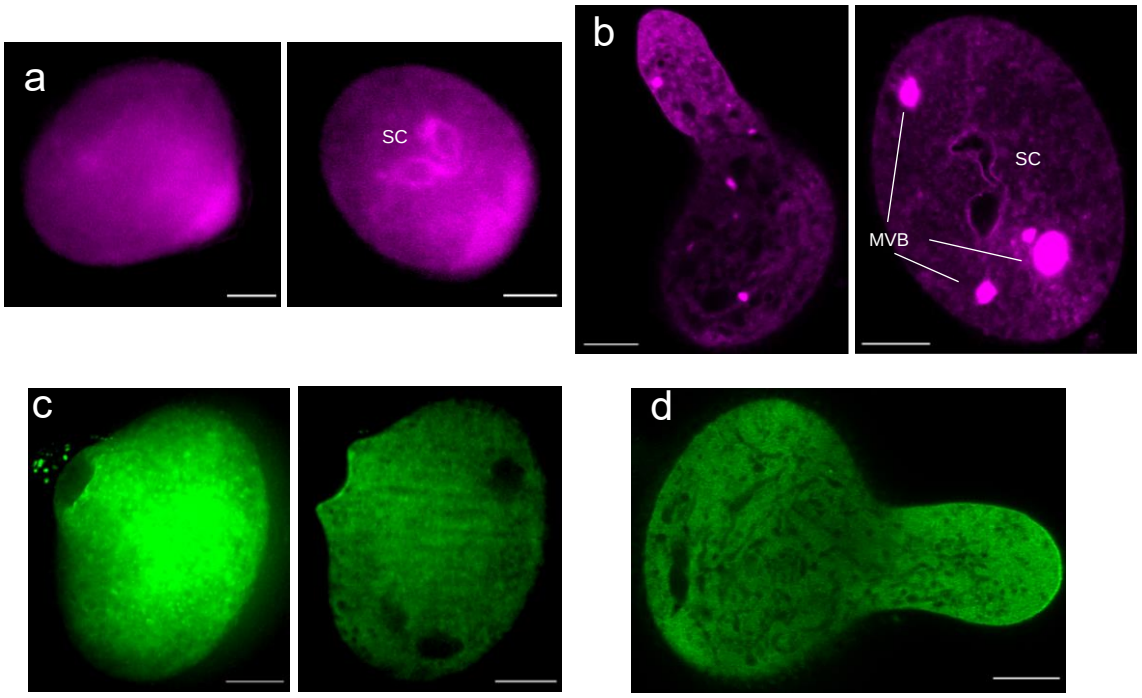

Fig.23 |PS and PtdInst(4,5)P_2 probes in pollen grains. (a,b) PS accumulates at the protrusion that later becomes the pollen tube and localizes to the sperm cells (SC).(b) PS accumulates at the PT tip and in highly fluorescent speckles that are thought to be multivesicular bodies (MVB). (c,d) PtdInst(4,5)P2 localizes to the apex of the pollen tube and accumulates at the protrusion site (c, left 3D visualization, right single image from the stack). The lines are overexpressing the probes under LAT52 promoter. Scale bar 5µm

When PTs are growing, the small apical vesicles and sperm cells are still enriched in PS but the distribution profiles along the plasma membrane are variable (fig.24 a,b,c). The apex of the PT is usually enriched in PS with variable size domains however, there are cases in which the shank is highly enriched after the first 20µm (fig.24 a, c) and other cases where it is more homogeneously distributed (fig.24 b). A

feature that is seen in many PTs is a PS depleted area around 10μm (fig.24 a, c), in close proximity to where the inversion point of ion fluxes happens. PtdInst(4,5)P_2 is exclusively enriched at the tip, and the rest of the plasma membrane has low to no abundance of this lipid (Fig.24 d). The high expression of the probe in the cytoplasm makes it difficult to ascertain whether the shank contains PtdInst(4,5)P2. This localization is expected because other works have shown that in PTs, the enzyme that synthesizes this lipid - PI4P5-Kinase – is localized at the PT tip (Ischebeck et al., 2008; Sousa et al., 2008).

The different lipid distribution of PS in variable domains was a good target to test whether these different distributions were affected by electro-diffusion as a consequence of the MPG variation. This could explain the lipid domains enriched at the tip and the more depleted domain of PS in the subapical region. By tracking membrane potential with VSDs in the PS or PtdInst(4,5)P_2 transgenic lines, one could investigate whether the variation in MPG size is correlated with differences of the lipid profile distributions. Unfortunately, when these transgenic plants were made, we had not established the VSDs and chose to fuse GFP to the PS and PtdInst(4,5)P_2 probe, but GFP excitation and emission spectra overlaps Annine-6plus and Fluovolt dyes spectra.

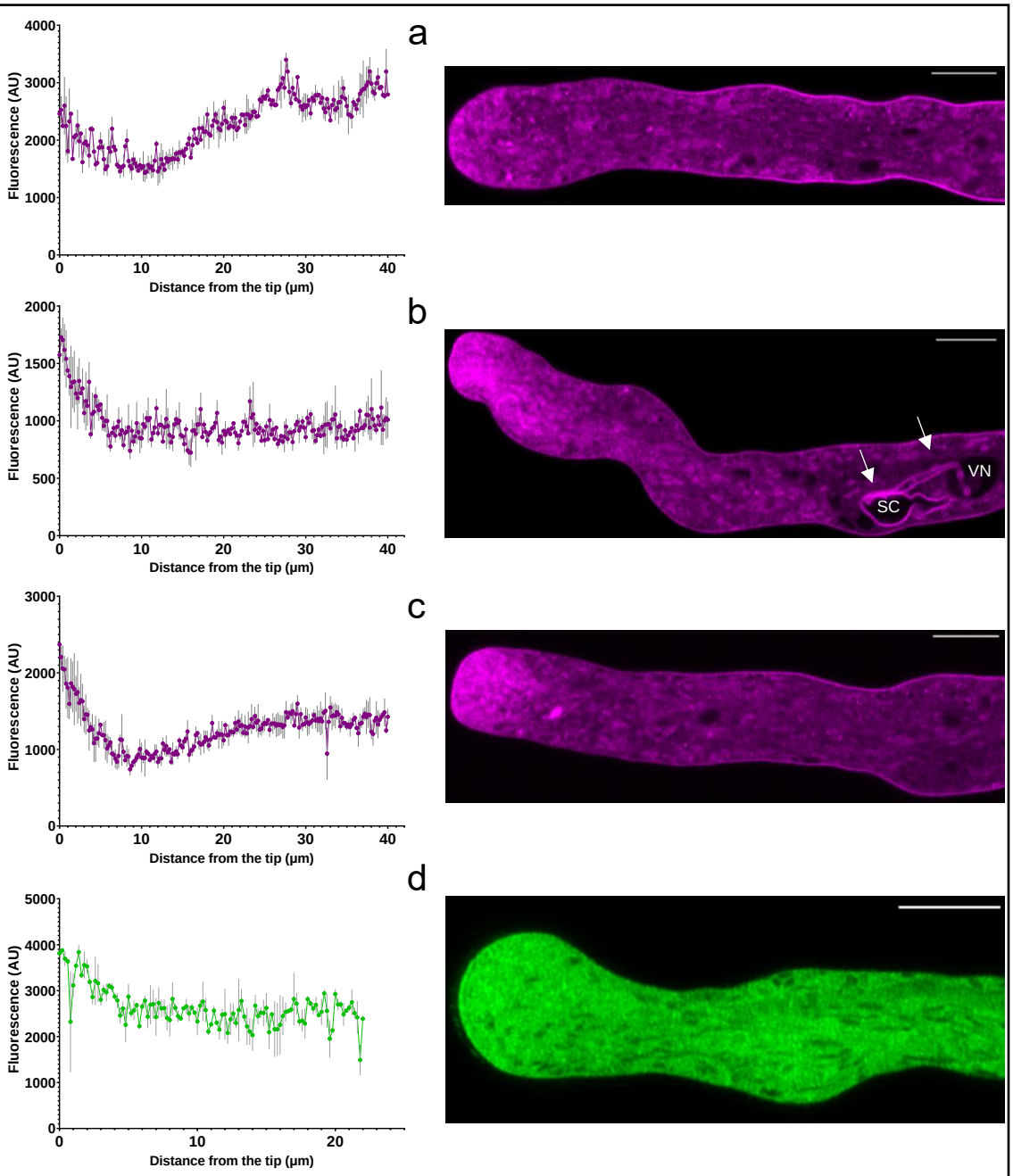

Fig. 24 |Exploring lipid domains in the pollen tube (a,b,c) PS probe in pollen tubes have different distribution profiles. (a) PS increases along the PT, (b,c) PS is highly labeled at the PT apex, followed by less accumulation in the subapical region (between 10-15um). Sperm cells (SC) membrane attaches the vegetative nucleus (VN) has high PS content. (d) PtdInst(4,5)P_2 localizes only at the very apex of the PT

4.2.2 Overexpression of lipid probes cause developmental phenotypes

Over the course of working with these transgenic lines, it was clear that the overexpression of the PS and PtdInst(4,5)P_2 probes cause developmental problems in pollen tubes. Most PTs in the PS transgenic lines showed many dents and constrictions throughout the tube, suggesting that PTs are changing direction more erratically or growing less uniformly (Fig.25 b,d). In some cases, PTs created protoplasts at the pollen tube tip, which can be induced experimentally by plasmolizing PTs and during recovery of turgor expose them to a solution of pectinase to soften the cell wall or in some ion channel mutants, such as GLRs (Wudick, Portes, et al., 2018). In PTs expressing the probe for PtdInst(4,5)P_2 there were also some cases of erratic growth, but the more common phenotype was tip ballooning, despite less severe than the PS probe.

Our reasoning was that the overexpression of the probes that are based in domains of other proteins fused with GFP may be hindering the binding of important proteins involved in polarity processes, hence creating defects in growth. As shown, the C2 domain of Lactadherin (Lact-C2 specific for PS)(Shao, Novakovic, Head, Seaton, & Gilbert, 2008) or the Plekstrin homoly domain from phospholipase C ($PLC\delta_1PH$ specific for PtdInst(4,5)P_2) (fig.25 a,c) (Várnai et al., 2002) are not negligible in size and carry a GFP molecule may obstruct the access to the lipids and membranes. Moreover, acquiring homozygous lines for PS probe proved to be quite difficult, which led me to test whether the transmission of the transgene was somehow related to the PTs developmental defects.

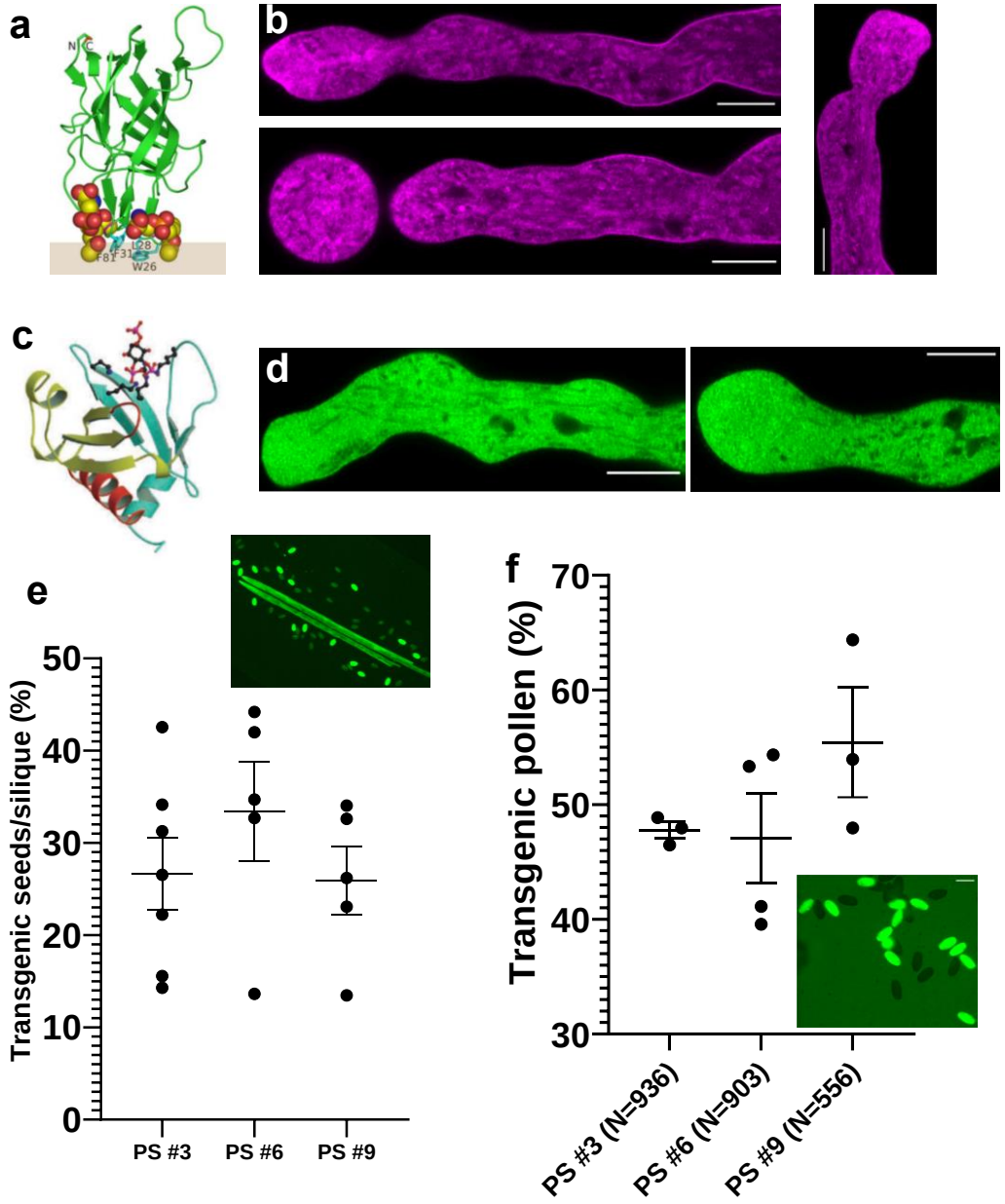

Fig. 25 |Developmental and fertility defects as a consequence of the lipid probes overexpression (a,b) PS probe and (c,d) PtdInst(4,5)P_2 probe. (a) PS and (b) PtdInst(4,5)P_2 probe crystal structure (Images (a) and (c) adapted from (Shao, Novakovic, Head, Seaton, & Gilbert, 2008) and (Várnai et al., 2002), respectively. (b,c) (e) Progeny from the cross between pollen from a heterozygous plants for the PS-probe transgene with WT flowers (3 independent lines). Every fruit tested had lower than 50% transgene transmission, implying that pollen tubes expressing the PS probe are performing worse than WT. (f) Percentage of pollen grains showing fluorescence from the 3 independent lines expressing PS-probe to check whether the plants had only one insertion of the transgene.

Heterozigous plants for the PS probe transgene were crossed to WT plants, and the number of seeds per silique carrying the transgene were counted, by the transgene marker that expressed GFP on the seed coat. All three independent lines showed that the transgene is always transmitted below 50% (the expected ratio), and overall transmission is about 30% indicating problems in PTs development *in planta* (fig.25e). To investigate if the lines had more than one insertion of the transgene, pollen grains of these heterozygous lines were counted to confirm that 50% of them express the probe. The observed values of fluorescent pollen grains were always around 50% (fig.25 f), indicating that the three independent lines have only one copy of the transgene and the lower transmission rates do not come from a distorted segregation or multiple transgene alleles segregating independently in the gametes. Instead, transmission rates may arise from developmental defects caused by PS overexpression, which consequently results in WT pollen outcompeting the transgenic ones. The lines with the probe for PtdInst(4,5)P_2 did not show any transmission problems.

4.2.3 The effect of electric fields on lipids lateral electro-diffusion

The goal in investigating anionic lipid domains was to understand how electric fields along the plasma membrane influence their distribution by a process called lateral electro-diffusion, in which the lipids can migrate along an electric field accordingly to their nominal charge. To test this, I used the depolarization protocols optimized for VSDs and applied them in these lines.

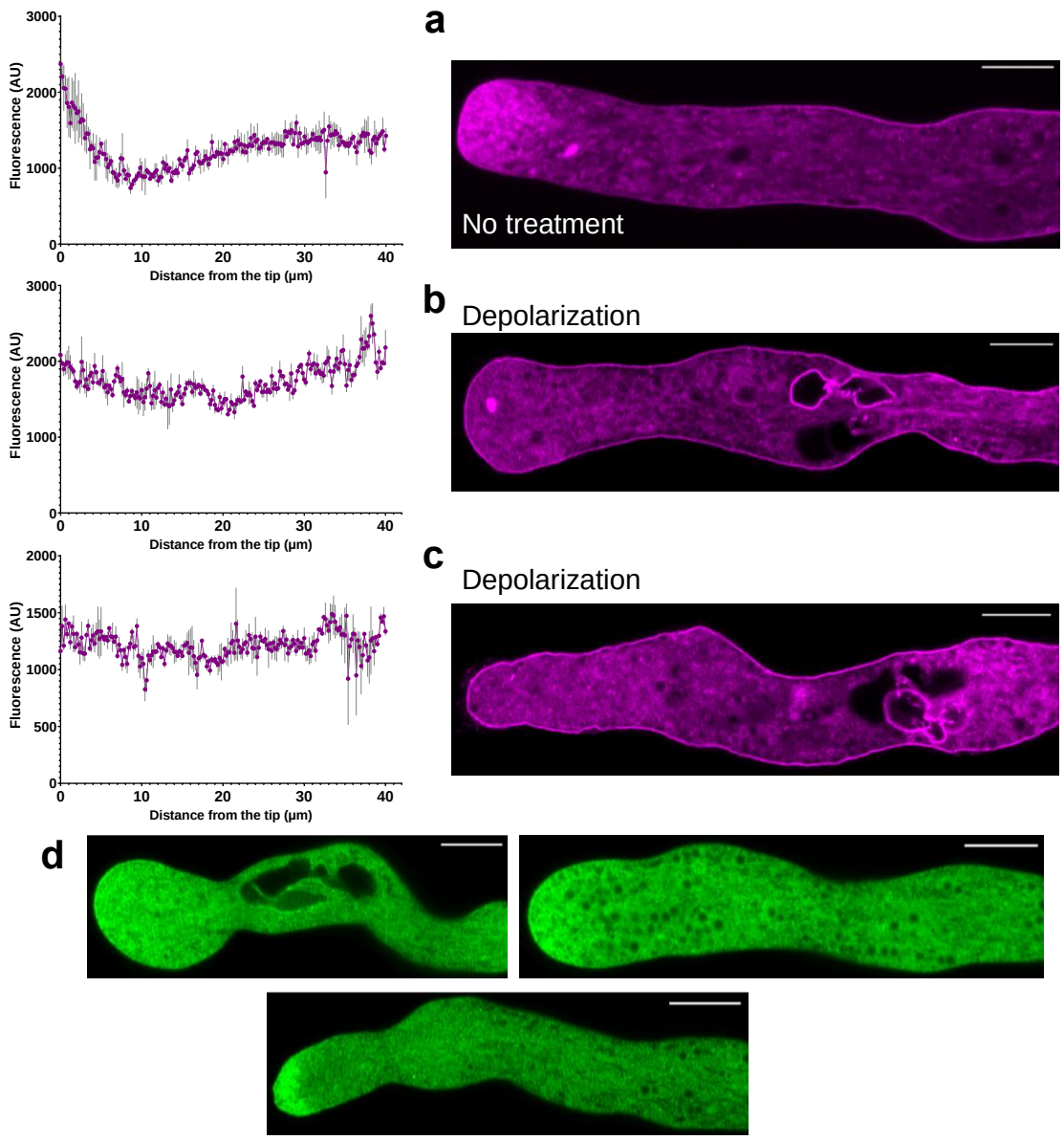

Fig.26 | Depolarization and salt stress effects on lipid distribution. Pollen tubes were treated with 30uM valinomycin and 150 mM KCl to induce membrane depolarization. (a) Control (b,c,d) depolarization protocols. PS becomes more uniformly distributed throughout the whole plasma membrane (b,c) whereas PtdInst(4,5)P_2 does not change the apical localization.

PTs expressing PtdInst(4,5)P_2 probe did not have significant alteration on the change of the apical domain of PtdInst(4,5)P_2 upon the depolarization protocol were

employed (fig. 26 d). The apical domain was maintained and in some cases it was clear that PtdInst(4,5)P_2 accumulates in the apical vesicles (fig. 26 d, bottom).

As for the PTs expressing the PS probe, the depolarization made the PS distribution profile more uniform along the entire tube and the inverted cone of apical vesicles disappeared because the depolarization induces growth arrest (fig.26 b, c). Although these results were somewhat promising, the depolarization protocols involve a salt stress response due to the use of 150mM KCl in the medium to dissipate the electrochemical gradient and salt stress was shown to change the lipid composition by triggering different lipid synthesis, especially PS and PtdInst(4,5)P_2 at similar time frames as our experiments (Lv et al., 2021). Thus, artificial depolarization protocols might not be the best approach to studying this phenomenon.

Given that the AHA mutants showed to be naturally depolarized, I crossed the lipid probe lines with *aha6/8* mutant to investigate whether the depolarization in these mutants affects the lipid distribution profiles. Although the mutant *aha6/8/9* was the prime choice because it is more depolarized, crosses with this mutant revealed to be unattainable because of the severe fertility and the low seed set phenotype. It was not possible to create the homozygous lines from the crosses between PtdInst(4,5)P_2 with *aha6/8*, as though the combination of the mutations with the overexpression line was somehow deleterious, and heterozygosity of AHA6 and 8 was favored.

Despite the PS probe transmission rates being low, the homozygous plant *aha6/8*+PS probe was obtained and PTs were imaged. The apical plasma membrane PS-enriched domain was maintain as previously described in the WT and the shank did

not show any differences either (fig.27). However, the inverted cone PS-enriched vesicles accumulate more in the apical region, likely related with the growth rate of *aha6/8* mutants. The slow growth rate implies less membrane incorporation and there may be accumulation of more PS-enriched vesicles that are ready to be delivered.

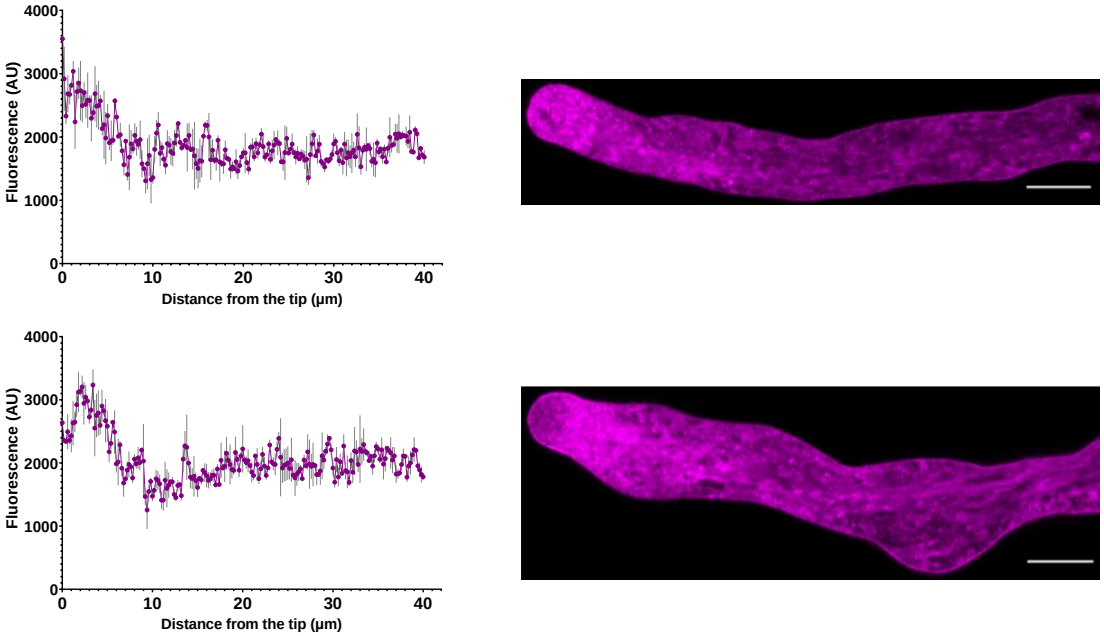

Fig.27 | PS distribution on aha6/8 mutants does not differ significantly. Two examples of aha6/8 mutants expressing the PS probe, not showing different distributions of PS despite being more depolarized. Inverted cone of apical vesicles is more noticeable and it advances farther in the shank than WT PTs.

4.3 Discussion

The main goal of studying anionic lipid domains associated with polarity was to understand how the MPG at the PT tip could influence lipid distribution but our approach proved to have some fundamental issues that were not easily solved without redoing the transgenic lines: 1) Lipid probes overexpression affected PTs development, 2) lipid probes fluorescence saturates the cytoplasm to a point where small differences in the lipid accumulation in the cytoplasm processes may be difficult to assess (like trafficking pathway) , 3) these probes are labeled with GFP, whose spectrum overlaps with the VSDs spectra, which does not allow for multiple probe acquisition for a correlation analysis between MPG and lipid domains.

Nevertheless, our preliminary results with these probes showed some interesting features of lipid distribution in the apical region that are worth testing further. PS-enriched apical domain is usually followed by the sub-apical area depleted in PS which correlates with the range of the MPG and the ion fluxes reversion points in PTs. The bacterial and yeast phosphatidylserine synthase (PSS), the enzyme that converts CDP-diacylglycerol (CDP-DG) and L-serine(Ser) to PS, was shown to have a pH dependency and the peak of activity above pH 7(Bae-Lee & Carman, 1984; Yamaoka et al., 2011). Although in plants PSS has a different function because it is thought to convert phosphatidylethanolamine (PE) in PS instead, we cannot discard the possibility that the enzyme is pH dependent (Yamaoka et al., 2011). In that case, the pH gradient in the cytosol could explain the apical PS-enriched vesicles because the pH at the tip is 7.5 and only becomes more acid along the shank, outside the peak of enzymatic activity – if we assume that PSS in Arabidopsis have similar pH-

dependency as in bacteria. PSS is a membrane protein with at least 9 transmembrane domains that localizes to the secretory pathway, which suggests that all the plasma membrane enrichment comes from the delivery of vesicles at the apical region. Thus, it is possible that the PS depleted area in the subapical region is the result of enzymatic activity that breaks down the PS to phosphatidylglycerol (PG) or PE. However, when this PS depleted area is detected, PS levels increase to parts of the shank farther from the tip which could suggest that the apical depleted area is under the influence of other factors like the electric field or enzymes that are restricted to that area do break down PS. In any case, it would be interesting to understand how this division in PS-enriched areas between the apex and the shank exist. Failure to control the PS-enriched area at the apex could promote vesicle fusion away in the sub-apical area and hinder directional growth.

PtdInst(4,5)P_2 probe only showed a small enriched area at the apex, correlating well with previous data on the localization of the enzymes that synthesize this lipid, PI4P5-Kinases (Ischebeck et al., 2008; Sousa et al., 2008). PI4P5K is anchored at the plasma membrane through lipid modifications in its structure, where it synthesizes PtdInst(4,5)P_2. Arabidopsis PI4P5K is an ortholog of the bacterial Ciona intestinalis Voltage Sensitive Phosphatase (Ci-VSP) and mammal's PTEN homologous inositol lipid phosphatase (Kurokawa et al., 2012). Ci-VSP has a voltage sensitive domain that was used as a tool to construct the genetically-encoded FRET voltage reporter VSFP (Dimitrov et al., 2007). Both Ci-VSP and PTEN orthologs have voltage-sensitive domains that are activated upon depolarization, synthesizing more PtdInst(4,5)P_2 (Kurokawa et al., 2012). The function of these orthologs points to a common function

that may be conserved in plants too. If that is the case, the MPG depolarization at the apex may be regulating the area where PtdInst(4,5)P_2 is synthesized and changes in PTs bioelectrical state may possibly have a big impact in PtdInst(4,5)P_2. This could explain the fact that we could never find a homozygous plant for the PtdInst(4,5)P_2 probe and *aha6/8* as the depolarization of these PTs may deregulate PtdInst(4,5)P_2 synthesis resulting in male gametophyte fertility problems. Surprisingly, the depolarization protocols did not have any effect in PtdInst(4,5)P_2 distribution, even knowing that salt stress increases the synthesis of this lipid (Zarza et al., 2020). There is the possibility that the overexpression of this lipid probe did not allow the detection of differences upon depolarization.

Furthermore, our results showed that the genetically encoded lipid probes may affect cellular processes. The lipid probes are based on domains that bind to specific lipids, and these domains may obstruct protein interactions with lipids. Both PS and PtdInst(4,5)P_2 are important lipids for cell polarity, involved in tethering proteins from the trafficking pathway (Yuelong Zhou et al., 2020) and exocyst (Bloch et al., 2016), which are pivotal for normal pollen tube growth. PS forms lipid nanodomains that anchor proteins that define polarity in the cell, like Rhop – GTPases (Platre et al., 2019). Disruption of ROP1 in pollen tubes creates ballooning in the pollen tube tip, because growth is not restricted to the apex, and growth becomes isometric (Gu et al., 2003), like we saw in some cases with the PtdInst(4,5)P_2 and PS probes. This suggests that the binding of the lipid probes covers the lipid electrostatics by impairing important cellular processes like polarity and vesicle delivery. Another aspect in which the lipid probes can affect normal physiology is at the ion homeostasis level because anionic

lipids are required for some ion channels to perform their functions properly (Hille et al., 2015; Pant et al., 2021; Tillman & Cascio, 2003). In plants, it has been shown that PtdInst(4,5)P_2 kinases are involved in polyamines-triggered K^+-efflux responses to abiotic stresses. The PtdInst(4,5)P_2 kinases are triggered by polyamines and produce more PtdInst(4,5)P_2 that may modulate the channels responsible for the K^+ efflux. Mutants for two PtdInst(4,5)P_2 kinases had 70% less K^+ efflux compared to WT when elicited with polyamines suggesting that not having an increase in the synthesis of PtdInst(4,5)P_2 at the plasma membrane affects K^+ channels.

Chapter 5: Plant Glutamate-Like Receptor in Root Wound Healing and Regeneration

5.1 Introduction

Plants have an astounding capacity to regenerate their organs after damage by establishing regions of growth and patterning. Root meristems are one such example in which after excising the root apical meristem with the quiescent center (stem cell niche) and its supporting cells, regeneration and growth ensues normally. Single-cell RNA sequencing and lineage tracing of root cells shows that multiple cell types can revert to stem cells. Before becoming stem cells, the transcriptome of the regenerating cells resembles that of an embryonic root progenitor (Efroni et al., 2016).

With this previous results, Birnbaum's group started working towards understanding the processes of chromatin remodeling that happen to the cells undergoing the reversion process to stem cell fate. To characterize these changes in cellular reprogramming, cells in the domain of the root tip or root stump were targeted

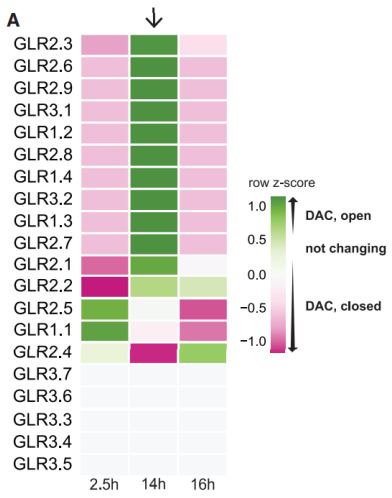

Fig.28 | The GLR family undergoes rapid chromatin modification and transcriptional regulation (A) Heatmap showing trends in chromatin accessibility among GLRs during regeneration at three time points representing hours post cut (DAC – differentially accessible chromatin). Color represents the relative accessibility as a row Z score, which is standard deviations from the row mean. Arrow points to a trend of opening chromatin at 14 h among a subset of GLRs.

for analysis in the first 24h after being excised. The expression marker of the root stem cell niche used was MONOPTEROS, that is removed by the excision but it reappears 2h after the damage in the stump (Cole et al., 2009). The cells expressing the marker were run on an Assay for Transposase Accessible Chromatin (ATAC)-sequencing protocol that aims to discover chromatin remodeling and accessibility and grossly correlates with changes in the transcriptional program of the cells. In the analysis, 12 members of the Glutamate-Like Receptor family were highly significant, showing that the chromatin of these genes were more accessible during the reprograming and hence, an indication that these genes should be required throughout the regeneration process (fig.28 a).

To test this hypothesis, they conducted root regeneration experiments with triple and quadruple mutants from the GLR family: (1) glr1.2/1.4/3.3, (2) glr3.1/3.2/3.3/3.6, and (3) glr1.2/1.4/2.2/3.3. To their surprise, all the triple and quadruple mutants had a higher % of regenerated roots than WT (fig.29 a). To test whether the GLRs function pre or post-wounding, they used GLR channels inhibitors by conditionally blocking GLR-mediated signaling after wounding. Gadolinium (Gd^{3+}) is a broad inhibitor of calcium channels, whereas AP5 and CNQX were originally described as antagonist of mammalian NMDA- and AMPA-type glutamate receptors, and later found to efficiently inhibit various GLR members in Physcomitrium and Arabidopsis (Michard et al., 2011; Ortiz-Ramírez et al., 2017; Wudick, Michard, Oliveira Nunes, & Feijó, 2018). The protocol of root excision was maintained, but roots were transferred to plates containing the aforementioned inhibitors after the cut. The

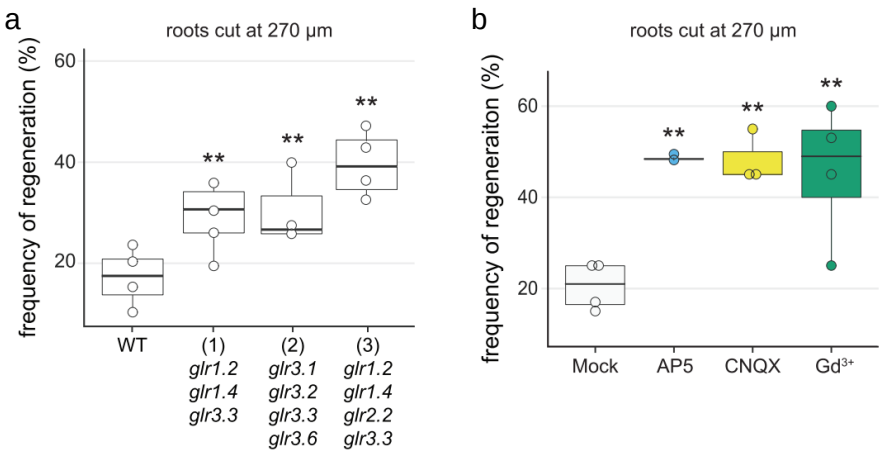

Fig.29 | Perturbation of GLR signaling improves regeneration in roots (a) Regeneration frequency of wild-type plants (Col-0) compared with triple and quadruple glr mutants: (1) glr1.2/1.4/3.3, (2) glr3.1/3.2/3.3/3.6, and (3) glr1.2/1.4/2.2/3.3 (chi-square test, Fisher's combined probability test; n > 19 for each genotype in each of 4 trials; **p < 10^{-7}). (b) Constitutive post-injury treatment (cut on treatment plates and kept on treatment plates for the duration of the experiment) of cut roots on various calcium signaling antagonists, showing enhanced regeneration on all treatments. Roots were grown on normal media, cut, and transferred to treatment plates (chi-square test, Fisher's combined probability test; n > 20 for each treatment in each of 4 trials, Gd3+ n > 12 one trial, **p < 10^{-11}).

three pharmacological treatments dramatically increased regeneration efficiency, up to 3-fold increase, even exceeding the effects seen in the glr mutants (fig.29 b). Tests on callus formation in leaves were conducted, a common technique used in tissue culture as a proxy to measure regeneration capability of the leaf tissues (fig.30). The percentage of leaves with callus formation was increased 20% on glr1.2/1.4/3.3 and 60% on glr1.2/1.4/2.2/3.3, but did not show any improvement in the clade 3 GLR quadruple mutant (2) (fig.30 a). This suggests that the GLRs from clade 3 may have a different role in roots than in the leaves. The use of CNQX in tissues culture yielded similar results, where the leaves treated with CNQX had increased callus formation more than 3-fold (fig.30 b) but the increase was not higher than in the *glr* quadruple mutant . The

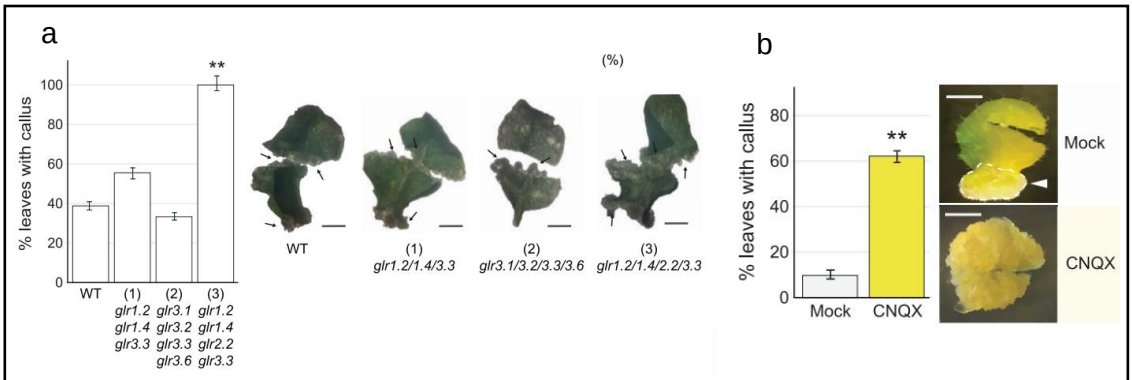

Fig.30 | Perturbation of GLR signaling improves callus formation (a) The glr quadruple mutant (3) shows enhanced callus formation, with bar graph showing percent of leaves that formed callus for each genotype, scored at 2 weeks post callus initiation. Right, representative images of callus formation in leaves. The error bars are proportional to the standard error of the pooled percentage computed using binomial distribution (chi-square test; n ≥ 32 for each genotype; $^{**}p < 10^{-9}$). Arrows indicate regions of callus formation. Scale bars, 0.5 cm. **(b)** Callus formation in leaves treated with the GLR antagonist CNQX is enhanced, showing percent of leaves with callus. The error bars are proportional to the standard error of the pooled percentage (chi-square test; n > 48 for each treatment; $^{*}p < 10^{-29}$) Scale bars, 0.5 cm.

higher increase in root regeneration and callus formation by pharmacological inhibition is likely a result of inhibiting more GLRs than the GLRs knocked out in the quadruple mutants, indicating that more GLRs function to suppress wound healing and regeneration.

To examine the downstream effects of pharmacologically blocked GLR signaling after wounding, an RNA-seq library was sequenced between Mock and CNQX treated roots and filtered the dataset for the top 10% most variable genes. In these cluster, most genes were identified as stress and defense –response GO terms (response to abiotic stimulus $p < 10^{-8}$, response to stress $p < 10^{-19}$, response to other organisms $p < 10^{-7}$). After analyzing the genes for the GO category defense, many genes were upregulated in the Mock samples but not in the CNQX treatment or glr

quadruple mutant. These results indicate that the CNQX treatment downregulates many stress response genes and that GLRs appear to be mediating the response to root damage.

Given the involvement of Jasmonic Acid (JA) in regeneration and in GLR-mediated defense (Mousavi, Chauvin, Pascaud, Kellenberger, & Farmer, 2013), the hypomorph mutant of CORONATINE-INSENSITIVE 1 (COI1) the primary receptor of JA were essayed (Katsir, Schilmiller, Staswick, Sheng, & Howe, 2008). If the GLR-mediated ion signaling inhibits regeneration through JA signaling, then the loss-of-function mutants in COI1 should phenocopy GLR mutants. Another gene tested because it is involved in defense was NONEXPRESSER OF PR GENES1 (NPR1), the primary receptor for salicylic acid (SA), that mediates pathogen responses overlapping with JA but also independent from JA (Ding et al., 2018). Moreover, the authors observed in several contexts that GLR inhibition improved regeneration in older tissues, which have higher levels of SA, suggesting that SA signaling pathway may be relevant to the defense response. The leaf explant results showed that *coi1-2* could not phenocopy the CNQX treatment or glr mutant phenotype, because the number of callus formed in the mutant was even lower than in WT leaves, even in the samples where CNQX or PAMD were used (PAMD is an SA inhibitor). However, the *npr1* mutants did phenocopy the regeneration levels in the Mock treatment to the same extent as in the CNQX and PAMD treatments (fig.31 a) and in the root regeneration experiments, regeneration increased in the *npr1* to higher levels in all the treatments (fig.31 b), which indicates that SA has a role in inhibition of regeneration post wounding and may be involved in the GLR signaling pathway. The *npr1* leaf explants also showed an increase

in root formation up to 100% in all the treatments, suggesting an inhibitory effect of SA in root formation in tissue culture (fig.31 c).

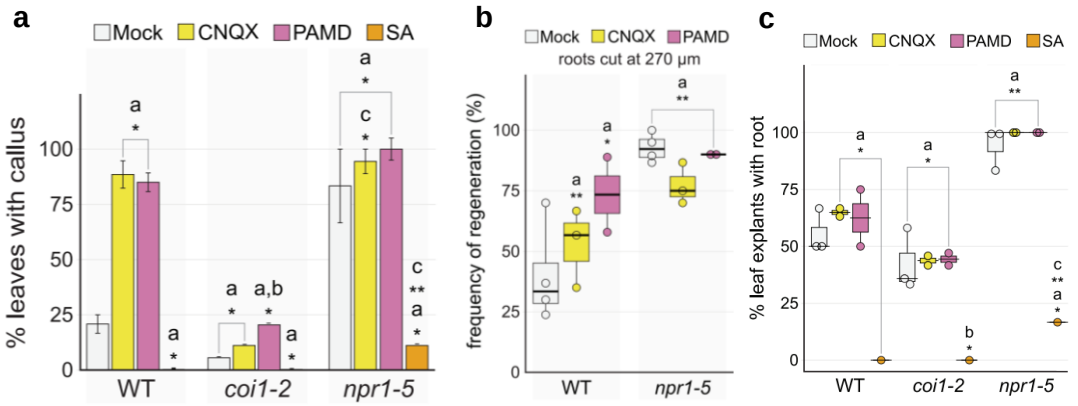

Fig.31 | Regeneration is associated with the SA pathway (a) Quantification of callus formation (chi-square test; n => 18 for each genotype in each treatment; a significant difference with respect to Col-0 Mock, *p < 10^{-6} , **p < 10^{-11}; b significant difference with respect to *coi1-2* Mock, *p = 0.003; c significant difference with respect to *npr1* Mock, *p < 0.04, **p < 10^{-9}). **(b)** Regeneration frequency of Col-0 and npr1–5 mutant on different constitutive post-injury treatments. The error bars are proportional to the standard error of the pooled percentage computed using binomial distribution (chi-square test, Fisher's combined probability test; n > 18 for each treatment in each genotype in each of 4 trials; a significant difference with respect to Col-0 Mock, *p < 0.05, **p < 10^{-6}) **(c)** Quantification of root-from-leaf regeneration (chi-square test, Fisher's combined probability test; n > 12 for each treatment in each genotype in each of 3 trials; a significant difference with respect to Col-0 Mock, *p < 0.03, **p < 10^{-7} ; b significant difference with respect to coi1-2 Mock, *p < 0.02; c significant difference with respect to npr1 Mock, *p < 10^{-20})

Here, we identity the ion signal responsible upon wounding that may be involved in plant regeneration instead of mounting a defense response against herbivory/mechanical damage

5.2 Results

All documented physiological implications of Arabidopsis GLRs so far are linked to their capability to permeate Ca^{2+} (Michard et al., 2011; Wudick, Portes, et al., 2018). The complexity of ion-mediated signaling was documented in maize root wounding experiments, it is documented (Meyer & Weisenseel, 1997). Maize roots wounded by deep incisions showed very fast membrane depolarizations, followed by periods of gradual re- or hyper-polarization. Maize root wounding also showed that the observed re-polarization was composed of major effluxes of K^+ and Cl^- and smaller influxes of Ca^{2+} and H^+, which could be expected given the concentration gradients of these ions.

Firstly, I measured the basal Ca^{2+} fluxes at the meristematic zone of the root, by screening about 100µm of this zone during 15 min, to assess whether there were any differences between WT and *glr1.2/1.4/2.2/3.3*. These measurements showed that there are no significantly different Ca^{2+} fluxes between the genotypes and the small fluxes measured were very close to the baseline (fig.32 a). Next, I performed root wounding experiments following the methodology employed by BirnBaum's group and measured Ca^{2+} fluxes until stabilization (approximately 15 min). In WT, Ca^{2+} influx peaks shortly after wouding and slowly decreases in magnitude for the first 10 minutes whereas in the glr mutant, the influx after wounding seem to be higher at the beginning but it recovers quickly in the first 5 minutes to lower levels than the WT (fig.31b). However, the fluxes in the glr mutant stabilize at a higher influx rate, one order of magnitude higher than WT, indicating that a larger Ca^{2+} influx is sustained in the mutant (fig.32b).

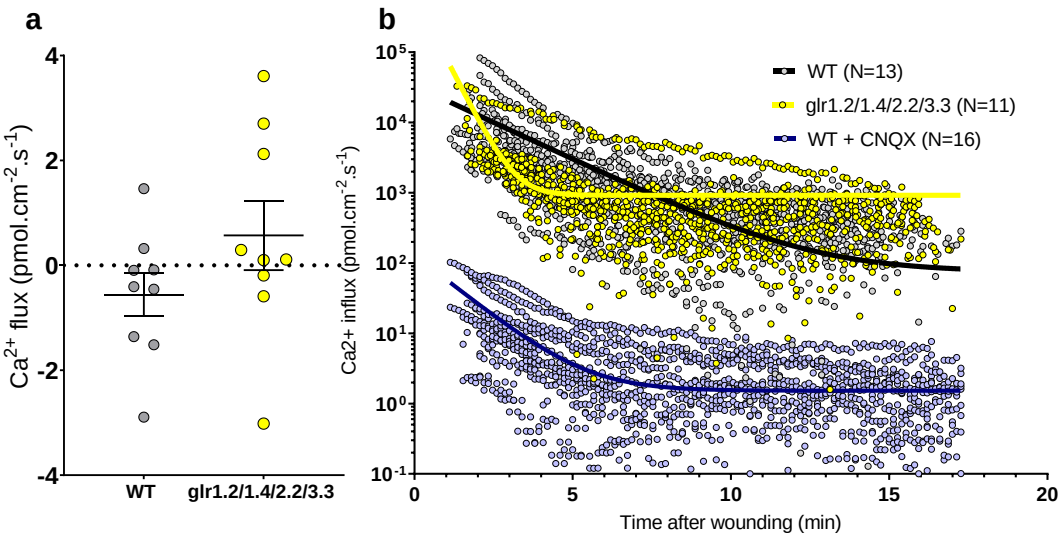

Fig.32 | Ca^{2+} Fluxes are disrupted when GLRs are blocked. (a) A. Extracellular Calcium fluxes were measured along the root meristematic zone for 15 min and were averaged both in wild type and glr1.2/1.4/2.2/3.3 mutant. There is no statistically significance of basal Calcium fluxes between the two genotypes (Welch's t test p=0.1705). **(b)** Vibrating probe measurements over time after root tip excision at the wound site show a higher calcium influx in the glr1.2/1.4.2.2/3.3 quadruple mutant compared with wild type (top) after stabilization. In wild type (bottom), treatment with CNQX decreases calcium influx 4-fold overall, showing a similar pattern of calcium influx over time compared with the mutant trend above.

Lower Ca^{2+} influx observed in the mutant immediately after injury could result from a direct contribution of the GLRs or an indirect consequence of an altered cellular physiology in the mutant. To distinguish these possibilities, I performed the same measurements on wild-type roots treated with CNQX before wounding, because this was the treatment that yielded a better percentage of regenerated roots. Upon the CNQX treatment, Ca^{2+} influx is severely affected, decreasing by four orders of magnitude. Nonetheless, a similar dynamic to glr mutant was observed, with the lowest Ca^{2+}-influx occurring at 6 min after wounding followed by sustained calcium levels in the recovery phase. The comparable dynamics of glr mutants and the transient CNQX-blocking of GLR function confirms an overall impairment in the kinetics of

homeostatic re-establishment of calcium after wounding further supporting that GLR channels mediate Ca^{2+} influxes in response to injury.

5.3 Discussion

The primary strategies used in plants upon damage are defense (immunity) and regeneration. Common to the two strategies are wound responses that trigger Ca^{2+}, reactive oxygen species and electrical signals (Chen, Sun, Xu, & Liu, 2016; Efroni et al., 2016; Florentin, Damri, & Grafi, 2013; Moeder, Phan, & Yoshioka, 2019; Mousavi et al., 2013; Savatin, Gramegna, Modesti, & Cervone, 2014). The key finding here is that GLR-mediated signals negatively regulate regeneration but positively regulate defense response, so the mechanisms that regulate defense and regeneration are antagonistic (Fig.33). The results show that the activation of the two processes can be decoupled. GLR-mediated signaling tunes responses in favor of defense, enhancing the expression of defense-related genes. At the same time, GLR signaling dampens the regeneration response, cellular reprogramming, and meristem recovery. The effects all appear to take place in the immediate vicinity of the wound without long-distance systemic signaling, as conditional GLR inhibition improved regeneration in isolated explants of leaves, where no systemic signaling is possible. Thus, the plant's wound

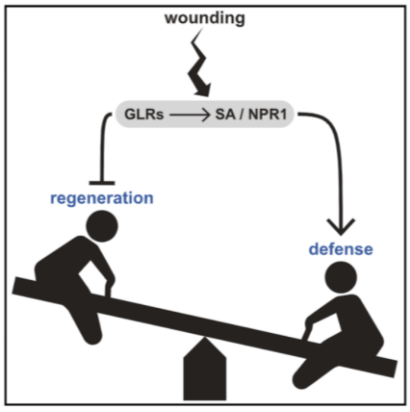

Fig. 33 | Wounding response trade-off between regeneration and defense. The diagram illustrates that after wounding, GLRs signaling triggers the SA pathway for defense, while blocking the regeneration pathway. If the GLRs or NPR1 are not present, the response favours regeneration.

response appears to be, at least to some degree, a trade-off between efficient repair and a robust defense response and the plant does not necessarily optimize wound responses for either process. The suppression of GLR function significantly increased regeneration in Arabidopsis roots while downregulating defense responses. Transient block experiments with chemical inhibitors of GLR signaling showed that suppression of GLR activity at the time of injury and for several additional hours improved regeneration, implying an immediate and extended role for GLRs in wound responses that mediate regeneration. Mutants in in the SA receptor, NPR1, showed dramatically higher regeneration efficiency than in wild type in roots and leaves, phenocopying the GLR inhibitor treatments and partly the *glr* mutants. Overall, SA may provide a less ‘‘conflicted’’ pathway to downregulate regeneration and upregulate defense and may be a better pathway to mediate the trade-off between the two.(Hernández-Coronado et al., 2022).

In a recent transcriptional study analyzing Arabidopsis pattern-triggered immunity, some members of the GLRs clade 2 were particularly upregulated. The perception of microbial or plant-derived molecular patterns by cell-surface-localized pattern recognition receptors (PRRs) induces pattern-triggered immunity, entailing a massive transcriptional reprogramming (Bjornson, Pimprikar, Nürnberger, & Zipfel, 2021). Calcium and electrical waves have been associated with herbivory responses in Arabidopsis as one of the hallmarks of the plant-immunity response (Mousavi et al., 2013; Toyota et al., 2018), which suggests that the physical damage to tissues may expose PRRs to the wound site, eventually modulating GLRs response to the biotic or abiotic stimulus (in case the PRR are produced by the plant), and in some cases

upregulate other GLRs in the tissues around the wound (Bjornson et al., 2021). These upregulated GLRs could be important for the next steps of wounding response.

My experiments with the glr quadruple mutant demonstrate an impairment of Ca^{2+} influxes that are highly reduced by pretreatment with CNQX. These results suggest that, without Ca^{2+} signaling, the default pathway reverts to favor regeneration. Another effect of wounding is the depolarization of the tissues around the excision, as it was shown previously in maize roots, which showed very fast membrane depolarizations in cells away from the wound up to 5 mm, followed by periods of gradual re- and hyperpolarization (Meyer & Weisenseel, 1997). A possible explanation for the reprogramming of the cells around the wound could come from the depolarization of the cells in the region, the same cells that start expressing MONOPTEROs, the stem cell niche marker. There is evidence that more depolarized cells are usually less differentiated (Levin & Stevenson, 2012) and in some cases, depolarization triggers dedifferentiation, a reversion of cell fate (Cone & Cone, 1976; Sundelacruz, Levin, & Kaplan, 2013), that may help in the process of regeneration. The trade-off between defense and regeneration is likely to be a compound signal from PRRs in the medium, ion and electrical signals that modulate the response for a tailored response, but in the case of the glr mutants, the lack of Ca^{2+} in the compound response favors the other mechanisms in place like regeneration and dedifferentiation, instead of defense and immunity.

Concluding remarks and future perspectives

Membrane potential gradient as a morphogenesis signal in apical growth

As we argue, spatially organized ion dynamics appear to be ubiquitous features of cells that undergo polarized cell growth. Examples of this phenomenon can be seen in fungi, algae, plants and neurons, where their apical domains drive intense ionic fluxes, predicted to depolarize the growth sites (Freeman et al., 1985; Nishiyama et al., 2008; Richard Nuccitelli & Jaffe, 1976). The ion fluxes are mainly carried by Cl^-, K^+, H^+ , and Ca^{2+}, generally giving rise to an external electric "circuit" that enters the growth pole and loops back through the mature regions of the cell, similarly to pollen tubes (Michard et al., 2016; Richard Nuccitelli, 1978). Pollen tubes show an average depolarization of approximately 35mV, but this number could be even higher at the apex, where the VSDs may be underestimating membrane potential. In fact, according to the passive membrane properties, the electric potential measured along the length of the axon gets smaller with distance from the site where current is injected due leakage, and this relationship is described by an exponential decay function (Purves, Augustine, George J., Fitzpatrick, Hall, LaMantia, & White, 2012). The apex of PT is where the depolarizing currents are 'injected' thus, the electric potential measurements at the apex of the PT should be exponentially more depolarized than our estimates between 5-10µm from the tip. The finely structured pattern of currents along the pollen tube suggests that ion channels are spatially organized in order to produce opposite currents in different regions of the pollen tubes, e.g. AHA pumps are confined to the shank and CHX antiporters and GLR3.4 localized at the tip. The spatial segregation of ion

currents create a profile of depolarizing currents at the apex and hyperpolarizing currents in the shank, creating an electric gradient and a silent zone where the currents are close to null, the inversion point of the ion fluxes.

Our model for pollen tube development proposes that this spatially organization starts in the pollen grain, when anionic lipid domains are formed at the site where the tube is going to emerge. These domains may be functional lipid micro-domains containing sterols and/or sphingolipids that maintain and bring together specific channels and receptors at the apex, but this information is still lacking due to the lack of probes for these lipids. The PS and PtdInst(4,5)P_2 enriched apex may recruit not only the cell machinery for vesicle delivery, but also specific channels that favor depolarizing currents, while the rest of the pollen grain plasma membrane would have channels that repolarize/hyperpolarize the membrane. This way, the depolarization at the emergence point is confined by hyperpolarizing unyielding currents in the rest of the tube. The nature of the depolarizing currents are likely to be composed by the main ions, Cl^-, K^+, Ca^{2+}, and H^+, because of the downstream effect they have in polarity, vesicle fusion, and enzyme activity. This initial depolarization may trigger other cellular processes for cellular growth and polarity, while self-sustaining the depolarization currents by activating voltage sensitive channels and other voltage sensitive proteins. The creation of an electric field generated by the MPG creates a positive feedback loop that can maintain directional cell growth and polarity.

Apical ion fluxes are known to be oscillatory, and it is expected that the electrical gradient will follow the oscillatory regime, but so far we have not been able to demonstrate this. Better imaging techniques, at smaller time frames are the next step

on understanding the MPG at the PT. Another approach to corroborate our results is an ongoing collaboration that uses a Quantum diamond microscope capable of imaging magnetic fields in biological samples with high spatial and temporal resolution (Barry et al., 2016; Glenn et al., 2015; Levine et al., 2019). Measurements of the magnetic field produced by the MPG-generated electric field will provide another estimate of the membrane potential gradient in PTs and will allow temporal resolution in the milliseconds, 2 orders of magnitude below the airy-disk confocal scanning microscopy used for this work. It would be exciting that this could show us the effect of ion oscillations in magnetic fields oscillations during PT's growth.

Co-option of depolarization signals from membrane repair mechanisms

The default bioelectrical state of a cell is hyperpolarization, a negative electrochemical gradient across the membrane where the cell holds much more negative charges than the outside. If the plasma membrane is breached, the electrochemical gradient is partly dissipated because the cytoplasm electrolyte solutions equilibrate with the medium, which results in a depolarization. The ions going out of the cell that could account for this depolarization are mainly K^+ and Cl^- (and other organic anions) because they are present at higher concentrations inside the cell, thus following the chemical gradient across the membrane. In the other hand, Ca^{2+} is maintained at very low intracellular levels because it is actively pumped out creating a very steep chemical gradient across the plasma membrane, from nanomolar intracellular concentrations to very high millimolar extracellular concentrations. When the integrity of the plasma membrane is compromised, a swift influx of Ca^{2+} generates

transient increases in cytosolic free Ca^{2+} concentration, localized to the injury site. It became established that Ca^{2+} influx is an absolute requirement for plasma membrane repair with early experiments in sea urchin eggs, which showed that without Ca^{2+} in the seawater, wounding the eggs resulted in cell death whereas in seawater with Ca^{2+}, wounds triggered a rapid surface reaction that would restore the egg's integrity.

After establishing that Ca^{2+} influx is necessary for plasma membrane repair, the focus shifted to identifying the targets of the Ca^{2+} signal in the cytosol. Both in animals in plants, membrane repair mechanisms are mostly overlapping: (1) Ca^{2+}-dependent cysteine protease calpain (DEKK1 ortholog in plants); (2) Annexins, which react to Ca^{2+} by binding to phospholipids creating membrane-associated scaffolds; (3) Synaptogamins, regulators of Ca^{2+}-regulated membrane fusion events; (4) SNARE complex, which helps in vesicle docking and fusion. The influx of Ca^{2+} inevitably triggers these membrane-bound components to fuse small vesicles that are in close proximity to the plasma membrane in a Ca^{2+} regulated exocytosis, subsequently patching the injury. The consensus that membrane repair involves a Ca^{2+} transient eventually ignored the bioelectrical component of membrane injury; a local depolarization that happens at the injury site which creates a transient electric field until the membrane is repaired. However, these two components, Ca^{2+} and bioelectrical signal, seem to be conserved throughout evolution, even in the most distinct specialized cells.

To illustrate this, let us take the pollen tube and the neuron, two highly specialized and polarized cells with completely distinct functions however, the mechanisms behind their functions are coincidental with many membrane repair

mechanisms. Both PTs and neurons rely on depolarization signals to perform their functions; PTs need to create a depolarized MPG to grow, whereas neurons need to propagate a depolarization signal so that neurotransmitters can be released and transduce the signal elsewhere. PTs and neurons rely on Ca^{2+} signals too, in one case to deliver vesicles that can create cell expansion, in the other case to fuse vesicles containing neurotransmitters. Both systems require annexins, synaptogamins and the SNARE complex to perform the fusion events that determines their functions. The similarities in these two processes are comparable to membrane repair mechanisms, except for the bioelectrical signal origin. While the depolarization during membrane injury comes from the breaking of the membrane, in PTs and neurons there are ion channels that create the depolarizing currents. In neurons it is well stablished that the depolarization triggers depolarization-sensitive Ca^{2+}-channels that can trigger the downstream events of vesicle fusion but, in plants, such channels have not been identified yet. Nevertheless, Ca^{2+} oscillations at the pollen tube tip could produce the same effect of activating downstream fusion events as similar as the membrane repair mechanisms. From my standpoint, depolarization and Ca^{2+} signals have evolved conjointly since primordial time in what we consider today as being a plasma membrane repair mechanism, and have been co-opted for other functions. In neurons, cells create depolarization signals so to activate the relay of the chemical signal through vesicles, while in pollen tubes, the cells create constant depolarizing currents as to recruit a constant repair mechanism that will lead to apical cell expansion. Furthermore, the local depolarization electric fields have an impact in proteins and vesicles movement and migration, as we now know through electrotaxy experiments under

electric fields, which can bring together many different cellular processes and proteins. For that reason, I think local depolarization signals constitute organizing events at a cellular scale that may activate downstream cascades relevant for cell polarity and growth.

Methods

Plant materials and growth conditions

Arabidopsis thaliana ecotype Columbia (Col-0) was used as the wild-type plant. Seeds were sown on plates with Murashige & Skoog media and stratified in darkness at 4 °C for 2 days before being transferred to climate light racks. Once the first pair of true leaves develops, plants are transferred to soil and placed into growth chambers where plants are maintained at 22 °C with 70% humidity and a 12 h light/12 h dark cycle (100 μmol m−2 s−1).

Tobacco (*Nicotiana tabacum* cultivars Petit Havana SR1) plants were grown on soil with a day/night regime of 12h/12h, and a temperature of 20 to 22°C until flowering for pollen collection. Pollen used in all assays was collected from anthers immediately after anthesis and used fresh.

Solanum licopersicum cultivar M82 plant were grown on soil with a day/night regime 16/8h, and a temperature of 20 to 22°C until flowering for pollen collection.

Arabidopsis pollen germination

Pollen grains were isolated in the morning from newly opened flowers. For this, flowers occupying a volume of about 500 µl were collected in a microcentrifuge tube and pollen germination medium: 5 mM CaCl2, 5 mM KCl, 1 mM MgSO4, 0.01% [w/v] H3BO3, 15% [w/v] sucrose, pH 7.5. 700 µl was added to each tube. The samples were vortexed for 2 min, and the pollen pelleted by centrifugation at 13,200g for 3 min. Flowers and medium were removed and the pollen pellet was resuspended in fresh pollen germination medium.

Tobacco pollen germination

Pollen used in all assays was collected from anthers immediately after anthesis and used fresh. Pollen was resuspended in tobacco pollen germination medium consisting in the following: 250 µM HEPES, 5 mM $CaCl_2$, and 1.6 mM H_3BO_3 and 10% D(+)-sucrose. The pH was adjusted to 5.7 with KOH.

Tomato pollen germination

Pollen used in all assays was collected during the first 2 days after the flowers had opened and were either used fresh or stored in a drierite chamber to maintain the humidity levels the lowest possible, which ensures the viability of the pollen grains. The collected pollen was resuspended in medium containing: 20 mM MES (pH 6), 0.8 mM $MgSO_4$, 1mM KNO_3, 1.6mM H_3BO_3, 3mM $Ca(NO_3)_2$, 2% D(+)-sucrose, 24% PEG 3350.

Annine-6-plus staining

For Annine-6-plus membrane potential measurements, wild-type and mutant pollen grains were collected and germinated as described above. Pollen grains were incubated at 21.5 °C for at least 2 h with the membrane potential dye Annine-6-plus to a final concentration of 10 µg.ml^{-1}.

FluoVolt staining and imaging

For FluoVolt membrane potential measurements, pollen grains were incubated at 21.5 °C for 1,5h first without the dye and then the germination medium containing the dye was added to the samples for another 1 hour until imaging. The reason pollen grains are not incubated with the dye throughout germination is because the dye mix requires the PowerLoad solution to make cell membranes permeable to the dye and this

was shown to decrease pollen germination rates and pollen tube development (PT showed strange shapes and bulging). In the other hand, experiments without the PowerLoad solution have little to almost no fluorescence. Using the dye after pollen tubes are already growing seems to have little effect in their development and growth. The original protocol from ThermoFischer Scientific was changed slightly to have enough fluorescence in the sample and to avoid cytotoxycity effects from the power load. The final concentration of the dye was 3x more concentrated than the protocol suggests and the PowerLoad concentration reduced to half.

Super Resolution Fluorescence imaging

Fluorescence images were acquired on a Zeiss LSM 980 Airyscan 2 Laser Scanning Confocal using an x63 NA1.4 oil immersion objective, in the Super-Resolution mode, and were processed with Airy Scan Super Resolution processing software in Zen lite. The estimated resolution was better than 0.2 µm. Filter settings were as follows: For annine-6plus, excitation 475 nm and emission 499–549 nm (dualband BP) and 573–627 nm (BP); for FluoVolt, excitation 488 nm, emission wavelength dualband BP 499-557 nm and 659-720 nm. Images were analyzed in ImageJ by drawing transects that were 0.2 µm apart and perpendicular to the pollen tube growth axis. Membrane fluorescence values were averaged from the three maxima pixels in each transect for both the left and right sides of the shank, corresponding to better than a tenth of the theoretical resolution, and well above the Nyquist criteria in terms of resolution and device pixel resolution oversampling. Images were acquired in strictly the same settings and normalized between different biological replicates by background fluorescence and average cytosolic fluorescence.

GEPII calibration and imaging

Arabidopsis pollen grains were collected as described in the Pollen germination section. The only difference in the germination medium was instead of 5 mM KCl, the final concentration was changed to 500 μM, which was shown before to be suitable for pollen tube germination and growth. This change was made in order to reach concentrations lower than 5 mM KCl for the calibration curve. After pollen tube germination (2,5h), 75μL of germination medium + 2x the final KCl concentration to be tested and 30 μM (final concentration) of valinomycin were slowly added to the sample, e.g. for the point of the curve at 400mM, 75μL solution at 800mM+ 60 μM valinomycin was added to the 75μL of the already germinated sample that was incubated for 2 hours.

For the valinomycin to have an effect and permeabilize the cells and balance out to the K^+ concentrations in the medium, the time elapsed was approximately 20 minutes after adding the ionophore solution. The time until the valinomycin effect takes place was assessed in time-lapses using the GEPII lines to see how long it would take for the sample to plateau at a lower fluorescent intensity due to the diffusion of the intracellular potassium (see also Depolarization protocols section). The 2x concentrated KCl solutions used were: 1, 5, 10, 50, 100, 200, 300, 500, 800mM. The images were acquired in the inverted wide-field DeltaVision microscope (Applied Precision Inc.) equipped with a 63x water objective 1.4NA and an EMCCD camera (Roper Cascade II or Roper Cascade 1024). The 2 channels used for the FRET mode were: CFP/CFP, CFP/YFP at 5% of the laser power with exposure times of 150ms. These images were processed in image J in order to transform them into ratiometric

pictures using Ratio Plus plug-in. After ratiometric-transformed, 3 areas in each pollen tube were selected and the YFP/CFP fluorescence ratio was averaged from those areas. 20-50 pollen tubes were measured for each KCl concentration in the curve. The higher concentration points have lesser pollen tubes because many do not survive the osmotic shock and either collapse or burst. Using Graphpad Prism 9.2.0 for the analysis, a non-linear fit for receptor-binding saturation was deployed using the one site- total binding mode to generate the calibration curve Y=Bmax*X/(Kd+X) + NS*X + Background .

For the K+ gradient estimation, a 15pixels-wide line was drawn through the center of the pollen tube, averaging the ratiometric fluorescence. The gradient profiles from 23 pollen tubes were analysed and a LOWESS curve fitting was deployed using 5 knots for the smoothing spline method.

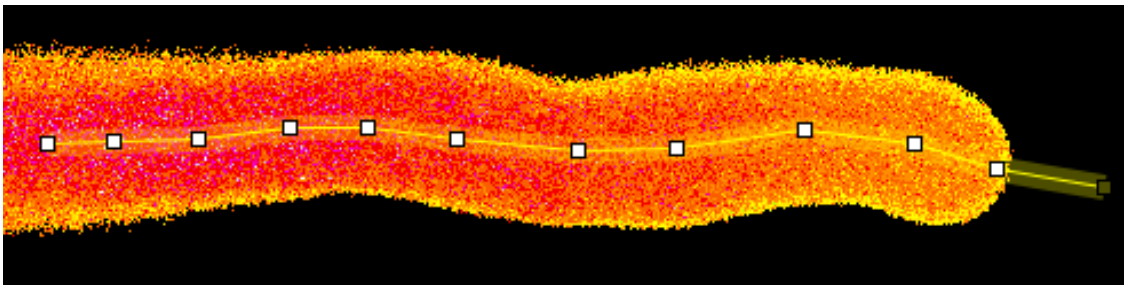

Thioflavin T staining and imaging

The cationic dye was used at different concentrations to asses any cytotoxic effects. Dye's Dose-response curve was done measuring germination rate and pollen tube length were measured in 3 replicates in each concentration: control, 1µM, 5 µM, 10 µM, 25 µM, and 50 µM. The sample size is over >346. For imaging, we used 10 µM ThT final concentration. The images were acquired in the inverted wide-field DeltaVision microscope (Applied Precision Inc.) equipped with a 63x water objective

1.4NA and an EMCCD camera (Roper Cascade II or Roper Cascade 1024). The excitation/emission wavelength used was CFP/CFP, 414-462nm/446-494nm.

BeRST staining and imaging

Pollen tubes were incubated with the dye BeRST or the dye was added after germination, always at a final concentration of 1µM, as indicated in the puclibation (Huang et al., 2015).. The images were acquired in the inverted wide-field DeltaVision microscope (Applied Precision Inc.) equipped with a 63x water objective 1.4NA and an EMCCD camera (Roper Cascade II or Roper Cascade 1024). The excitation/emission wavelength used was Cy5/Cy5, 610-654nm/642-710nm.

VSFP

The images were acquired in the inverted wide-field DeltaVision microscope (Applied Precision Inc.) equipped with a 63x water objective 1.4NA and an EMCCD camera (Roper Cascade II or Roper Cascade 1024). The 2 channels used for the FRET mode were: CFP/CFP, CFP/YFP at 5% of the laser power.

Plasmolysis experiments

Plasmolysis was induced using 500mM mannitol and images were acquired promptly after the osmotic shock.

Depolarization protocols

To depolarize pollen tubes, a solution 2x concentrated was added to the medium after 2,5h of germination, to a final concentration of: Valinomycin (30µM), Nigericin (25µM), Niflumic acid (10µM), and 150mM KCl. Valinomycin dissipates the K^+ chemical gradient, Nigericin functions as an antiporter H^+/K^+ and dissipates chemical

gradient H^+, niflumic acid blocks anion channels, and 150mM KCl to enhance the effect of the ionophores and depolarize pollen tubes faster. The concentrations for valinomycin were assessed using GEPII, to visualize the K^+ chemical gradient dissipation.

VSDs calibrations

The calibrations of the VSDs were done using KCl at different concentrations and 5µM valinomycin as a final concentration, because the experiments with GEPII showed that this valinomycin concentration does not dissipate the K^+ chemical gradient. Pollen tubes were germinated in 75µL and prior do imaging, another 75µL of Germination medium with KCl and valinomycin was added to the solution (KCl and valinomyciun were 2x concentrated to account for the dilution factor). PTs were imaged 15 min after the addition of KCl and valinomycin solution.

Seed count and crosses

Heterozygous plants for the transgenic lipid probe were crossed with WT plant onde day after emasculating flower to prevent self-pollination. After the siliques dried up, siliques were blotted on a double side tape on a cover slide, in order to open the fruit and spread the seeds into the adhesive surface. Slides were brought to an epifluorescence scope and pictures were acquired in the GFP channel, in order to see the seed coat GFP. This is possible because our transgene has a selection marker that expresses GFP driven by the OLE1 promotor, specific for sead coat.

Lipids imaging

Fluorescence images were acquired on a Zeiss LSM 980 Airyscan 2 Laser Scanning Confocal using an x63 NA1.4 oil immersion objective, in the Super-Resolution mode with an excitation for GFP of 488nm at 0.7% and emission filters dualband BP 499-557 nm and 659-720 nm

Extracellular Ca2+ flux measurements after wounding

The ion-selective vibrating probe was used to estimate extracellular calcium flux at the wounding site (as per (Wudick, Portes, et al., 2018)) between 1–2 min after the cut due to the constrains in the technique. Arabidopsis roots were hydrated approximately 1 h before the measurements to equilibrate with the Basic Measuring Solution (BMS): 0.5 mM KCl, 0.1 mM CaCl2, pH 5.5 (unbuffered) (Shabala, Shabala, Van Volkenburgh, & Newman, 2005) or BMS+CNQX (50 μM). All the roots were cut and measured in BMS. The vibrating probe was moved with an excursion of 10μm, completing the cycle of acquisition in 10 s. Each of the roots was measured until the fluxes stabilized at approximately 10–15 min after starting the measures. All the points were plotted, and an exponential decay fit was employed to extract the asymptote (plateau) and the decay constant (k) that were then compared with the extra sum of squares F-test. The statistics and fitting of the data were run on Graphpad Prism.

Genotyping

Primer #	designation	sequence from 5' to 3'
C125	aha6-1_LB	CGTTTATTTCGGCGTGTAGG
C126	aha6-1_RP	TGTGCTCTTCTCTTTGTTTCTCC
C127	aha6-1_LP	TGCGATTGATACTTCCATTGTT
C128	aha8-1_LB	AAACGTCCGCAATGTGTTATT
C129	aha8-1_RP	CTCTCAACAAGGTGCCATCA
C130	aha8-1_LP	TTCGTGTGCTTTTCTTTTAGTCTC
C131	aha9-4_LB	CGTCAATTTGTTTACACAGTAGTATAATC
C132	aha9-4_RP	GTAAGCCCATTTTCTGAGGAAC
C133	aha9-4_LP	TCGAGTAAGTGTATGTGTTGATCTTC
B424	SAIL_162_A07_LP3	GGTTTGGGAGAGTCGTATGT
B425	SAIL_162_A07_RP3	AACTATGCGTGTGTGAGGAA
B322	CHX23_SALK_035909_LP3	TACATGGACGCAAGCTAAGAC
B323	CHX23_SALK_035909_RP3	ccatgccaaaactcaaactca
B5	Salk_LB1.3	ATTTTGCCGATTTCGGAAC

These were the primer pairs used to genotype the T-DNA in the mutant lines for AHA6 and 8, CHX21 and 23.

aha6-1 Sail_1293_D09

WT PCR - C126/C127 | tDNA PCR - C126/C125

aha8-1 Sail_823_E09

WT PCR - C129/C130 | tDNA PCR - C129/C128

Chx21 Sail_162_A07

WT PCR - B424/B425 | tDNA PCR - C128/B425

Chx23 Salk_035909

WT PCR - B322/B323 | tDNA PCR - B322/B5

CLONING

Intermediate and Source Vectors

p266 pLat52-pK7FWG2

Published in Science (Wudick et al., Science 360, 533–536 (2018) 4 May 2018)

p333 XL071 Lat52 Lyn24::GFP

The C-Terminal Hypervariable Domain Targets Arabidopsis ROP9 to the Invaginated Pollen Tube Plasma Membrane, Molecular Plant • Volume 6 • Number 4 • Pages 1362–1364 • July 2013

p358 pGreenII-pOLE1::OLE1::eGFP, Lat52-Gateway-Destination

Published in Science (Wudick et al., Science 360, 533–536 (2018) 4 May 2018)

p366 XL071 pLat52::Lyn24::GFP

PCR was performed to amplify pLat52::Lyn24::GFP from vector lyn24_ve (source) with primers B119 and B120. XL071 (source) was digested with SpeI and KpnI, and the pLat52::Lyn24::GFP PCR product was cloned into the backbone via GIA resulting in vector p366.

p369 pGreenII-KanR-(PstI/SacI Blunted) Intermediate vector

p403, digested with PstI and SacI, was purified and treated with DNA polymerase I Klenow fragment to blunt the ends. Blunted product was purified and ligated to create intermediate cloning vector p369.

p375 pGreenII-KanR-Lat52-Gateway-Destination

PCR using p358 as template was performed with primers B193 and B204 to amplify the pLat52 Gateway cassette. Product was subsequently cloned into p369 digested with KpnI and EcoRI via GIA resulting in vector p375.

p383 pGreenII-Hyg-Lat52-Gateway-Destination

PCR using p366 as template was performed with primers B314 and B315 to amplify the Hygromycin resistance gene driven by the NOS promoter. Product was subsequently cloned into p375 digested with SphI and SacII via GIA resulting in vector p383.

p403 pGreenII-MIGS2.2(FF573)

Addgene 35248

p423 pH7RWG2-Lat52

PCR using PK7FWG2-Lat52 as template was performed with primers B378 and B379 to amplify the Lat52 promoter. Product was then cloned into pH7RWG2 digested with SpeI and HindIII by GIA resulting in destination vector p423.

p424 pLat52::CHX23::RFP

(Pollen Tubes Lacking a Pair of K+ Transporters Fail to Target Ovules in Arabidopsis, Yongxian Lu, Salil Chanroj, Lalu Zulkifli, Mark A. Johnson, Nobuyuki Uozumi, Alice Cheung, Heven SzeThe Plant Cell, Volume 23, Issue 1, January 2011, Pages 81–93)

p668 pMOD-B2101

Addgene 91060

p698_Lact-C2-GFP

Addgene 22852

p699_GFP-C1-PLCdelta-PH

Addgene 21179

p759 MCS+

Addgene 90412

p766 pDONR207-GoldenGate(SapI)

PCR using p668 as template was performed with primer pair B988/B989 and product was subsequently cloned into pDONR207 (Invitrogen) using BP Clonase II via standard protocols to yield vector p766

p809 pGGF-OLE1p-OLE1-GFP

PCR using p358 as template was performed with primer pairs C59/C60, C61/C62, and C63/C64. PCR products were subsequently cloned into pGGF000 via the Pyrite Method using BsaI and T4 DNA Ligase to yield vector p809.

(Pyrite cloning: a single tube and programmed reaction cloning with restriction enzymes, Matthew D. Fischer, Emmanuel Mgboji & Zhongchi Liu, Plant Methods volume 14, Article number: 91 (2018))

p810 pGGA-Lat52p

PCR using p266 as template was performed with primer pair C53/C54. Product and pGGA000 was digested with BsaI. The pGGA000 digest was CIP treated. The digested vector and PCR product were column purified and ligated via T4 DNA Ligase to yield vector p810.

pGGZ003 – Empty Destination Vector (ccdB) Plant resistance at LB – Addgene 48869

GreenGate - A Novel, Versatile, and Efficient Cloning System for Plant Transgenesis, Athanasios Lampropoulos, Zoran Sutikovic, Christian Wenzl, Ira Maegele, Jan U. Lohmann*, Joachim Forner, Plos One December 2013 | Volume 8 | Issue 12 | e83043

pGGB003 – B-dummy (default random sequence if no specific N-tag is desired) Addgene 48821

GreenGate - A Novel, Versatile, and Efficient Cloning System for Plant Transgenesis, Athanasios Lampropoulos, Zoran Sutikovic, Christian Wenzl, Ira Maegele, Jan U. Lohmann*, Joachim Forner, Plos One December 2013 | Volume 8 | Issue 12 | e83043

pGGD002 – D-dummy (default random sequence with stop codon if no specific C-tag is desired) Addgene 48834

GreenGate - A Novel, Versatile, and Efficient Cloning System for Plant Transgenesis, Athanasios Lampropoulos, Zoran Sutikovic, Christian Wenzl, Ira Maegele, Jan U. Lohmann*, Joachim Forner, Plos One December 2013 | Volume 8 | Issue 12 | e83043

pGGE009 – atUBQ10 terminator (Addgene 48841)

GreenGate - A Novel, Versatile, and Efficient Cloning System for Plant Transgenesis, Athanasios Lampropoulos, Zoran Sutikovic, Christian Wenzl, Ira Maegele, Jan U. Lohmann*, Joachim Forner, Plos One December 2013 | Volume 8 | Issue 12 | e83043

chx21-GFP

p695_pDONR207-CHX21-gDNA

PCR using col0 gDNA as template was performed with primer pair B884/B885. PCR product was subsequently cloned into pDONR207 (Invitrogen) via BP Clonase II via standard protocols resulting in vector p695.

p707_pGreenII-OLE1-GFP_Lat52p-CHX21gDNA-T35S

A Gateway reaction using LR Clonase II was performed with destination vector p358 and entry clone p695 containing CHX21-gDNA via standard protocols resulting in vector p707.

chx23-RFP

p435 pDONR201-Chx23 (cDNA with C-terminal truncation)

A Gateway reaction using BP Clonase II was performed with expression vector p424 and donor vector pDONR201 (Invitrogen) via standard protocols resulting in vector p435.

p453 pDONR201-CHX23 (cDNA full length)

PCR using p435 as template was performed with primer pairs B383/B384 and B385/B386. Products were simultaneously cloned via GIA into p435 digested with XbaI and PvuII resulting in vector p453.

p456 pH7RWG2-pLat52::CHX23(full cDNA)

A Gateway reaction using LR Clonase II was performed with destination vector p423 and entry clone p453 containing Chx23 cDNA via standard protocols resulting in vector p456.

PI Sensor

p737_pDONR207-GFP-C1-PLCdelta-PH

PCR using p699 was performed with primer pair B914/B916. PCR product was subsequently cloned into pDONR207 (Invitrogen) via BP Clonase II via standard protocols resulting in vector p737.

p751 pGreenII-OLE1-GFP Lat52p-GFP-C1-PLCdelta-PH

A Gateway reaction using LR Clonase II was performed with destination vector p358 and entry clone p737 containing GFP-C1-PLCdelta-PH via standard protocols resulting in vector p751.

PS Sensor

p736_pDONR207-Lact-C2-GFP

PCR using p698 was performed with primer pair B914/B915. PCR product was subsequently cloned into pDONR207 (Invitrogen) via BP Clonase II via standard protocols resulting in vector p736.

p750 pGreenII-OLE1-GFP Lat52p-Lact-C2-GFP

A Gateway reaction using LR Clonase II was performed with destination vector p358 and entry clone p736 containing Lact-C2-GFP via standard protocols resulting in vector p750.

MSC+ sensor

p770 pDONR207-GG-MCS+

PCR using p759 as template was performed with primer pair B984/B985 and the product was subsequently cloned into p766 using SapI in a Golden Gate reaction to yield donor vector p770

p776 pGreenII-KanR-Lat52 MCS+

A Gateway reaction using LR Clonase II was performed with destination vector p375 and entry clone p770 containing MCS+ via standard protocols resulting in vector p776.

p781 pGreenII-Hyg-Lat52-MCS+

A Gateway reaction using LR Clonase II was performed with destination vector p383 and entry clone p770 containing MCS+ via standard protocols resulting in vector p781.

GEPII

p808 pcDNA3.1(-) GEPII 2.15 (untargeted)

NGFI – Next Generation Fluorescence Imaging (http://ngfi.eu)

p812 pGGC - GEPII-2.15

PCR using p808 as template was performed with primer pairs C65/C69 and C70/C71. Products were cloned into pGGC000 using BsaI in a Golden Gate Reaction.

p818 pGGZ003 Lat52p GEPII-2.15 OLE1p-OLE1-GFP

The following vectors were combined in a Golden Gate reaction using BsaI: pGGZ003, p810, pGGB003, p812, pGGD002, pGGE009, and p809. This yielded transformation vector p818.

Appendix A – Ion selective vibrating probe in Tomato pollen tubes

Table IV - Medium optimization for tomato PTs. Ion concentrations and buffers must be changed so not to affect the sensitivity of the probe in VP method.

	Normal	VP
MES/HEPES(mM)	**20**	**0.125**
$Ca(NO_3)_2$ (mM)	**3**	**0.125**
H_3BO_3 (mM)	**1.6**	**0.8**
KNO_3 (mM)	**1**	**0.5**
$MgSO_4$ (mM)	**0.8**	**0.4**
Sucrose	**2%**	**3%**
PEG	**24%**	**24%**

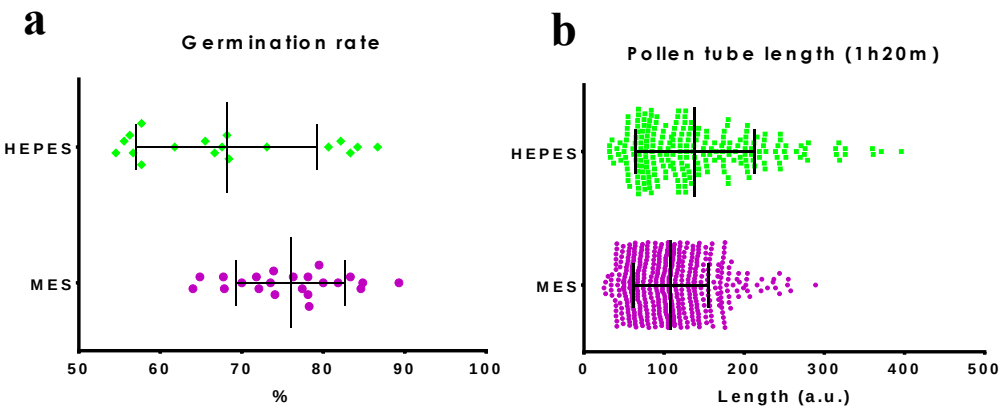

Supplemental figure 1 – Changing buffers does not change dramatically PT development. (a) germination rate seems to be affected by the HEPES buffer but pollen tube length (b) increases slightly so we decided to use HEPES for the VP medium

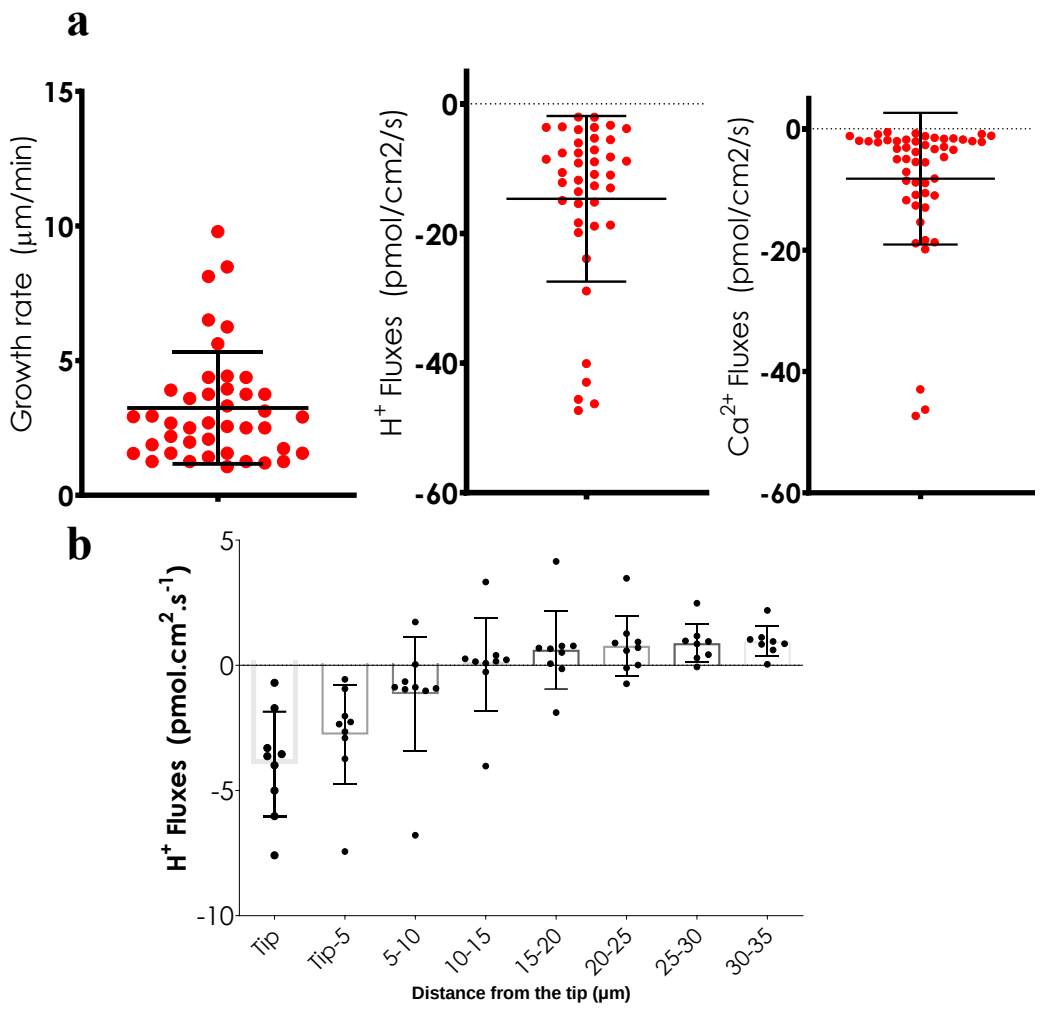

Supplemental figure 2 | Cation dynamics in tomato pollen tubes

(a) Growth rate, Apical H+ and Ca2+ fluxes in tomato pollen tubes

(b) H+ flux profiles along the pollen tube (n=7)

This was the first time cation fluxes were measured in tomato pollen tubes and it required optimization. I optimized the medium concentrations so that the probe was not affected by it, while keeping the levels of germination and growth (S1 a,b,)

Appendix B – Do mitochondria shape PTs apical Ca^{2+} gradient?

MICU-1 is an EF-hand Ca^{2+} binding protein which is part of the mitochondrial Ca^{2+} uniporter complex (MCUC). Although there are more regulatory subunits in the MCUC in the mammalian counterpart, in Arabidopsis there is only MICU-1. We

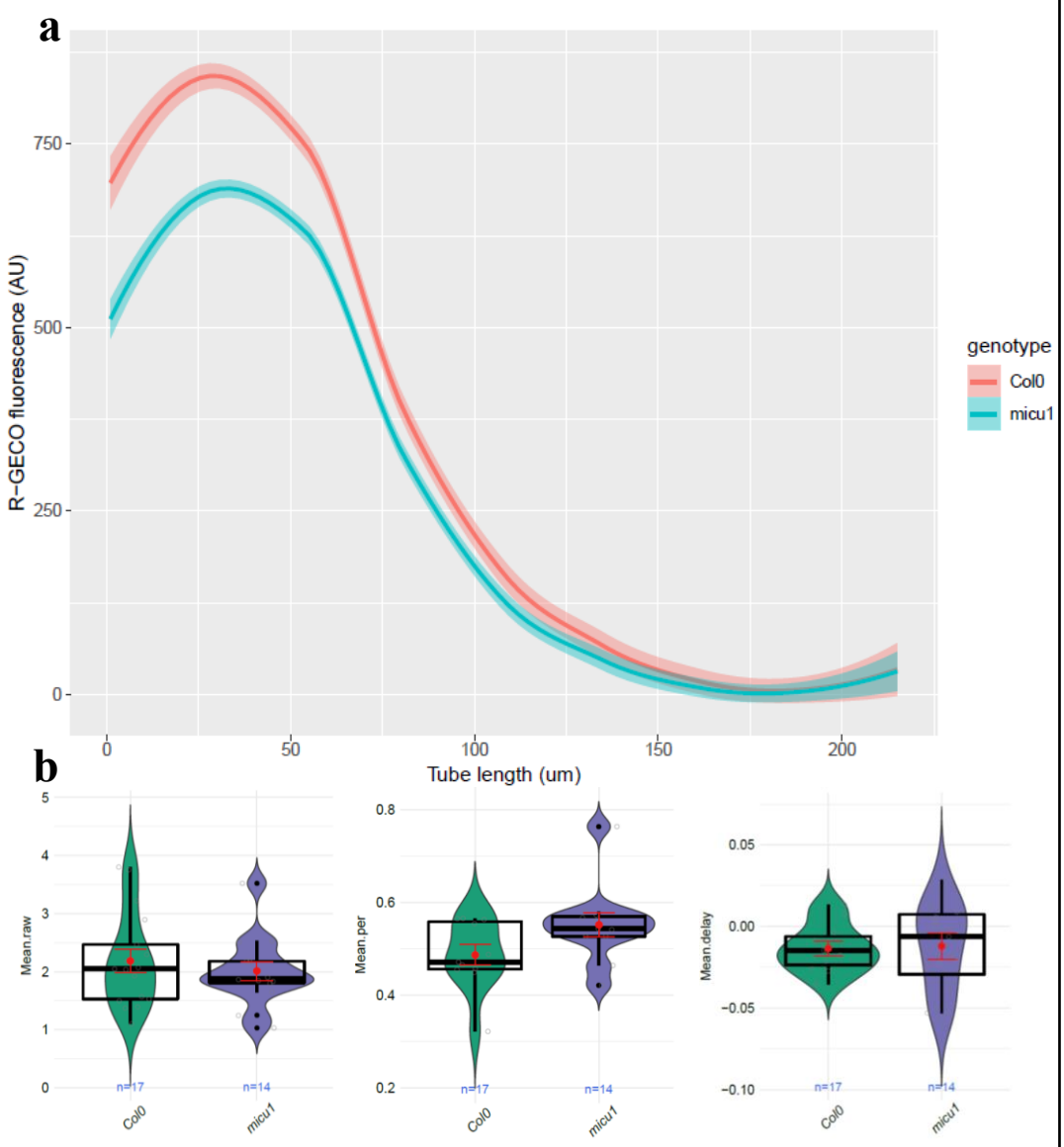

Supplemental figure 3 | (a) Ca2+ gradient in *micu-1* mutant pollen tubes have a less steep gradient compared to WT. (b) left : comparison of growth rate, middle: mean period of Ca2+ oscillations, right: mean delay between oscillations and growth change. None of this comparison was significant

transformed *micu-1* mutant with R-Geco, a genetically encoded cytosolic Ca^{2+} reporter to understand whether mitochondria can act as an endomembrane compartment for Ca^{2+} dissipation from the cytosol. We hypothesized that if mitochondria are intaking cytosolic calcium through MICU-1 complex, then the mutant would have a different Ca^{2+} gradient steepness.

Appendix C – Evidence of the MPG in root hairs another apical growing cell

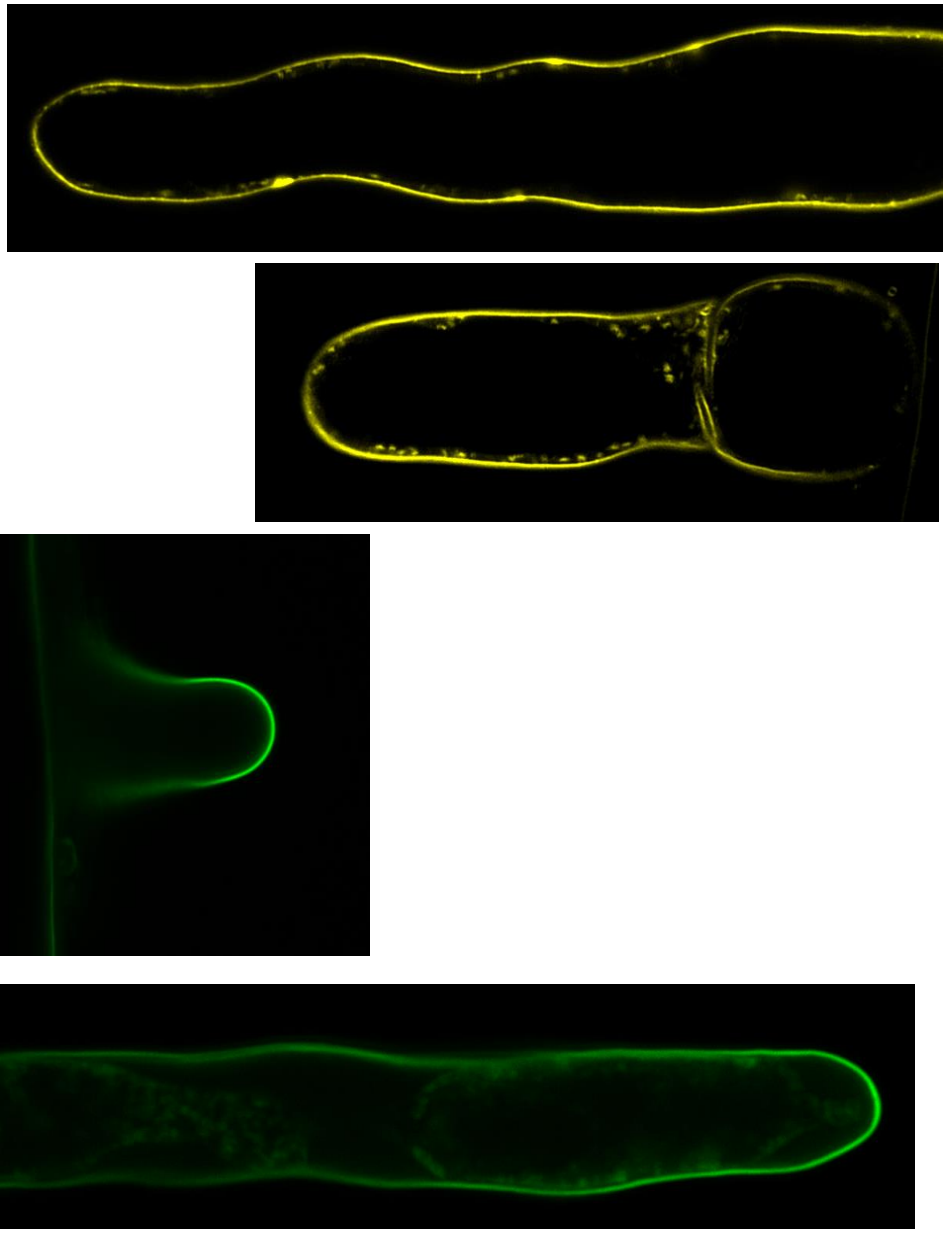

Supplemental figure 4 | Roots hairs labelled with FluoVolt and Annine reveal a MPG. Mature roots hairs tend to not have differences in fluorescence between the apical region and the shank (Annine in yellow, FluoVolt in green)

Bibliography

Abbott, L. F., & Kepler, T. B. (1952). Model neurons: From Hodgkin-Huxley to hopfield. *Statistical Mechanics of Neural Networks*, 5–18. https://doi.org/10.1007/3540532676_37

Altizer, A. M., Moriarty, L. J., Bell, S. M., Schreiner, C. M., Scott, W. J., & Borgens, R. B. (2001). Endogenous electric current is associated with normal development of the vertebrate limb. *Developmental Dynamics*, *221*(4), 391–401. https://doi.org/10.1002/dvdy.1158

Amien, S., Kliwer, I., Márton, M. L., Debener, T., Geiger, D., Becker, D., & Dresselhaus, T. (2010). Defensin-like ZmES4 mediates pollen tube burst in maize via opening of the potassium channel KZM1. *PLoS Biology*, *8*(6). https://doi.org/10.1371/journal.pbio.1000388

Bae-Lee, M. S., & Carman, G. M. (1984). Phosphatidylserine synthesis in Saccharomyces cerevisiae. Purification and characterization of membrane-associated phosphatidylserine synthase. *Journal of Biological Chemistry*, *259*(17), 10857–10862. https://doi.org/10.1016/s0021-9258(18)90592-2

Barry, J. F., Turner, M. J., Schloss, J. M., Glenn, D. R., Song, Y., Lukin, M. D., … Walsworth, R. L. (2016). Optical magnetic detection of single-neuron action potentials using quantum defects in diamond. *Proceedings of the National Academy of Sciences of the United States of America*, *113*(49), 14133–14138. https://doi.org/10.1073/pnas.1601513113

Beane, W. S., Morokuma, J., Lemire, J. M., & Levin, M. (2013). Bioelectric signaling regulates head and organ size during planarian regeneration. *Development*, *140*(2), 313–322. https://doi.org/10.1242/dev.086900

Becker, D., Geiger, D., Dunkel, M., Roller, A., Bertl, A., Latz, A., … Hedrich, R. (2004). AtTPK4, an Arabidopsis tandem-pore K+ channel, poised to control the pollen membrane voltage in a pH- and Ca2+-dependent manner. *Proceedings of the National Academy of Sciences of the United States of America*, *101*(44), 15621–15626. https://doi.org/10.1073/pnas.0401502101

Bedut, S., Seminatore-Nole, C., Lamamy, V., Caignard, S., Boutin, J. A., Nosjean, O.,

… Coge, F. (2016). High-throughput drug profiling with voltage-and calcium-sensitive fluorescent probes in human iPSC-derived cardiomyocytes. *American Journal of Physiology - Heart and Circulatory Physiology*, *311*(1), H44–H53. https://doi.org/10.1152/ajpheart.00793.2015

Bernstein, J. (1912). *Elektrobiologie, die Lehre von den elektrischen Vorgängen im Organismus auf moderner Grundlage dargestellt*. Braunschweig, F. Vieweg.

Bezanilla, F., & Perozo, E. (2003). The voltage sensor and the gate in ion channels. *Advances in Protein Chemistry*, *63*(2), 211–241. https://doi.org/10.1016/S0065-3233(03)63009-3

Bischof, H., Rehberg, M., Stryeck, S., Artinger, K., Eroglu, E., Waldeck-Weiermair, M., … Malli, R. (2017). Novel genetically encoded fluorescent probes enable real-Time detection of potassium in vitro and in vivo. *Nature Communications*, *8*(1), 1–11. https://doi.org/10.1038/s41467-017-01615-z

Bjornson, M., Pimprikar, P., Nürnberger, T., & Zipfel, C. (2021). The transcriptional landscape of Arabidopsis thaliana pattern-triggered immunity. *Nature Plants*, *7*(5), 579–586. https://doi.org/10.1038/s41477-021-00874-5

Blackiston, D. J., McLaughlin, K. A., & Levin, M. (2009). Bioelectric controls of cell proliferation: Ion channels, membrane voltage and the cell cycle. *Cell Cycle*, *8*(21), 3527–3536. https://doi.org/10.4161/cc.8.21.9888

Bloch, D., Pleskot, R., Pejchar, P., Potocký, M., Trpkošová, P., Cwiklik, L., … Žárský, V. (2016). Exocyst SEC3 and phosphoinositides define sites of exocytosis in pollen tube initiation and growth. *Plant Physiology*, *172*(2), 980–1002. https://doi.org/10.1104/pp.16.00690

Borgens, R. B. (1982). What is the Role of Naturally Produced Electric Current in Vertebrate Regeneration and Healing? *International Review of Cytology*, *76*(C), 245–298. https://doi.org/10.1016/S0074-7696(08)61793-3

Borgens, R. B., & Shi, R. (1995). Uncoupling histogenesis from morphogenesis in the vertebrate embryo by collapse of the transneural tube potential. *Developmental Dynamics*, *203*(4), 456–467. https://doi.org/10.1002/aja.1002030408

Bosch Calero, C., Selga, E., Brugada, R., Scornik, F. S., & Pérez, G. J. (2014). The smooth muscle-type β1 subunit potentiates activation by DiBAC4(3) in

recombinant BK channels. *Channels*, *8*(1), 95–102. https://doi.org/10.4161/chan.27212

Bose, J. C. (1913). *Researches on Irritability of Plants*. London: Longmans, Green and Co.

Bose, J. C. (1926). *The Nervous Mechanisms of Plants*. London: Longmans, Green and Co.

Bove, J., Vaillancourt, B., Kroeger, J., Hepler, P. K., Wiseman, P. W., & Geitmann, A. (2008). Magnitude and direction of vesicle dynamics in growing pollen tubes using spatiotemporal image correlation spectroscopy and fluorescence recovery after photobleaching. *Plant Physiology*, *147*(4), 1646–1658. https://doi.org/10.1104/pp.108.120212

Breygina, M. A., Matveeva, N. P., & Ermakov, I. P. (2009). The role of Cl- in pollen germination and tube growth. *Russian Journal of Developmental Biology*, *40*(3), 157–164. https://doi.org/10.1134/S1062360409030047

Breygina, M. A., Matveyeva, N. P., Andreyuk, D. S., & Yermakov, I. P. (2012). Transmembrane transport of K + and Cl - during pollen grain activation in vivo and in vitro. *Russian Journal of Developmental Biology*, *43*(2), 85–93. https://doi.org/10.1134/S1062360412020038

Breygina, M. A., Smirnova, A. V., Matveeva, N. P., & Yermakov, I. P. (2009). Membrane potential changes during pollen germination and tube growth. *Cell and Tissue Biology*, *3*(6), 573–582. https://doi.org/10.1134/S1990519X0906011X

Breygina, M., Smirnova, A., Matveeva, N., & Yermakov, I. (2010). The role of anion channels in pollen germination and tube growth. *Pollen: Structure, Types and Effects*, (September), 235–253.

Brown, D. A., & Rose, J. K. (1992). Sorting of GPI-anchored proteins to glycolipid-enriched membrane subdomains during transport to the apical cell surface. *Cell*, *68*(3), 533–544. https://doi.org/10.1016/0092-8674(92)90189-J

Burr, H. S. (1944). The meaning of bio-electrical potentials. *Yale Journal of Biology and Medicine*, (16), 354–360.

Burr, H. S. (1973). *The fields of life: Our links with the universe* (Vol. 23559). Ballantines Books.

Burr, H. S., & Northrop, F. (1935). THE ELECTRO-DYNAMIC THEORY OF LIFE. *Quarterly Review of Biology*, (10), 322–333.

Carland, F. M., Fujioka, S., Takatsuto, S., Yoshida, S., & Nelson, T. (2002). The identification of CVP1 reveals a role for sterols in vascular patterning. *Plant Cell*, *14*(9), 2045–2058. https://doi.org/10.1105/tpc.003939

Catterall, W. A. (2010). Ion channel voltage sensors: Structure, function, and pathophysiology. *Neuron*, *67*(6), 915–928. https://doi.org/10.1016/j.neuron.2010.08.021

Certal, A. C., Almeida, R. B., Carvalho, L. M., Wong, E., Moreno, N., Michard, E., … Feijo, J. A. (2008). Exclusion of a Proton ATPase from the Apical Membrane Is Associated with Cell Polarity and Tip Growth in Nicotiana tabacum Pollen Tubes. *The Plant Cell Online*, *20*(3), 614–634. https://doi.org/10.1105/tpc.106.047423

Chang, F., & Minc, N. (2014). Electrochemical control of cell and tissue polarity. *Annual Review of Cell and Developmental Biology*, *30*(1), 317–336. https://doi.org/10.1146/annurev-cellbio-100913-013357

Chebli, Y., Kroeger, J., & Geitmann, A. (2013). Transport logistics in pollen tubes. *Molecular Plant*, *6*(4), 1037–1052. https://doi.org/10.1093/mp/sst073

Chen, L., Sun, B., Xu, L., & Liu, W. (2016). Wound signaling: The missing link in plant regeneration. *Plant Signaling and Behavior*, *11*(10), 1–3. https://doi.org/10.1080/15592324.2016.1238548

Cheung, A. Y., Duan, Q. H., Costa, S. S., De Graaf, B. H. J., Di Stilio, V. S., Feijo, J., & Wu, H. M. (2008). The dynamic pollen tube cytoskeleton: Live cell studies using actin-binding and microtubule-binding reporter proteins. *Molecular Plant*, *1*(4), 686–702. https://doi.org/10.1093/mp/ssn026

Choi, C. H., Webb, B. A., Chimenti, M. S., Jacobson, M. P., & Barber, D. L. (2013). Ph sensing by FAK-His58 regulates focal adhesion remodeling. *Journal of Cell Biology*, *202*(6), 849–859. https://doi.org/10.1083/jcb.201302131

Churchill, F. B. (1969). From Machine-Theory to Entelechy : Two Studies in Developmental Teleology. *Journal of the History of Biology*, *2*(1), 165–185.

Cohen, A. E., & Venkatachalam, V. (2014). Bringing Bioelectricity to Light. *Annual Review of Biophysics*, *43*(1), 211–232. https://doi.org/10.1146/annurev-biophys-

051013-022717

Cole, M., Chandler, J., Weijers, D., Jacobs, B., Comelli, P., & Werr, W. (2009). DORNRÖSCHEN is a direct target of the auxin response factor MONOPTEROS in the Arabidopsis embryo. *Development*, *136*(10), 1643–1651. https://doi.org/10.1242/dev.032177

Cone, C. D. (1971). Unified theory on the basic mechanism of normal mitotic control and oncogenesis. *Journal of Theoretical Biology*, *30*(1), 151–181. https://doi.org/10.1016/0022-5193(71)90042-7

Cone, C. D., & Cone, C. M. (1976). Induction of mitosis in mature neurons in central nervous system by sustained depolarization. *Science*, *192*(4235), 155–158. https://doi.org/10.1126/science.56781

Cooper, M. S., & Keller, R. E. (1984). Perpendicular orientation and directional migration of amphibian neural crest cells in dc electrical fields. *Proceedings of the National Academy of Sciences of the United States of America*, *81*(1 I), 160–164. https://doi.org/10.1073/pnas.81.1.160

Croswell, W. F., Cecchini, Ro., & Pelosi, G. (1992). Alessandro Volta and His Battery. *IEEE Transactions on Antennas and Propagation*, *34*(2), 30–37. Retrieved from https://www.researchgate.net/publication/269107473_What_is_governance/link/548173090cf22525dcb61443/download%0Ahttp://www.econ.upf.edu/~reynal/Civil wars_12December2010.pdf%0Ahttps://think-asia.org/handle/11540/8282%0Ahttps://www.jstor.org/stable/41857625

Damineli, D. S. C., Portes, M. T., & Feijó, J. A. (2017). Oscillatory signatures underlie growth regimes in Arabidopsis pollen tubes: Computational methods to estimate tip location, periodicity, and synchronization in growing cells. *Journal of Experimental Botany*, *68*(12), 3267–3281. https://doi.org/10.1093/jxb/erx032

De Loof, A. (2015). How to deduce and teach the logical and unambiguous answer, namely L = ∑C, to "What is Life?" using the principles of communication? *Communicative and Integrative Biology*, *8*(5), 1–11. https://doi.org/10.1080/19420889.2015.1059977

De Loof, A. (2016). The cell's self-generated "electrome": The biophysical essence of the immaterial dimension of Life? *Communicative & Integrative Biology*, *9*(5),

e1197446. https://doi.org/10.1080/19420889.2016.1197446

Denker, S. P., & Barber, D. L. (2002). Cell migration requires both ion translocation and cytoskeletal anchoring by the Na-H exchanger NHE1. *Journal of Cell Biology*, *159*(6), 1087–1096. https://doi.org/10.1083/jcb.200208050

Dimitrov, D., He, Y., Mutoh, H., Baker, B. J., Cohen, L., Akermann, W., & Knöpfel, T. (2007). Engineering and characterization of an enhanced fluorescent protein voltage sensor. *PLoS ONE*, *2*(5), 2–6. https://doi.org/10.1371/journal.pone.0000440

Ding, Y., Sun, T., Ao, K., Peng, Y., Zhang, Y., Li, X., & Zhang, Y. (2018). Opposite Roles of Salicylic Acid Receptors NPR1 and NPR3/NPR4 in Transcriptional Regulation of Plant Immunity. *Cell*, *173*(6), 1454-1467.e10. https://doi.org/10.1016/j.cell.2018.03.044

Domingos, P., Dias, P. N., Tavares, B., Portes, M. T., Wudick, M. M., Konrad, K. R., … Feijó, J. A. (2019). Molecular and electrophysiological characterization of anion transport in Arabidopsis thaliana pollen reveals regulatory roles for pH, Ca2+ and GABA. *New Phytologist*, *223*(3), 1353–1371. https://doi.org/10.1111/nph.15863

Efroni, I., Mello, A., Nawy, T., Ip, P. L., Rahni, R., Delrose, N., … Birnbaum, K. D. (2016). Root Regeneration Triggers an Embryo-like Sequence Guided by Hormonal Interactions. *Cell*, *165*(7), 1721–1733. https://doi.org/10.1016/j.cell.2016.04.046

Emri, M., Balkay, L., Krasznai, Z., Trón, L., & Márián, T. (1998). Wide applicability of a flow cytometric assay to measure absolute membrane potentials on the millivolt scale. *European Biophysics Journal*, *28*(1), 78–83. https://doi.org/10.1007/s002490050186

Fairn, G. D., Hermansson, M., Somerharju, P., & Grinstein, S. (2011). Phosphatidylserine is polarized and required for proper Cdc42 localization and for development of cell polarity. *Nature Cell Biology*, *13*(12), 1424–1430. https://doi.org/10.1038/ncb2351

Fan, L. M., Wang, Y. F., Wang, H., & Wu, W. H. (2001). In vitro Arabidopsis pollen germination and characterization of the inward potassium currents in Arabidopsis

pollen grain protoplasts. *Journal of Experimental Botany*, *52*(361), 1603–1614. https://doi.org/10.1093/jxb/52.361.1603

Feijó, J. A., Sainhas, J., Hackett, G. R., Kunkel, J. G., & Hepler, P. K. (1999a). Growing pollen tubes possess a constitutive alkaline band in the clear zone and a growth-dependent acidic tip. *Journal of Cell Biology*, *144*(3), 483–496. https://doi.org/10.1083/jcb.144.3.483

Feijó, J. A., Sainhas, J., Hackett, G. R., Kunkel, J. G., & Hepler, P. K. (1999b). Growing pollen tubes possess a constitutive alkaline band in the clear zone and a growth-dependent acidic tip. *Journal of Cell Biology*, *144*(3), 483–496. https://doi.org/10.1083/jcb.144.3.483

Field, K. A., Holowka, D., & Baird, B. (1997). Compartmentalized activation of the high affinity immunoglobulin E receptor within membrane domains. *Journal of Biological Chemistry*, *272*(7), 4276–4280. https://doi.org/10.1074/jbc.272.7.4276

Flickinger, B., Berghöfer, T., Hohenberger, P., Eing, C., & Frey, W. (2010). Transmembrane potential measurements on plant cells using the voltage-sensitive dye ANNINE-6. *Protoplasma*, *247*(1), 3–12. https://doi.org/10.1007/s00709-010-0131-y

Florentin, A., Damri, M., & Grafi, G. (2013). Stress induces plant somatic cells to acquire some features of stem cells accompanied by selective chromatin reorganization. *Developmental Dynamics*, *242*(10), 1121–1133. https://doi.org/10.1002/dvdy.24003

Foster, L. J., De Hoog, C. L., & Mann, M. (2003). Unbiased quantitative proteomics of lipid rafts reveals high specificity for signaling factors. *Proceedings of the National Academy of Sciences of the United States of America*, *100*(10), 5813–5818. https://doi.org/10.1073/pnas.0631608100

Freeman, J. A., Manis, P. B., Snipes, G. J., Wikswo, J. P., Freeman, D. B., Mayes, B. N., & Samson, P. C. (1985). Steady Growth Cone Currents Revealed by a Novel Circularly Vibrating Probe : A Possible Mechanism Underlying Neurite Growth. *Journal of Neuroscience Research*, (13), 257–283.

Fromherz, P. (1995). Model for Symmetrical, 7188–7192.

Fromherz, P., Hübener, G., Kuhn, B., & Hinner, M. J. (2008). ANNINE-6plus, a

voltage-sensitive dye with good solubility, strong membrane binding and high sensitivity. *European Biophysics Journal*, *37*(4), 509–514. https://doi.org/10.1007/s00249-007-0210-y

Galindo-Trigo, S., Gray, J. E., & Smith, L. M. (2016). Conserved roles of CrRLK1L receptor-like kinases in cell expansion and reproduction from algae to angiosperms. *Frontiers in Plant Science*, *7*(AUG2016), 1–10. https://doi.org/10.3389/fpls.2016.01269

Gao, R. chi, Zhang, X. dong, Sun, Y. hui, Kamimura, Y., Mogilner, A., Devreotes, P. N., & Zhao, M. (2011). Different roles of membrane potentials in electrotaxis and chemotaxis of Dictyostelium cells. *Eukaryotic Cell*, *10*(9), 1251–1256. https://doi.org/10.1128/EC.05066-11

Gerth, K., Lin, F., Menzel, W., Krishnamoorthy, P., Stenzel, I., Heilmann, M., & Heilmann, I. (2017). Guilt by Association: A Phenotype-Based View of the Plant Phosphoinositide Network. *Annual Review of Plant Biology*, *68*, 349–374. https://doi.org/10.1146/annurev-arplant-042916-041022

Glenn, D. R., Lee, K., Park, H., Weissleder, R., Yacoby, A., Lukin, M. D., … Connolly, C. B. (2015). Single-cell magnetic imaging using a quantum diamond microscope. *Nature Methods*, *12*(8), 736–738. https://doi.org/10.1038/nmeth.3449

Gomez-Porras, J. L., Riaño-Pachón, D. M., Benito, B., Haro, R., Sklodowski, K., Rodríguez-Navarro, A., & Dreyer, I. (2012). Phylogenetic analysis of K+ transporters in bryophytes, lycophytes, and flowering plants indicates a specialization of vascular plants. *Frontiers in Plant Science*, *3*(AUG), 1–13. https://doi.org/10.3389/fpls.2012.00167

Gow, N. A. R. (1984). Transhyphal electrical currents in fungi. *Journal of General Microbiology*, *130*(12), 3313–3318. https://doi.org/10.1099/00221287-130-12-3313

Gray, R. A., Mashburn, D. N., Sidorov, V. Y., & Wikswo, J. P. (2013). Quantification of transmembrane currents during action potential propagation in the heart. *Biophysical Journal*, *104*(1), 268–278. https://doi.org/10.1016/j.bpj.2012.11.007

Gu, Y., Vernoud, V., Fu, Y., & Yang, Z. (2003). ROP GTPase regulation of pollen tube growth through the dynamics of tip-localized F-actin. *Journal of Experimental*

Botany, *54*(380), 93–101. https://doi.org/10.1093/jxb/erg035

Gurtovenko, A. A., & Vattulainen, I. (2007). Lipid transmembrane asymmetry and intrinsic membrane potential: Two sides of the same coin. *Journal of the American Chemical Society*, *129*(17), 5358–5359. https://doi.org/10.1021/ja070949m

Gurtovenko, A. A., & Vattulainen, I. (2008). Membrane potential and electrostatics of phospholipid bilayers with asymmetric transmembrane distribution of anionic lipids. *Journal of Physical Chemistry B*, *112*(15), 4629–4634. https://doi.org/10.1021/jp8001993

Gutermuth, T., Herbell, S., Lassig, R., Brosché, M., Romeis, T., Feijó, J. A., … Konrad, K. R. (2018). Tip-localized Ca2+-permeable channels control pollen tube growth via kinase-dependent R- and S-type anion channel regulation. *New Phytologist*, 1089–1105. https://doi.org/10.1111/nph.15067

Haupt, A., & Minc, N. (2017). Gradients of phosphatidylserine contribute to plasma membrane charge localization and cell polarity in fission yeast. *Molecular Biology of the Cell*, *28*(1), 210–220. https://doi.org/10.1091/mbc.E16-06-0353

Heilmann, I., & Ischebeck, T. (2016). Male functions and malfunctions: the impact of phosphoinositides on pollen development and pollen tube growth. *Plant Reproduction*, *29*(1–2), 3–20. https://doi.org/10.1007/s00497-015-0270-6

Hepler, P. K. (2016). The Cytoskeleton and Its Regulation by Calcium and Protons. *Plant Physiology*, *170*(1), 3–22. https://doi.org/10.1104/pp.15.01506

Hepler, P. K., & Winship, L. J. (2015). The pollen tube clear zone: Clues to the mechanism of polarized growth. *Journal of Integrative Plant Biology*, *57*(1), 79–92. https://doi.org/10.1111/jipb.12315

Herman, P., Malinsky, J., Plasek, J., & Vecer, J. (2004). Pseudo real-time method for monitoring of the limiting anisotropy in membranes. *Journal of Fluorescence*, *14*(1), 79–85. https://doi.org/10.1023/B:JOFL.0000014664.60479.f2

Herman, Petr, Vecer, J., Opekarova, M., Vesela, P., Jancikova, I., Zahumensky, J., & Malinsky, J. (2015). Depolarization affects the lateral microdomain structure of yeast plasma membrane. *FEBS Journal*, *282*(3), 419–434. https://doi.org/10.1111/febs.13156

Hernández-Coronado, M., Dias Araujo, P. C., Ip, P. L., Nunes, C. O., Rahni, R.,

Wudick, M. M., … Birnbaum, K. D. (2022). Plant glutamate receptors mediate a bet-hedging strategy between regeneration and defense. *Developmental Cell*, *57*(4), 451-465.e6. https://doi.org/10.1016/j.devcel.2022.01.013

Heslop-Harrison, J., & Heslop-Harrison, Y. (1982). The growth of the grass pollen tube: 1. Characteristics of the polysaccharide particles ("P-particles") associated with apical growth. *Protoplasma*, *112*(1–2), 71–80. https://doi.org/10.1007/BF01280217

Hille, B. (2001). *Ion Channels of Excitable Membranes*. (I. Sinauer associates, Ed.) (3rd ed.). Sunderland.

Hille, B., Dickson, E. J., Kruse, M., Vivas, O., & Suh, B. C. (2015). Phosphoinositides regulate ion channels. *Biochimica et Biophysica Acta - Molecular and Cell Biology of Lipids*, *1851*(6), 844–856. https://doi.org/10.1016/j.bbalip.2014.09.010

Hoffmann, R. D., Portes, M. T., Olsen, L. I., Damineli, D. S. C., Hayashi, M., Nunes, C. O., … Palmgren, M. (2020). Plasma membrane H+-ATPases sustain pollen tube growth and fertilization. *Nature Communications*, *11*(1), 1–15. https://doi.org/10.1038/s41467-020-16253-1

Hotary, K. B., & Robinson, K. R. (1992). Evidence of a role for endogenous electrical fields in chick embryo development. *Development*, *114*(4), 985–996. https://doi.org/10.1242/dev.114.4.985

Hotary, K. B., & Robinson, K. R. (1994). Endogenous Electrical Currents and Voltage Grandients in Xenopus Embryos and the Consequences of their Distribution.

Huang, Y. L., Walker, A. S., & Miller, E. W. (2015). A Photostable Silicon Rhodamine Platform for Optical Voltage Sensing. *Journal of the American Chemical Society*, *137*(33), 10767–10776. https://doi.org/10.1021/jacs.5b06644

Inaba, M., Yamanaka, H., & Kondo, S. (2012). Pigment Pattern Formation by Contact-Dependent Depolarization. *Science*, *335*(6069), 677–677. https://doi.org/10.1126/science.1212821

Ischebeck, T., Stenzel, I., & Heilmann, I. (2008). Type B phosphatidylinositol-4-phosphate 5-kinases mediate Arabidopsis and Nicotiana tabacum pollen tube growth by regulating apical pectin secretion. *Plant Cell*, *20*(12), 3312–3330. https://doi.org/10.1105/tpc.108.059568

Ischebeck, T., Vu, L. H., Jin, X., Stenzel, I., Löfke, C., & Heilmann, I. (2010). Functional cooperativity of enzymes of phosphoinositide conversion according to synergistic effects on pectin secretion in tobacco pollen tubes. *Molecular Plant*, *3*(5), 870–881. https://doi.org/10.1093/mp/ssq031

Jaffe, L. F. (1981). The role of ionic currents in establishing developmental pattern. *Philosophical Transactions of the Royal Society of London. Series B, Biological Sciences*, *295*(1078), 553–566. https://doi.org/10.1098/rstb.1981.0160

Jaffe, Lionel F. (1966). Electrical currents through the developing fucus egg. *Proceedings of the National Academy of Sciences*, *56*, 1102–1109.

Jaffe, Lionel F. (1977). Electrophoresis along cell membranes. *Nature*, *265*(5595), 600–602. https://doi.org/10.1038/265600a0

Jaffe, Lionel F., & Nuccitelli, R. (1974). An Ultrasensitive Vibrating Probe for Measuring Steady Extracellular Currents. *The Journal of Cell Biology*, *63*(6), 614–628.

Jaffe, Lionel F., & Nuccitelli, R. (1977). Electrical Controls of Develpment. *Annual Review of Biophysics and Bioengineering*, *7*(10), 16–19. https://doi.org/10.1007/978-3-658-34622-5_10

Jaffe, Lionel F., & Stern, Cl. D. (1979). Strong Electrical Currents Leave the Primitive Streak of Chick Embryos Author. *American Association for the Advancement of Science*, *206*(4418), 569–571.

Jenkins, L. S., Duerstock, B. S., & Borgens, R. B. (1996). Reduction of the current of injury leaving the amputation inhibits limb regeneration in the red spotted newt. *Developmental Biology*, *178*(2), 251–262. https://doi.org/10.1006/dbio.1996.0216

Katsir, L., Schilmiller, A. L., Staswick, P. E., Sheng, Y. H., & Howe, G. A. (2008). COI1 is a critical component of a receptor for jasmonate and the bacterial virulence factor coronatine. *Proceedings of the National Academy of Sciences of the United States of America*, *105*(19), 7100–7105. https://doi.org/10.1073/pnas.0802332105

Kellaway, P. (1946). The part played by electric fish in the early history of bioelectricity and electrotherapy. *Bulletin of the History of Medicine*, *20*(2), 112–

137. Retrieved from http://europepmc.org/abstract/MED/20277440%5Cnhttp://www.ncbi.nlm.nih.gov/pubmed/20277440

Kessler, S. A., Lindner, H., Jones, D. S., & Grossniklaus, U. (2015). Functional analysis of related Cr RLK 1L receptor-like kinases in pollen tube reception . *EMBO Reports*, *16*(1), 107–115. https://doi.org/10.15252/embr.201438801

Ketelaar, T., Galway, M. E., Mulder, B. M., & Emons, A. M. C. (2008). Rates of exocytosis and endocytosis in Arabidopsis root hairs and pollen tubes. *Journal of Microscopy*, *231*(2), 265–273. https://doi.org/10.1111/j.1365-2818.2008.02031.x

Kim, T., Kao, M. T., Hasselbrink, E. F., & Meyhöfer, E. (2007). Active alignment of microtubules with electric fields. *Nano Letters*, *7*(1), 211–217. https://doi.org/10.1021/nl061474k

Kline, D., Robinson, K. R., & Nuccitelli, R. (1983). Ion currents and membrane domains in the cleaving Xenopus egg. *Journal of Cell Biology*, *97*(6), 1753–1761. https://doi.org/10.1083/jcb.97.6.1753

Korohoda, W., Mycielska, M., Janda, E., & Madeja, Z. (2000). Immediate and long-term galvanotactic responses of Amoeba proteus to dc electric fields. *Cell Motility and the Cytoskeleton*, *45*(1), 10–26. https://doi.org/10.1002/(SICI)1097-0169(200001)45:1<10::AID-CM2>3.0.CO;2-T

Kuhn, B., & Fromherz, P. (2003). Anellated hemicyanine dyes in a neuron membrane: Molecular Stark effect and optical voltage recording. *Journal of Physical Chemistry B*, *107*(31), 7903–7913. https://doi.org/10.1021/jp0345811

Kuhn, B., & Roome, C. J. (2019). Primer to voltage imaging with ANNINE dyes and two-photon microscopy. *Frontiers in Cellular Neuroscience*, *13*(July), 1–15. https://doi.org/10.3389/fncel.2019.00321

Kurokawa, T., Takasuga, S., Sakata, S., Yamaguchi, S., Horie, S., Homma, K. J., … Okamura, Y. (2012). 3′ Phosphatase activity toward phosphatidylinositol 3,4-bisphosphate [PI(3,4)P 2] by voltage-sensing phosphatase (VSP). *Proceedings of the National Academy of Sciences of the United States of America*, *109*(25), 10089–10094. https://doi.org/10.1073/pnas.1203799109

Lambacher, A., & Fromherz, P. (2001). Orientation of hemicyanine dye in lipid

membrane measured by fluorescence interferometry on a silicon chip. *Journal of Physical Chemistry B*, *105*(2), 345–346. https://doi.org/10.1021/jp002843i

Lancelle, S. A., & Hepler, P. K. (1992). Ultrastructure of freeze-substituted pollen tubes of Lilium longiflorum. *Protoplasma*, *167*(3–4), 215–230. https://doi.org/10.1007/BF01403385

Lang, V., Pertl-Obermeyer, H., Safiarian, M. J., & Obermeyer, G. (2014). Pump up the volume - a central role for the plasma membrane H+ pump in pollen germination and tube growth. *Protoplasma*, *251*(3), 477–488. https://doi.org/10.1007/s00709-013-0555-2

Levin, M. (2012). Molecular bioelectricity in developmental biology: New tools and recent discoveries: Control of cell behavior and pattern formation by transmembrane potential gradients. *BioEssays*, *34*(3), 205–217. https://doi.org/10.1002/bies.201100136

Levin, M., & Stevenson, C. G. (2012). Regulation of cell behavior and tissue patterning by bioelectrical signals: Challenges and opportunities for biomedical engineering. *Annual Review of Biomedical Engineering*, *14*, 295–323. https://doi.org/10.1146/annurev-bioeng-071811-150114

Levine, E. V., Turner, M. J., Kehayias, P., Hart, C. A., Langellier, N., Trubko, R., … Walsworth, R. L. (2019). Principles and techniques of the quantum diamond microscope. *Nanophotonics*, *8*(11), 1945–1973. https://doi.org/10.1515/nanoph-2019-0209

Li, X., & Kolega, J. (2002). Effects of direct current electric fields on cell migration and actin filament distribution in bovine vascular endothelial cells. *Journal of Vascular Research*, *39*(5), 391–404. https://doi.org/10.1159/000064517

Lin, F., Baldessari, F., Gyenge, C. C., Sato, T., Chambers, R. D., Santiago, J. G., & Butcher, E. C. (2008). Lymphocyte Electrotaxis In Vitro and In Vivo. *The Journal of Immunology*, *181*(4), 2465–2471. https://doi.org/10.4049/jimmunol.181.4.2465

Lipchinsky, A. (2018). Electromechanics of polarized cell growth. *BioSystems*, *173*(September), 114–132. https://doi.org/10.1016/j.biosystems.2018.10.004

Liu, L., Zheng, C., Kuang, B., Wei, L., Yan, L., & Wang, T. (2016). Receptor-Like

Kinase RUPO Interacts with Potassium Transporters to Regulate Pollen Tube Growth and Integrity in Rice. *PLoS Genetics*, *12*(7), 1–23. https://doi.org/10.1371/journal.pgen.1006085

Liu, M., Wang, Z., Hou, S., Wang, L., Huang, Q., Gu, H., … Qu, L. J. (2021). AtLURE1/PRK6-mediated signaling promotes conspecific micropylar pollen tube guidance. *Plant Physiology*, *186*(2), 865–873. https://doi.org/10.1093/PLPHYS/KIAB105

Lovy-Wheeler, A. (2006). Oscillatory Increases in Alkalinity Anticipate Growth and May Regulate Actin Dynamics in Pollen Tubes of Lily. *The Plant Cell Online*, *18*(9), 2182–2193. https://doi.org/10.1105/tpc.106.044867

Lovy-Wheeler, Alenka, Cárdenas, L., Kunkel, J. G., & Hepler, P. K. (2007). Differential organelle movement on the actin cytoskeleton in lily pollen tubes. *Cell Motility and the Cytoskeleton*, *64*(3), 217–232. https://doi.org/10.1002/cm.20181

Lu, Y., Chanroj, S., Zulkifli, L., Johnson, M. A., Uozumi, N., Cheung, A., & Sze, H. (2011). Pollen tubes lacking a pair of K+ transporters fail to target ovules in Arabidopsis. *Plant Cell*, *23*(1), 81–93. https://doi.org/10.1105/tpc.110.080499

Lund, E. J. (1923). Electrical Control of Organic Polarity in the Egg of Fucus. *Botanical Gazette*, *76*(3), 288–301.

Luther, P. W., Peng, H. B., & Lin, J. J. C. (1983). Changes in cell shape and actin distribution induced by constant electric fields. *Nature*, *303*(5912), 61–64. https://doi.org/10.1038/303061a0

Lv, S., Tai, F., Guo, J., Jiang, P., Lin, K., Wang, D., … Li, Y. (2021). Phosphatidylserine Synthase from Salicornia europaea Is Involved in Plant Salt Tolerance by Regulating Plasma Membrane Stability. *Plant and Cell Physiology*, *62*(1), 66–79. https://doi.org/10.1093/pcp/pcaa141

Maksimov, N., Evmenyeva, A., Breygina, M., & Yermakov, I. (2018). The role of reactive oxygen species in pollen germination in Picea pungens (blue spruce). *Plant Reproduction*, *31*(4), 357–365. https://doi.org/10.1007/s00497-018-0335-4

Malhó, R., Feijó, J. A., & Pais, M. S. S. (1992). Effect of electrical fields and external ionic currents on pollen-tube orientation. *Sexual Plant Reproduction*, *5*(1), 57–63.

https://doi.org/10.1007/BF00714558

Malhó, Rui, Read, N. D., Trewavas, A. J., & Pais, M. S. (1995). Calcium channel activity during pollen tube growth and reorientation. *Plant Cell*, *7*(8), 1173–1184. https://doi.org/10.2307/3870093

Marcel, D., Müller, T., Hedrich, R., & Geiger, D. (2010). K+ transport characteristics of the plasma membrane tandem-pore channel TPK4 and pore chimeras with its vacuolar homologs. *FEBS Letters*, *584*(11), 2433–2439. https://doi.org/10.1016/j.febslet.2010.04.038

Markham, J. E., Li, J., Cahoon, E. B., & Jaworski, J. G. (2006). Separation and identification of major plant sphingolipid classes from leaves. *Journal of Biological Chemistry*, *281*(32), 22684–22694. https://doi.org/10.1074/jbc.M604050200

Marsh, G., & Beams, H. W. (1947). Electrical control of growth polarity in regenerating Dugesia tigrina. *Federation Proceedings*, (6), 163–164.

Marsh, G., & Beams, H. W. (1949). Electrical control of axial polarity in a regenerating annelid. *Anatomical Records*, (105), 513–514.

Marsh, G., & Beams, H. W. (1952). Electrical control of morphogenesis in regenerating Dugesia tigrina: Relation of axial polarity and field strength. *Journal of Cell and Comparative Physiology*, (39), 191–213.

Martin, S. W., Glover, B. J., & Davies, J. M. (2005). Lipid microdomains - plant membranes get organized. *Trends in Plant Science*, *10*(6), 260–263. https://doi.org/10.1016/j.tplants.2005.04.001

Maynard Smith, J. (1986). *The Problems of Biology*. Oxford: Oxford University Press.

McLaughlin, S., & Poo, M. M. (1981). The role of electro-osmosis in the electric-field-induced movement of charged macromolecules on the surfaces of cells. *Biophysical Journal*, *34*(1), 85–93. https://doi.org/10.1016/S0006-3495(81)84838-2

McPheeters, M. T., Wang, Y. T., Werdich, A. A., Jenkins, M. W., & Laurita, K. R. (2017). An infrared optical pacing system for screening cardiac electrophysiology in human cardiomyocytes. *PLoS ONE*, *12*(8), 1–19. https://doi.org/10.1371/journal.pone.0183761

Messerli, M. A., Danuser, G., & Robinson, K. R. (1999). Pulsatile influxes of H+, K+ and Ca2+ lag growth pulses of Lilium longiflorum pollen tubes. *Journal of Cell Science*, *112*(10), 1497–1509. https://doi.org/10.1242/jcs.112.10.1497

Meyer, A. J., & Weisenseel, M. H. (1997). Wound-induced changes of membrane voltage, endogenous currents, and ion fluxes in primary roots of maize. *Plant Physiology*, *114*(3), 989–998. https://doi.org/10.1104/pp.114.3.989

Michard, E., Alves, F., & Feijó, J. A. (2009). The role of ion fluxes in polarized cell growth and morphogenesis: The pollen tube as an experimental paradigm. *International Journal of Developmental Biology*, *53*(8–10), 1609–1622. https://doi.org/10.1387/ijdb.072296em

Michard, E., Dias, P., & Feijó, J. A. (2008). Tobacco pollen tubes as cellular models for ion dynamics: Improved spatial and temporal resolution of extracellular flux and free cytosolic concentration of calcium and protons using pHluorin and YC3.1 CaMeleon. *Sexual Plant Reproduction*, *21*(3), 169–181. https://doi.org/10.1007/s00497-008-0076-x

Michard, E., Lima, P. T., Borges, F., Silva, A. C., Portes, M. T., Carvalho, J. E., … Feijó, J. A. (2011). Glutamate Receptor – Like Genes Form Ca 2+ Channels in Pollen Tubes and Are Regulated by Pistil. *Science*, *332*, 434–437.

Michard, E., Simon, A. A., Tavares, B., Wudick, M. M., & Feijo, J. A. (2016). Signaling with ions: the keystone for apical cell growth and morphogenesis in pollen tubes. *Plant Physiology*, *173*(January), pp.01561.2016. https://doi.org/10.1104/pp.16.01561

Minc, N., & Chang, F. (2010). Electrical Control of Cell Polarization in the Fission Yeast Schizosaccharomyces pombe. *Current Biology*, *20*(8), 710–716. https://doi.org/10.1016/j.cub.2010.02.047

Moeder, W., Phan, V., & Yoshioka, K. (2019). Ca2+ to the rescue – Ca2+channels and signaling in plant immunity. *Plant Science*, *279*(April 2018), 19–26. https://doi.org/10.1016/j.plantsci.2018.04.012

Mongrand, S., Morel, J., Laroche, J., Claverol, S., Carde, J. P., Hartmann, M. A., … Bessoule, J. J. (2004). Lipid rafts in higher plant cells: Purification and characterization of triton X-100-insoluble microdomains from tobacco plasma

membrane. *Journal of Biological Chemistry*, *279*(35), 36277–36286. https://doi.org/10.1074/jbc.M403440200

Moscatelli, A., Gagliardi, A., Maneta-Peyret, L., Bini, L., Stroppa, N., Onelli, E., … Moreau, P. (2015). Characterisation of detergent-insoluble membranes in pollen tubes of Nicotiana tabacum (L.). *Biology Open*, *4*(3), 378–399. https://doi.org/10.1242/bio.201410249

Mouline, K., Véry, A. A., Gaymard, F., Boucherez, J., Pilot, G., Devic, M., … Sentenac, H. (2002). Pollen tube development and competitive ability are impaired by disruption of a Shaker K+ channel in Arabidopsis. *Genes and Development*, *16*(3), 339–350. https://doi.org/10.1101/gad.213902

Mousavi, S. A. R., Chauvin, A., Pascaud, F., Kellenberger, S., & Farmer, E. E. (2013). GLUTAMATE RECEPTOR-LIKE genes mediate leaf-to-leaf wound signalling. *Nature*, *500*(7463), 422–426. https://doi.org/10.1038/nature12478

Mycielska, M. E., & Djamgoz, M. B. A. (2004). Cellular mechanisms of direct-current electric field effects: Galvanotaxis and metastatic disease. *Journal of Cell Science*, *117*(9), 1631–1639. https://doi.org/10.1242/jcs.01125

Nishimura, K. Y., Isseroff, R. R., & Nucciteili, R. (1996). Human keratinocytes migrate to the negative pole in direct current electric fields comparable to those measured in mammalian wounds. *Journal of Cell Science*, *109*(1), 199–207. https://doi.org/10.1242/jcs.109.1.199

Nishiyama, M., Von Schimmelmann, M. J., Togashi, K., Findley, W. M., & Hong, K. (2008). Membrane potential shifts caused by diffusible guidance signals direct growth-cone turning. *Nature Neuroscience*, *11*(7), 762–771. https://doi.org/10.1038/nn.2130

Noack, L. C., & Jaillais, Y. (2020). Functions of Anionic Lipids in Plants. *Annual Review of Plant Biology*, *71*, 71–102. https://doi.org/10.1146/annurev-arplant-081519-035910

Nuccitelli, R. (2003). Endogenous electric fields in embryos during development, regeneration and wound healing. *Radiation Protection Dosimetry*, *106*(4), 375–383. https://doi.org/10.1093/oxfordjournals.rpd.a006375

Nuccitelli, Richard. (1978). Oöplasmic segregation and secretion in the Pelvetia egg is

accompanied by a membrane-generated electrical current. *Developmental Biology*, *62*(1), 13–33. https://doi.org/10.1016/0012-1606(78)90089-1

Nuccitelli, Richard, & Jaffe, L. F. (1975). The Pulse Current Pattern Generated by Developing Fucoid Eggs. *The Journal of Cell Biology*, *64*, 636–643.

Nuccitelli, Richard, & Jaffe, L. F. (1976). The ionic components of the current pulses generated by developing fucoid eggs. *Developmental Biology*, *49*(2), 518–531. https://doi.org/10.1016/0012-1606(76)90193-7

Nuccitelli, Richard, Poo, M. M., & Jaffe, L. F. (1977). Relations between ameboid movement and membrane-controlled electrical currents. *The Journal of General Physiology*, *69*(6), 743–763. https://doi.org/10.1085/jgp.69.6.743

Obermeuer, G., & Kolb, H. (1993). K + Channels in the Plasma Membrane of Lily Pollen Protoplasts. *Botanica Acta*, *106*, 26–31.

Obermeyer, G., & Blatt, M. R. (1995). Electrical properties of intact pollen grains of Lilium longiflorum: Characteristics of the non-germinatingpollen grain. *Journal of Experimental Botany*, *46*(7), 803–813. https://doi.org/10.1093/jxb/46.7.803

Olivotto, M., Arcangeli, A., Carla, M., & Wanke, E. (1996). Electric fields at the plasma membrane level: a neglected element in the mechanism of cell signaling. *BioEssays*, *18*(6), 495–504.

Onuma, E. K., & Hui, S. W. (1988). Electric field-directed cell shape changes, displacement, and cytoskeletal reorganization are calcium dependent. *Journal of Cell Biology*, *106*(6), 2067–2075. https://doi.org/10.1083/jcb.106.6.2067

Orida, N., & Poo, M. M. (1978). Electrophoretic movement and localization of acetylcholine receptors in the embryonic muscle cell membrane. *Nature*, *275*(5675), 31–35. https://doi.org/10.1038/275031a0

Ortiz-Ramírez, C., Michard, E., Simon, A. A., Damineli, D. S. C., Hernández-Coronado, M., Becker, J. D., & Feijó, J. A. (2017). GLUTAMATE RECEPTOR-LIKE channels are essential for chemotaxis and reproduction in mosses. *Nature*, *549*(7670), 91–95. https://doi.org/10.1038/nature23478

Pakhomov, A. G., Semenov, I., Casciola, M., & Xiao, S. (2017). Neuronal excitation and permeabilization by 200-ns pulsed electric field: An optical membrane potential study with FluoVolt dye. *Biochimica et Biophysica Acta* -

Biomembranes, *1859*(7), 1273–1281. https://doi.org/10.1016/j.bbamem.2017.04.016

Palmgren, M. G. (2001). Plant Plasma Membrane H+-ATPases: Powerhouses for Nutrient Uptake. *Evolution*, *52*, 817–845. https://doi.org/10.1146/annurev.arplant.52.1.817

Pan, L., & Borgens, R. Ben. (2010). Perpendicular organization of sympathetic neurons within a required physiological voltage. *Experimental Neurology*, *222*(1), 161–164. https://doi.org/10.1016/j.expneurol.2009.12.002

Pant, S., Zhang, J., Kim, E. C., Lam, K., Chung, H. J., & Tajkhorshid, E. (2021). PIP2-dependent coupling of voltage sensor and pore domains in Kv7.2 channel. *Communications Biology*, *4*(1). https://doi.org/10.1038/s42003-021-02729-3

Patel, H., & Barber, D. L. (2005). A developmentally regulated Na-H exchanger in Dictyostelium discoideum is necessary for cell polarity during chemotaxis. *Journal of Cell Biology*, *169*(2), 321–329. https://doi.org/10.1083/jcb.200412145

Patel, N., & Poo, M. M. (1982). Orientation of neurite growth by extracellular electric fields. *Journal of Neuroscience*, *2*(4), 483–496. https://doi.org/10.1523/jneurosci.02-04-00483.1982

Pedersen, M. G. (2011). On depolarization-evoked exocytosis as a function of calcium entry: Possibilities and pitfalls. *Biophysical Journal*, *101*(4), 793–802. https://doi.org/10.1016/j.bpj.2011.06.061

Piccolino, M. (1997). Luigi Galvani and animal electricity: Two centuries after the foundation of electrophysiology. *Trends in Neurosciences*, *20*(10), 443–448. https://doi.org/10.1016/S0166-2236(97)01101-6

Platre, M. P., Bayle, V., Armengot, L., Bareille, J., del Mar Marquès-Bueno, M., Creff, A., … Jaillais, Y. (2019). Developmental control of plant Rho GTPase nano-organization by the lipid phosphatidylserine. *Science*, *364*(6435), 57–62. https://doi.org/10.1126/science.aav9959

Platre, M. P., & Jaillais, Y. (2017). Anionic lipids and the maintenance of membrane electrostatics in eukaryotes. *Plant Signaling and Behavior*, *12*(2), 1–5. https://doi.org/10.1080/15592324.2017.1282022

Platre, M. P., Noack, L. C., Doumane, M., Bayle, V., Simon, M. L. A., Maneta-Peyret,

L., … Jaillais, Y. (2018). A Combinatorial Lipid Code Shapes the Electrostatic Landscape of Plant Endomembranes. *Developmental Cell*, *45*(4), 465-480.e11. https://doi.org/10.1016/j.devcel.2018.04.011

Podolyan, A., Luneva, O., Klimenko, E., & Breygina, M. (2021). Oxygen radicals and cytoplasm zoning in growing lily pollen tubes. *Plant Reproduction*, *34*(2), 103–115. https://doi.org/10.1007/s00497-021-00403-6

Poo, M. (1981). In situ electrophoresis of membrane components. *Annual Review of Biophysics and Bioengineering*, *10*, 245–276. https://doi.org/10.1146/annurev.bb.10.060181.001333

Portes, M. T., Damineli, D. S. C., Moreno, N., Colaço, R., Costa, S., & Feijó, J. A. (2015). The Pollen Tube Oscillator: Integrating Biophysics and Biochemistry into Cellular Growth and Morphogenesis BT - Rhythms in Plants: Dynamic Responses in a Dynamic Environment. In S. Mancuso & S. Shabala (Eds.) (pp. 121–156). Cham: Springer International Publishing. https://doi.org/10.1007/978-3-319-20517-5_6

Potapova, T. V., Aslanidi, K. B., Belozerskaya, T. A., & Levina, N. N. (1988). Transcellular ionic currents studied by intracellular potential recordings in Neurospora crassa hyphae Transfer of energy from proximal to apical cells. *FEBS Letters*, *241*(1–2), 173–176. https://doi.org/10.1016/0014-5793(88)81054-8

Prindle, A., Liu, J., Asally, M., Ly, S., Garcia-Ojalvo, J., & Süel, G. M. (2015). Ion channels enable electrical communication in bacterial communities. *Nature*, *527*(7576), 59–63. https://doi.org/10.1038/nature15709

Purves, D., Augustine, George J., Fitzpatrick, D., Hall, W. C., LaMantia, A.-S., & White, L. E. (2012). *Neuroscience*. (R. D. Mooney & L. E. Platt, Eds.) (Fifth edit). Sinauer Associates, Inc.

Radhakrishnan, A., & McConnell, H. M. (2000). Electric field effect on cholesterol-phospholipid complexes. *Proceedings of the National Academy of Sciences of the United States of America*, *97*(3), 1073–1078. https://doi.org/10.1073/pnas.97.3.1073

Rajnicek, A., Gow, N., & McCaig, C. (1992). Electric field-induced orientation of rat hippocampal neurones in vitro. *Experimental Physiology*, *77*(1), 229–232.

https://doi.org/10.1113/expphysiol.1992.sp003580

Rajnicek, A. M., McCaig, C. D., & Gow, N. A. R. (1994). Electric fields induce curved growth of Enterobacter cloacae, Escherichia coli, and Bacillus subtilis cells: Implications for mechanisms of galvanotropism and bacterial growth. *Journal of Bacteriology*, *176*(3), 702–713. https://doi.org/10.1128/jb.176.3.702-713.1994

Ramakrishnan, S., Bera, M., Coleman, J., Rothman, J. E., & Krishnakumar, S. S. (2020). Synergistic roles of synaptotagmin-1 and complexin in calcium-regulated neuronal exocytosis. *ELife*, *9*, 1–18. https://doi.org/10.7554/eLife.54506

Ramos, C., & Teissié, J. (2000). Electrofusion: A biophysical modification of cell membrane and a mechanism in exocytosis. *Biochimie*, *82*(5), 511–518. https://doi.org/10.1016/S0300-9084(00)00200-5

Rathore, K. S., Cork, R. J., & Robinson, K. R. (1991). A cytoplasmic gradient of Ca2+ is correlated with the growth of lily pollen tubes. *Developmental Biology*, *148*(2), 612–619. https://doi.org/10.1016/0012-1606(91)90278-B

Reid, B., Nuccitelli, R., & Zhao, M. (2007). Non-invasive measurement of bioelectric currents with a vibrating probe. *Nature Protocols*, *2*(3), 661–669. https://doi.org/10.1038/nprot.2007.91

Riveline, D., Ott, A., Jülicher, F., Winkelmann, D. A., Cardoso, O., Lacapère, J. J., … Prost, J. (1998). Acting on actin: The electric motility assay. *European Biophysics Journal*, *27*(4), 403–408. https://doi.org/10.1007/s002490050147

Salerno, S., Garten, K., Smith, G. L., Stølen, T., & Kelly, A. (2020). Two-photon excitation of FluoVolt allows improved interrogation of transmural electrophysiological function in the intact mouse heart. *Progress in Biophysics and Molecular Biology*, *154*, 11–20. https://doi.org/10.1016/j.pbiomolbio.2019.08.007

Sato, M. J., Kuwayama, H., Van Egmond, W. N., Takayama, A. L. K., Takagi, H., Van Haastert, P. J. M., … Ueda, M. (2009). Switching direction in electric-signal-induced cell migration by cyclic guanosine monophosphate and phosphatidylinositol signaling. *Proceedings of the National Academy of Sciences of the United States of America*, *106*(16), 6667–6672. https://doi.org/10.1073/pnas.0809974106

Savatin, D. V., Gramegna, G., Modesti, V., & Cervone, F. (2014). Wounding in the plant tissue: The defense of a dangerous passage. *Frontiers in Plant Science*, *5*(SEP), 1–11. https://doi.org/10.3389/fpls.2014.00470

Savtchenko, L. P., Poo, M. M., & Rusakov, D. A. (2017). Electrodiffusion phenomena in neuroscience: A neglected companion. *Nature Reviews Neuroscience*, *18*(10), 598–612. https://doi.org/10.1038/nrn.2017.101

Schäffer, E., & Thiele, U. (2004). Dynamic domain formation in membranes: Thickness-modulation-induced phase separation. *European Physical Journal E*, *14*(2), 169–175. https://doi.org/10.1140/epje/i2003-10147-x

Schlegel, R. A., & Williamson, P. (2001). Phosphatidylserine, a death knell. *Cell Death and Differentiation*, *8*(6), 551–563. https://doi.org/10.1038/sj.cdd.4400817

Schnepf, E. (1986). Cellular Polarity. *Annual Review of Plant Physiology*, *37*(1), 23–47. https://doi.org/10.1146/annurev.pp.37.060186.000323

Schreurs, W. J., & Harold, F. M. (1988). Transcellular proton current in Achlya bisexualis hyphae: relationship to polarized growth. *Proceedings of the National Academy of Sciences of the United States of America*, *85*(5), 1534–1538. https://doi.org/10.1073/pnas.85.5.1534

Shao, C., Novakovic, V. A., Head, J. F., Seaton, B. A., & Gilbert, G. E. (2008). Crystal structure of lactadherin C2 domain at 1.7 A° resolution with mutational and computational analyses of its membrane-binding motif. *Journal of Biological Chemistry*, *283*(11), 7230–7241. https://doi.org/10.1074/jbc.M705195200

Shepherd, V. A. (1999). Bioelectricity and the rhythms of sensitive plants - The biophysical research of Jagadis Chandra Bose. *Current Science*, *77*(1), 189–195. Retrieved from //wos

Sheridan, D. M., Isseroff, R. R., & Nuccitelli, R. (1996). Imposition of a physiologic DC electric field alters the migratory response of human keratinocytes on extracellular matrix molecules. *Journal of Investigative Dermatology*, *106*(4), 642–646. https://doi.org/10.1111/1523-1747.ep12345456

Simon, M. L. A., Platre, M. P., Marquès-Bueno, M. M., Armengot, L., Stanislas, T., Bayle, V., … Jaillais, Y. (2016). A PtdIns(4)P-driven electrostatic field controls cell membrane identity and signalling in plants. *Nature Plants*, *2*(7), 1–10.

https://doi.org/10.1038/NPLANTS.2016.89

Smokvarska, M., Jaillais, Y., & Martiniere, A. (2021). Function of membrane domains in rho-of-plant signaling. *Plant Physiology*, *185*(3), 663–681. https://doi.org/10.1093/PLPHYS/KIAA082

Song, B., Zhao, M., Forrester, J. V., & McCaig, C. D. (2002). Electrical cues regulate the orientation and frequency of cell division and the rate of wound healing in vivo. *Proceedings of the National Academy of Sciences of the United States of America*, *99*(21), 13577–13582. https://doi.org/10.1073/pnas.202235299

Sousa, E., Kost, B., & Malho, R. (2008). Arabidopsis Phosphatidylinositol-4-Monophosphate 5-Kinase 4 Regulates Pollen Tube Growth and Polarity by Modulating Membrane Recycling. *The Plant Cell Online*, *20*(11), 3050–3064. https://doi.org/10.1105/tpc.108.058826

Spira, F., Mueller, N. S., Beck, G., Von Olshausen, P., Beig, J., & Wedlich-Söldner, R. (2012). Patchwork organization of the yeast plasma membrane into numerous coexisting domains. *Nature Cell Biology*, *14*(6), 640–648. https://doi.org/10.1038/ncb2487

Stracke, R., Böhm, K. J., Wollweber, L., Tuszynski, J. A., & Unger, E. (2002). Analysis of the migration behaviour of single microtubules in electric fields. *Biochemical and Biophysical Research Communications*, *293*(1), 602–609. https://doi.org/10.1016/S0006-291X(02)00251-6

Sun, Y., Do, H., Gao, J., Zhao, R., Zhao, M., & Mogilner, A. (2013). Keratocyte fragments and cells utilize competing pathways to move in opposite directions in an electric field. *Current Biology*, *23*(7), 569–574. https://doi.org/10.1016/j.cub.2013.02.026

Sundelacruz, S., Levin, M., & Kaplan, D. L. (2013). Depolarization alters phenotype, maintains plasticity of predifferentiated mesenchymal stem cells. *Tissue Engineering*, *19*(17–18), 1889–1908. https://doi.org/10.1089/ten.tea.2012.0425.rev

Sze, H. (1985). H+-Translocating ATPases: Advances Using Membrane Vesicles. *Annual Review of Plant Physiology*, *36*, 175–208.

Sze, H., & Chanroj, S. (2018). Plant endomembrane dynamics: Studies of K+/H+

antiporters provide insights on the effects of pH and ion homeostasis. *Plant Physiology*, *177*(3), 875–895. https://doi.org/10.1104/pp.18.00142

Sze, H., Padmanaban, S., Cellier, F., Honys, D., Cheng, N. H., Bock, K. W., … Hirschi, K. D. (2004). Expression patterns of a novel AtCHX gene family highlight potential roles in osmotic adjustment and K+ homeostasis in pollen development. *Plant Physiology*, *136*(1), 2532–2547. https://doi.org/10.1104/pp.104.046003

Szumlanski, A. L., & Nielsen, E. (2009). The rab GTPase RabA4d regulates pollen tube Tip growth in Arabidopsis thaliana. *Plant Cell*, *21*(2), 526–544. https://doi.org/10.1105/tpc.108.060277

Thiel, G., MacRobbie, E. A. C., & Blatt, M. R. (1992). Membrane Transport in Stomatal Guard Cells: the Importance of Voltage Control. *Journal of Membrane Biology*, *126*, 1–18.

Tillman, T. S., & Cascio, M. (2003). Effects of membrane lipids on ion channel structure and function. *Cell Biochemistry and Biophysics*, *38*(2), 161–190. https://doi.org/10.1385/CBB:38:2:161

Toyota, M., Spencer, D., Sawai-Toyota, S., Jiaqi, W., Zhang, T., Koo, A. J., … Gilroy, S. (2018). Glutamate triggers long-distance, calcium-based plant defense signaling. *Science*, *361*(6407), 1112–1115. https://doi.org/10.1126/science.aat7744

Urrego, D., Tomczak, A. P., Zahed, F., Stühmer, W., & Pardo, L. A. (2014). Potassium channels in cell cycle and cell proliferation. *Philosophical Transactions of the Royal Society B: Biological Sciences*, *369*(1638), 1–9. https://doi.org/10.1098/rstb.2013.0094

Van Meer, G., Voelker, D. R., & Feigenson, G. W. (2008). Membrane lipids: Where they are and how they behave. *Nature Reviews Molecular Cell Biology*, *9*(2), 112–124. https://doi.org/10.1038/nrm2330

Várnai, P., Lin, X., Lee, S. B., Tuymetova, G., Bondeva, T., Spät, A., … Balla, T. (2002). Inositol lipid binding and membrane localization of isolated pleckstrin homology (PH) domains. Studies on the PH domains of phospholipase C δ1 and p130. *Journal of Biological Chemistry*, *277*(30), 27412–27422. https://doi.org/10.1074/jbc.M109672200

Véry, A. A., & Davies, J. M. (2000). Hyperpolarization-activated calcium channels at the tip of Arabidopsis root hairs. *Proceedings of the National Academy of Sciences of the United States of America*, *97*(17), 9801–9806. https://doi.org/10.1073/pnas.160250397

Wang, H., Han, S., Siao, W., Song, C., Xiang, Y., Wu, X., … Zhao, H. (2015). Arabidopsis Synaptotagmin 2 Participates in Pollen Germination and Tube Growth and Is Delivered to Plasma Membrane via Conventional Secretion. *Molecular Plant*, *8*(12), 1737–1750. https://doi.org/10.1016/j.molp.2015.09.003

Wang, L. (2012). Measurements and implications of the membrane dipole potential. *Annual Review of Biochemistry*, *81*, 615–635. https://doi.org/10.1146/annurev-biochem-070110-123033

Wang, Y., & Wu, W. H. (2013). Potassium transport and signaling in higher plants. *Annual Review of Plant Biology*, *64*, 451–476. https://doi.org/10.1146/annurev-arplant-050312-120153

Wang, Y., & Wu, W. H. (2017). Regulation of potassium transport and signaling in plants. *Current Opinion in Plant Biology*, *39*, 123–128. https://doi.org/10.1016/j.pbi.2017.06.006

Weisenseel, M., Nuccitelli, R., & Jaffe, L. F. (1975). Large electrical currents traverse growing pollen tubes. *The Journal of Cell Biology*, *66*, 556–567.

Wiese, A., Reiners, J. O., Brandenburg, K., Kawahara, K., Zähringer, U., & Seydel, U. (1996). Planar asymmetric lipid bilayers of glycosphingolipid or lipopolysaccharide on one side and phospholipids on the other: Membrane potential, porin function, and complement activation. *Biophysical Journal*, *70*(1), 321–329. https://doi.org/10.1016/S0006-3495(96)79573-5

Woodruff, R. I., & Telfer, W. H. (1980). Electrophoresis of proteins in intercellular bridges. *Nature*, *286*(5768), 84–86. https://doi.org/10.1038/286084a0

Wudick, M. M., Michard, E., Oliveira Nunes, C., & Feijó, J. A. (2018). Comparing plant and animal glutamate receptors: Common traits but different fates? *Journal of Experimental Botany*, (May), 1–13. https://doi.org/10.1038/pr.2015.58

Wudick, M. M., Portes, M. T., Michard, E., Rosas-santiago, P., Lizzio, M. A., Oliveira Nunes, C., … Feijó, J. A. (2018). CORNICHON sorting and regulation of GLR

channels underlie pollen tube Ca 2+ homeostasis. *Science*, *536*(May), 533–536. https://doi.org/10.1126/science.aar6464

Yamada, A., Gaja, N., Ohya, S., Muraki, K., Narita, H., Ohwada, T., & Imaizumi, Y. (2001). Usefulness and limitation of DiBAC4(3), a voltage-sensitive fluorescent dye, for the measurement of membrane potentials regulated by recombinant large conductance Ca2+-activated K+ channels in HEK293 cells. *Japanese Journal of Pharmacology*, *86*(3), 342–350. https://doi.org/10.1254/jjp.86.342

Yamaoka, Y., Yu, Y., Mizoi, J., Fujiki, Y., Saito, K., Nishijima, M., … Nishida, I. (2011). PHOSPHATIDYLSERINE SYNTHASE1 is required for microspore development in Arabidopsis thaliana. *Plant Journal*, *67*(4), 648–661. https://doi.org/10.1111/j.1365-313X.2011.04624.x

Yang, Y., Niu, Y., Chen, T., Zhang, H., Zhang, J., Qian, D., … Xiang, Y. (2022). The phospholipid flippase ALA3 regulates pollen tube growth and guidance in Arabidopsis. *The Plant Cell*, *34*(10), 3718–3736. https://doi.org/10.1093/plcell/koac208

Yoneda, A., Ohtani, M., Katagiri, D., Hosokawa, Y., & Demura, T. (2020). Hechtian strands transmit cell wall integrity signals in plant cells. *Plants*, *9*(5). https://doi.org/10.3390/plants9050604

Yonezawa, N., Nishida, E., & Sakai, H. (1985). pH control of actin polymerization by cofilin. *Journal of Biological Chemistry*, *260*(27), 14410–14412. https://doi.org/10.1016/s0021-9258(17)38580-0

Zarza, X., Van Wijk, R., Shabala, L., Hunkeler, A., Lefebvre, M., Rodriguez-Villalón, A., … Munnik, T. (2020). Lipid kinases PIP5K7 and PIP5K9 are required for polyamine-triggered K+ efflux in Arabidopsis roots. *Plant Journal*, *104*(2), 416–432. https://doi.org/10.1111/tpj.14932

Zaydman, M. A., Silva, J. R., Delaloye, K., Li, Y., Liang, H., Larsson, H. P., … Cui, J. (2013). Kv7.1 ion channels require a lipid to couple voltage sensing to pore opening. *Proceedings of the National Academy of Sciences of the United States of America*, *110*(32), 13180–13185. https://doi.org/10.1073/pnas.1305167110

Zhang, X., Liu, W., Nagae, T. T., Takeuchi, H., Zhang, H., Han, Z., … Chai, J. (2017). Structural basis for receptor recognition of pollen tube attraction peptides. *Nature*

Communications, *8*(1), 1–8. https://doi.org/10.1038/s41467-017-01323-8

Zhao, M., Agius-Fernandez, A., Forrester, J. V., & McCaig, C. D. (1996). Orientation and directed migration of cultured corneal epithelial cells in small electric fields are serum dependent. *Journal of Cell Science*, *109*(6), 1405–1414. https://doi.org/10.1242/jcs.109.6.1405

Zhou, X., Lu, J., Zhang, Y., Guo, J., Lin, W., Van Norman, J. M., … Yang, Z. (2021). Membrane receptor-mediated mechano-transduction maintains cell integrity during pollen tube growth within the pistil. *Developmental Cell*, *56*(7), 1030-1042.e6. https://doi.org/10.1016/j.devcel.2021.02.030

Zhou, Y. C. (2012). Electrodiffusion of lipids on membrane surfaces. *Journal of Chemical Physics*, *136*(20). https://doi.org/10.1063/1.4722196

Zhou, Yong, Wong, C. O., Cho, K. J., Van Der Hoeven, D., Liang, H., Thakur, D. P., … Hancock, J. F. (2015). Membrane potential modulates plasma membrane phospholipid dynamics and K-Ras signaling. *Science*, *349*(6250), 873–876. https://doi.org/10.1126/science.aaa5619

Zhou, Yuelong, Yang, Y., Niu, Y., Fan, T. T., Qian, D., Luo, C., … Xiang, Y. (2020). The tip-localized phosphatidylserine established by Arabidopsis ALA3 is crucial for rab GTPase-mediated vesicle trafficking and pollen tube growth. *Plant Cell*, *32*(10), 3170–3187. https://doi.org/10.1105/tpc.19.00844

Zonia, L., Cordeiro, S., Tupy, J., & Feijo, J. A. (2002). Oscillatory chloride efflux at the pollen tube apex has a role in growth and cell volume regulation and is targeted by inositol 3,4,5,6-tetrakisphosphate. *Plant Cell*, *14*(9), 2233–2249. https://doi.org/10.1105/tpc.003830.these

Curriculum Vitae

Custódio de Oliveira Nunes, Ph.D.

Education

2015-2022 **Ph.D**
Biological Sciences – Physiological Systems, University of Maryland, College Park
Dissertation title: "Molecular and biophysical bases of intracellular electric fields in pollen tubes"
Chair: José A. Feijó, Ph.D

2012-2014 **Masters in Evolutionary and Developmental Biology**
Faculdade de Ciências da Universidade de Lisboa
Thesis title: ""Characterisation of a novel family of putative Glutamate Receptor-like interacting proteins in *Arabidopsis thaliana*"

2008-2012 **Bachelor in Biology**
Faculdade de Ciências da Universidade de Lisboa

Awards & Fellowships

- Dean's Fellowship, UMD, College Park (2017)
- Graduate School Summer Research Fellowship, UMD, College Park (2019)
- Carrol E. Cox Award for the outstanding work in botany, UMD, College park (2019)
- Graduate School's Outstanding Research Assistant Award, UMD, College park (2021)

Work Experience and Training

- **Lab technician**
  Dr. Jörg Becker, Plant Genomics group
  Work under the supervision of Post-doc Leonor Boavida in her research project "*The other Side of the Mirror: mRNA Transport and Non-Cell-Autonomous Activity in the Male Germ Unit*" funded by FCT
  Instituto Gulbenkian de Ciência, Oeiras, Portugal
  December 2014 – June 2015

- **Internship in the scope of the Masters of Evolutionary and Developmental Biology**
  Masters thesis : "*Characterisation of a novel family of putative Glutamate Receptor-like interacting proteins in Arabidopsis thaliana*"
  Dr. José A.B.M. Feijó, Cell Biophysics and Development group
  Research project at Instituto Gulbenkian de Ciência, Oeiras, Portugal
  August 2013- September 2014

- **Introductory Bioinformatics Course**
  Gulbenkian Training Program in Bioinformatics (GTPB), IGC
  April 2014

- **6th Course on Optical Microscopy Imaging for Biosciences**
  Institute of Molecular and Cell Biology (IBMC), Porto
  Course contents: Theory of image formation, The anatomy of an optical microscope, light contrast techniques, fluorescence wide-field and laser scanning microscopy, Digital imaging and image processing, live cell imaging and advanced applications for molecular analysis, high-content screening analysis and quantitative microscopy, mesoscopy.
  7th - 11th of April 2014

- **Trainee**
  Fellowship researcher André Alcântara
  Laboratory assistant, helping to develop the research: 'Physiological responses of two *Medicago truncatula* lines overexpressing ATPS1 genes towards water deficit'
  Faculdade de Ciências da Universidade de Lisboa, Departamento de Biologia Vegetal, Portugal
  August 2012

Publications

- Wudick MM, Portes MT, Michard E, Oliveira Nunes C, *et al*. **CORNICHON sorting and regulation of GLR channels underlie pollen tube Ca 2+ homeostasis**. *Science*, 2018;(May):533-536. doi:10.1126/science.aar6464

- Wudick MM, Michard E, Oliveira Nunes C, Feijó JA. **Comparing plant and animal glutamate receptors: Common traits but different fates?** *Journal of Experimental Botany*, 2018;(May):1-13. doi:10.1038/pr.2015.58

- Hoffmann, RD, Portes MT, Oliveira Nunes, C, *et al.* **Plasma membrane H^+-ATPases regulate an oscillating cytosolic pH and sustain actin organization in pollen tubes.** *Nature Communications*, 2020 (May):*14;11(1):2395. doi: 10.1038/s41467-020-16253-1*

- Hernandez Coronado, M, Oliveira Nunes, C, *et al.* **Repel or Repair: Plant Glutamate Receptor-Like Channels Mediate a Defense vs. Regeneration Tradeoff**. Developmental Cell, 2022 (Feb) 28;57(4):451-465.e6. doi: 10.1016/j.devcel.2022.01.013.

Conferences and Symposiums:

- Fundação Calouste Gulbenkian 2007/2008 "Na fronteira da Ciência"
- Cycle of conferences: Darwin no Caminho da Evolução (2008)
- Cycle of conferences: A Evolução de Darwin (2009). Speakers: Lynn Margulis, J. Watson, Frias Martins, Peter and Rosemary Grant
- TiBE 2012, Trends in Biodiversity and Evolution: Abordagens Integrativas em Biologia Evolutiva (CIBIO/UP)
- IX Portuguese Evolutionary Biology Meeting (ENBE), 2013, IGC
- 17th International Workshop on Plant Membrane Biology; June 5th - 10th, 2016, Annapolis, MD, USA
- Pollen Network- Imaging Workshop, 5-10 April 2017, UMD, College park, MD, USA

- MAS-ASPB /University of Maryland Plant Symposium – Joint meeting, May 30th – 31st, 2018, UMD, College park, USA
- 18th International Workshop on Plant Membrane Biology: July 7th - 12th, 2019, Glasgow, Scotland, UK (**Poster** "Ion fluxes in pollen tubes: patterning a membrane potential gradient?")
- MAS-ASPB/University of Maryland Plant Symposium – Joint meeting, May 27th-28th, 2020 (Virtual meeting) (**Oral presentation** "Bioelectrical signals in pollen tubes: a beacon for apical morphogenesis and chemotropism?")
- 26th ICSPR Plant Reproduction 2022 – June 20-24th, **Poster** presentation "Integration of ion dynamics into a Membrane Potential Gradient in pollen tubes"

Teaching experience

Fall 2015, 2016, 2018	BSCI 454 – University of Maryland, College park Neurobiology Laboratory
Spring 2016, 2017, 2018, 2019	BSCI 442/ PLS 400 – University of Maryland, College park Plant Physiology laboratory